INFLUENCES OF CHEMICAL SPECIATION AND SOLID PHASE PARTITIONING ON MICROBIAL TOXICITY: SINGLE ORGANISM TO IN SITU COMMUNITY RESPONSE

by

James Gill Moberly

A dissertation submitted in partial fulfillment
of the requirements for the degree

of

Doctor of Philosophy

in

Engineering

MONTANA STATE UNIVERSITY
Bozeman, Montana

April 2010

APPROVAL

of a dissertation submitted by

James Gill Moberly

This dissertation has been read by each member of the dissertation committee and has been found to be satisfactory regarding content, English usage, format, citation, bibliographic style, and consistency, and is ready for submission to the Division of Graduate Education.

Dr. Brent M. Peyton

Approved for the Department Chemical and Biological Engineering

Dr. Ron Larsen

Approved for the Division of Graduate Education

Dr. Carl A. Fox

STATEMENT OF PERMISSION TO USE

In presenting this dissertation in partial fulfillment of the requirements for a doctoral degree at Montana State University, I agree that the Library shall make it available to borrowers under rules of the Library. I further agree that copying of this dissertation is allowable only for scholarly purposes, consistent with "fair use" as prescribed in the U.S. Copyright Law. Requests for extensive copying or reproduction of this dissertation should be referred to ProQuest Information and Learning, 300 North Zeeb Road, Ann Arbor, Michigan 48106, to whom I have granted "the exclusive right to reproduce and distribute my dissertation in and from microform along with the non-exclusive right to reproduce and distribute my abstract in any format in whole or in part."

James Gill Moberly

April 2010

DEDICATION

I dedicate this dissertation firstly to my wonderful wife who has stuck with me throughout school, marriage, five children, and moves to three states nearly every year, through thick and thin, in the pursuit of my dreams. Also this dedication is to my children, Cardin, Isabella, Jackson, John, and Meredith who have been born into "a student's life" and put up with it, while enriching mine. I would like to thank my parents who supported me in my first forays of life and science, with continued help and support along the way. I would like to include the important people who have shaped my career and education path, those who taught me in school, my 5th grade teacher Mr. Abbley, who set me on the path in science, Mr. Jeff Butler and Mrs. Mary Margaret Pratt, my high school physics, calculus, and chemistry teachers, for helping show me the joy in discovery. Lastly, this dedication is to my committee, Drs. Abigail Richards, Robin Gerlach, David Cummings, Albert Parker, and especially my advisor Dr. Brent Peyton, who took a chance hiring me and without whom, I would have floundered on the rocky shores of ignorance.

TABLE OF CONTENTS

TABLE OF CONTENTS (CONTINUED)

LIST OF TABLES

LIST OF FIGURES

Figure Page

ABSTRACT

The waters and sediments of Lake Coeur d'Alene (LCDA) in northern Idaho have been contaminated by heavy metals because of decades of mining operations. Metal speciation is critical in assessing toxicity because it may vary considerably with pH and is dependent on other aqueous constituents. There has been little research on integrated investigations of the effects of heavy metal speciation on indigenous microbes from LCDA, especially large scale community analysis. The focus of this research in the LCDA system was to determine the effect of heavy metal speciation on toxicity, first in a defined single organism system, followed by *in situ* studies.

Combined results of thermodynamic modeling, statistical analysis, and batch culture studies using *Arthrobacter* sp. JM018 suggest that the toxic species is not solely limited to the free ion, but also includes $ZnHPO_4^0(aq)$. Cellular uptake of $ZnHPO_4^0(aq)$ through the inorganic phosphate transporter (*pit* family), which requires a neutral metal phosphate complex for phosphate transport, may explain the observed toxicity. These findings show the important role of "minor" Zn species in organism toxicity and have wider implications since the *pit* inorganic phosphate transport system is widely distributed in bacteria, archaea, and eukaryotes.

Using a multivariate statistical approach, correlations between the microbial community (via 16S rDNA microarray) in sediment cores and operationally defined heavy metal phases (via continuous sequential extractions) were explored. Candidate phyla *NC10, OP8* and *LD1PA* were only present in metal contaminated cores and diversity doubled among *Natronoanaerobium* in metal contaminated cores which may suggest some increased fitness of these phyla in contaminated sediments. Correlations show decreases in diversity from presumed sulfate reducing lineages within most taxa from *Desulfovibrionales* and *Bdellovibrionales* and from metal reducing bacterial lineages *Shewanellaceae, Geobacteraceae,* and *Rhodocyclaceae* with increases in the ratio of more bioavailable Pb exchangeable/carbonate to less bioavailable Pb oxyhydroxide. This is the first time these techniques have been used in combination to describe a contaminated system.

CHAPTER 1

INTRODUCTION

Lake Coeur d'Alene Metal Contamination

Lake Coeur d'Alene (LCDA), a natural lake in northern Idaho between the Selkirk and Coeur d'Alene Mountains, was formed by glacial meltwaters which overflowed from Lake Missoula approximately 14,000 years ago [1-3]. LCDA is joined on the southern portion of the lake by the St. Joe (STJOE) and Coeur d'Alene River (CDAR) [1-5]. These two rivers contribute approximately 94% of the influent flow into LCDA [3]. The CDAR is composed of two main rivers; 1) the South Fork of the CDAR and its tributaries which flow through the Coeur d'Alene Mining District and 2) the North Fork which joins the South Fork before continuing through an area of lateral lakes and deltas and into LCDA [1-4]. The South Fork of the CDAR is of particular interest as it and its tributaries are the primary drainage source for the Coeur d'Alene Mining District [1, 3].

Though in the recent past only two out of over 90 mines were in operation, the Coeur d'Alene Mining district has been a world class producer of Ag, Pb, Zn and Sb [1, 3-4, 6]. Over 3 million tons of Zn, 34 thousand tons of Ag, and 7 million tons of Pb have been mined from the Coeur d'Alene Mining district, stretching from Coeur d'Alene, Idaho to Superior, Montana [7].

The history of this district as well as the type of ore deposits and mineralogy has been summarized by Leach and others [7-11]. The mineralogy of the Coeur d'Alene

Mining District consists primarily of quartz [SiO_2] and siderite [$FeCO_3$] veins containing deposits of galena [PbS], sphalerite [ZnS], and tetrahedrite [$Cu_{12}Sb_4S_{13}$] [7]. Pyrite [FeS_2], chalcopyrite [$CuFeS_2$], and pyrrhotite [Fe_xS x=0.8,1] are also locally abundant [7]. Fe minerals including siderite, magnetite, pyrite, pyrrhotite, goethite, hematite, and ferrihydrite have been reported in sediments of LCDA and in the upstream Mining district [12-14].

Analyses of the sediment and water in the Coeur d'Alene system have been examined by others focusing on geology and geochemistry [8-10, 13, 15], as well as surface and subsurface sediment contamination and benthic transport [1-3, 5, 14, 16-24]. Contamination of lateral lakes adjacent to the delta [17, 25-26], CDAR and upstream tributary contamination [20, 22, 27-33], and downstream of LCDA [34], have also been studied. In a study of LCDA, Horowitz [3] found the CDAR was the most heavily contaminated. Heavy metals in the delta region of LCDA appear to be associated with an operationally defined sulfidic phase [18], while those elsewhere in LCDA appear to be predominantly associated with the more mobile hydroxides [3, 24], though there is some controversy on this point [35].

Historical data (1991-2007) from the US Geological Survey database (http://waterdata.usgs.gov/id/nwis/) show a strong positive correlation ($p<0.0001$) between heavy metals (Pb, Zn) and redox active elements (Fe, Mn) in filtered and unfiltered samples. Fe and Mn in unfiltered samples show a negative correlation with river temperature ($p<0.0033$ and $p<0.0002$, respectively) and to a lesser extent pH ($p<0.055$, and $p<0.0073$, respectively). This high correlation between heavy metals and

redox active elements may suggest co-transport of metal (hydr)oxides with sorbed heavy metals (unfiltered), or reductive dissolution and consequent release of heavy metals from sorbed (hydr)oxides (filtered).

Of concern in the LCDA system is the potential contamination of unpolluted sediment from re-mobilization of heavy metals in the fine fraction. Remobilization may occur from any of the following processes: (i) physical entrainment of the small heavy-metal-laden particles from the upper sediment column into the river [36], (ii) adsorption of toxic metals to metal (hydr)oxides (e.g., ferrihydrite), clays, and organic compounds (e.g., humics, fulvics, citrate) followed by particle-based transport of these bound metals within the water column [6, 31, 37], and (iii) reductive dissolution of mineral phases resulting in release of adsorbed or co-precipitated heavy metals [38-39].

Dry grain size fractioning by Moberly *et al.* [33] revealed that the majority, by mass, of sediment particles in CDAR samples were in the smallest size fraction, below 75 μm (this fraction contains primarily silt (2-50 μm) and clay (< 2 μm) sized particles) and that this distribution is most pronounced in the upper 5 cm of sediment. Horowitz *et al.* [1] and Grosbois *et al.* [34] reported that the majority of metal contamination within LCDA is contained within the smallest fractions (<63 μm) and that metal concentration is inversely proportional to particle size. Micron and smaller-scale particles are often more reactive and can be more bio-available [40]. Because the majority of the smallest particles are within the top 5 cm, this may pose a potential metal remobilization issue when these sediments are disturbed by flooding, bioturbation [41], or anthropogenic activities, such as dredging [36].

Although total metal content is important, the mobility, reactivity, and bioavailability of heavy metals is dictated by crystallinity, particle size, mineral phase, and associated chemistry in which these metals partition [42]. For a better understanding of the mineralogy and thus bioavailability, fate, and transport of heavy metals in this system, it was desirable to combine both macro- and micro-scale analyses. For the first time with CDAR sediments, Moberly *et al.* [33] applied a combination of bulk X-ray diffraction (XRD), extended X-ray absorption fine structure (EXAFS) spectroscopy, and synchrotron based micro-focused XRD combined with micro-focused X-ray fluorescence (μXRF) mapping techniques to provide high-resolution analyses of minerals and metal associations at the micron scale. Their analyses indicate the presence of crystalline Pb and Zn-bearing mineral phases of dundasite [$Pb_2Al_4(CO_3)_4(OH)_8 \bullet 3H_2O$], coronadite [$PbMn_8O_{16}$], stolzite [$PbWO_4$], mattheddleite [$Pb_{10}(SiO_4)_{3.5}(SO_4)_2Cl_2$], bindheimite [$Pb_2Sb_2O_7$], and smithsonite [$ZnCO_3$]. Likely phases for Zn and Pb adsorption were ferrihydrite, diaspore [AlO(OH)], manganite [$Mn^{(III)}O(OH)$], muscovite [$KAl_2(Si_3Al)O_{10}(OH,F)_2$], biotite [$K(Fe,Mg)_3AlSi_3O_{10}(F,OH)_2$], and montmorillonite [$Na_{0.3}(Al,Mg)_2Si_4O_{10}(OH)_2 \bullet 8H_2O$]. Moberly *et al.* [33] suggests the large predominance of Fe and Mn (hydr)oxides over other sorbent minerals suggests that the metal sorption behavior is dominated by these (hydr)oxide phases.

Metal Toxicity to Biota

Heavy metals are toxic and carcinogenic to biota including humans [43], can alter anti-predatory behaviors in snails, caddis flies [44], and fish [45], and can bio-accumulate

in the ecosystem [46-48]. Metal toxicity in bacteria has been shown to depend on speciation and chemical properties as well as cell associated surfaces that affect local metal concentration [49-52]. It is known that a variety of ligands can alter metal toxicity to microbes in aqueous medium by chelation with pyrithiones [53], pyrophosphates [52], ethylene di-amine tetra acetic acid (EDTA) [52, 54], nitrilotriacetic acid (NTA) [55], and precipitation with inorganic compounds such as phosphates [56], and sulfides [56-57]. At higher concentrations, metals may interact with nucleic acids and enzyme active sites, and may lead to a rapid decline in membrane integrity, which is generally manifested as leakage of mobile cellular solutes (e.g., K^+) and cell death [58]. Toxic effects in bacteria are believed to result from the displacement and/or substitution of essential ions from cellular sites, and from blocking functional groups of important biochemical molecules such as enzymes, polynucleotides, and essential nutrient transport systems [43]. This causes disruption of the cell-membrane resulting in denaturation and inactivation of enzymes [59]. Metal toxicity can manifest as decreases in specific growth rates of an organism, decreases in cellular yields, increased lag-time associated with inhibition, or failure to grow.

Mineral/Microbe Interactions

Microbial growth, metal detoxification, and biogeochemical cycling of metals can be linked to mineral phases in environmental settings. It is theorized that iron reducing bacteria (IRB) and sulfate reducing bacteria (SRB) contribute significantly to metal cycling in the LCDA system though the main mechanisms are not well understood [3, 60-

62]. In studies with the sulfate-reducer *Desulfovibrio desulfuricans* G20, Sani *et al.* [63-64] found that mineralization of uranium (VI) was controlled by the availability of a carbon source, and that biogenically reduced uraninite could be reoxidized in the presence of hematite, goethite, and ferrihydrite. Studies with aluminum, nickel, and cobalt substituted goethite and co-precipitated nickel/hydrous ferric oxides showed release of these metals upon reduction of the ferric oxide [38, 65-66]. In co-precipitated Ni-hydrous ferric oxide, nickel showed an inhibitory effect on Fe reduction [38]. Additionally, oxidation of metastable authigenic and sedimentary Fe sulfide minerals can release surface absorbed and co-precipitated heavy metals into the environment [57]. Microbes in LCDA are capable of dissimilatory reduction of reducible metals such as arsenate and ferric Fe [17, 60, 62, 67]. Maximum concentrations of As and Fe at the sediment water interface suggest post-depositional mobilization of these elements potentially mediated by microorganisms [12, 17, 67]. IRB can release absorbed or coprecipitated metals by reducing Fe and manganese hydroxides [12, 38, 68]. In contrast, SRB catalyze reactions that detoxify their environment that can lead to community bio-protection by biogenic production of highly reactive sulfides [69-70]. Sulfide complexes have low solubility and can readily precipitate (e.g., ZnS, PbS, CuS, HgS) while soluble complexes (e.g., $Zn(HS)_2$, $ZnS(HS)^-$) are thought to be less bioavailable [69]. Other elements such as zinc, lead, and cadmium may undergo mobilization with changes in pH, redox-potential, and binding to organic matter, mediated by microbial populations [71].

Methods for Estimating Heavy Metal Bioavailability

Aqueous heavy metals speciation and thus predicted bioavailability can be determined in a number of ways. Recent advances in electrochemistry have allowed application of a variety of stripping voltammetry methods to determine aqueous speciation and redox state of elements, as well as attempt to predict bioavailability [72-75]. However, there are limitations to voltammetry, such as difficulty in preparing standards of unknown or very transient species. Thermodynamic aqueous speciation modeling has been employed to predict partitioning of heavy metals with associated ligands [76-77]. Speciation models have been employed to study the LCDA system and give valuable information for predictions of fate and transport, stability, environmental management and planning, and further hypothesis testing [5-6, 31, 78]. Toxicity models [72-73, 79-81] have been developed that employ chemical speciation information to predict the effects of these chemical interactions with biota. These models suggest that the activity of the free metal ion in aqueous solution [80, 82] or metal sorption to biological surfaces [72-73, 82-83] dictate the toxicity to microorganisms.

Methods for solid phase characterization have used multiple techniques to predict partitioning and bioavailable fractions. Multiple methods are available for chemical extractions to target specific metal phases [18, 26, 84-88], or simulate *in vivo* digestive processes [89]; all are operationally defined by extractants and methods of extraction. The main limitations to chemical extraction are unknown dissolution kinetics of each heavy metal phase, redistribution of extracted metals onto other phases during extraction, and non-specific extractions. These issues are being overcome with the introduction of

more specific chemical extractants and the use of continuous extraction systems which limit redistribution and kinetic problems [86]. Additional advances in spectroscopic techniques, especially in smaller scale analysis through X-ray microprobe and synchrotron radiation, have been gaining in use to identify mineralogy, redox state, and element correlation, even in complex environmental samples [33, 90-91].

Scope of Thesis

The geochemistry of LCDA has been relatively well characterized, including solid phase partitioning and aqueous chemistry. There have been limited microbial studies, falling under two classes: culture dependent techniques [12, 17, 62, 92-94], and culture independent techniques [60, 93, 95]. However, there has been little research on integrated investigations of the effects of heavy metal speciation on indigenous microbes from LCDA, especially large scale community analysis. The following chapters focus on research in the LCDA system determining the effect of heavy metal speciation to microorganisms in two systems: 1) single organism isolated from LCDA in defined growth medium and 2) *in situ* characterization of natural microbial communities and correlation to heavy metal phase association. Chapter four focuses on future work in speciation related toxicity with specifics to LCDA. The following are areas for further investigation into chemical speciation and its effects on microorganisms.

In single species systems, future work could focus on other well characterized microorganisms, such as *E. coli*, to verify the findings demonstrated in *Arthrobacter* sp.

JM018. Zn also may behave differently than other divalent heavy metal cations and further investigation with other heavy metals would be desirable.

Future work in the LCDA system could begin by verifying these linear models with laboratory and environmental isolate strains from identified taxa with mineral identified in the LCDA system. Presumed metabolic functions based on families for exploratory analysis were used in this study, but further work in this area should quantify metabolic functions of active populations using meta-genomic analyses, for example 454 sequencing [96], functional gene microarrays [97] and/or employ live/dead extraction procedures [98] for more complete picture of the environment. Additionally, only Pb, Zn, Mn, and Fe were studied, but further work could examine other factors including, but not limited to, Hg, Cu, As, and Cd.

CHAPTER 2

ZINC ION SPECIES TOXICITY: INHIBITION OF CELL YIELDS AND GROWTH RATES OF *ARTHROBACTER* SP. ISOLATED FROM HEAVY METAL CONTAMINATED SEDIMENTS

Abstract

Chapter has been submitted to Environmental Science and Technology.

Due to its high solubility over a wide range of pH conditions, Zn is found in many natural and anthropogenic aqueous systems. Zn speciation is critical in assessing Zn toxicity to microorganisms because it varies considerably with pH and is dependent on other aqueous constituents. Combined results of thermodynamic modeling, statistical analysis, and batch culture studies using *Arthrobacter* sp. JM018 suggest that the toxic species may not solely be limited to the free ion, but also includes $ZnHPO_4^0$(aq). Cellular uptake of $ZnHPO_4^0$(aq) through the inorganic phosphate transporter (*pit* family), which requires a neutral metal phosphate complex for phosphate transport, may explain the observed toxicity. Based on visual MINTEQ (v2.52) modeling, at 50 μM total Zn, $ZnHPO_4^0$(aq) contributes 33, 70, and 76% of the neutral metal phosphate pool at pH 6, 7, and 8, respectively. At 50 μM total Zn, cultures supplied with organic phosphate (glycerol-3-phosphate) show no significant response to pH (p=0.20) while inhibition of inorganic phosphate supplemented cultures whose neutral metal phosphates are increasingly dominated by $ZnHPO_4^0$(aq) show significant pH dependence (p=9.5e-7). These findings show the important role of "minor" Zn species in organism toxicity and have wider

implications since the *pit* inorganic phosphate transport system is widely distributed in bacteria, archaea, and eukaryotes.

Introduction

The waters and sediments of the Coeur d'Alene River in northern Idaho have been impacted by decades of mining operations within the Coeur d'Alene Mining district. However, sediment samples in the heavy metal contaminated Coeur d'Alene River which showed average concentrations of 0.75% mass of Zn and 0.5% mass of lead [33], provide a unique habitat for the cultivation of heavy metal tolerant microorganisms.

Arthrobacter species are commonly isolated from a variety of metal contaminated and non-contaminated sites [99-105]. *Arthrobacter* are pleomorphic, changing membrane properties from Gram-negative rods in young cultures to Gram-positive cocci in older cultures [100]. It has been suggested that the ability for *Arthrobacter* to alter its membrane characteristics may aid in this genus' success in survival in extreme environments [100].

Arthrobacter species have been found to be tolerant of aluminum, lead, cadmium, mercury, cobalt, chromium, and Zn [103, 106-109]. It is hypothesized [110] that because of the high solubility and availability of Zn under normal environmental conditions Zn may be the most toxic of heavy metals. Zn exhibited higher toxicity than lead, copper, cadmium, nickel, and manganese in studies with *Pseudomonads*, *Micrococci*, and *Bacilli* in crude oil and aromatic hydrocarbon degradation [111-112]. Zn also plays a significant role in many enzyme active sites as well as being an important structural molecule [113]. Toxic effects of Zn and other heavy metals in bacteria are believed to result from the

displacement and/or substitution of essential ions from cellular sites, and from blocking functional groups of important biochemical molecules such as enzymes, polynucleotides, and essential nutrient transport systems [43].

Metal toxicity in bacteria has been shown to depend on speciation and chemical properties as well as cell associated surfaces that affect local concentration [49-52]. It is known that a variety of ligands can alter metal toxicity to microbes in aqueous medium by chelation with pyrithiones [53], pyrophosphates [52], ethylene di-amine tetra acetic acid (EDTA) [52, 54], nitrilotriacetic acid (NTA) [55], and precipitation with inorganic compounds such as phosphates [56], and sulfides [56-57]. Toxicity models [72-73, 79-81] have been developed to begin to predict the effects of these chemical interactions. Many of these models maintain that the activity of the free metal ion in aqueous solution dictates the toxicity to microorganisms and biota [80, 82]. However, the free ion does not always accurately predict toxicity. In studies with two species of freshwater green algae, De Schamphelaere *et al.* [83] found that surface-bound and cytoplasmic copper better predicted toxicity than free copper. To improve our understanding of the role of Zn species in bacterial toxicity we employed thermodynamic models to predict the Zn species distribution under changes in medium pH. This study was focused on characterizing the growth inhibition of *Arthrobacter sp.* JM018 under changing Zn species distributions and correlating the toxic effects to specific aqueous Zn species.

Materials and Methods

Bacterial Isolation and Characterization

Arthrobacter sp. JM018 was isolated from sediment samples in heavy metal contaminated Coeur d'Alene River which showed average concentrations of 0.75% mass of Zn and 0.5% mass of lead [33] and provides a unique habitat for cultivation of heavy metal tolerant organisms. Clone-libraries and 16S rDNA microarrays from the sediments samples taken at that time indicate that *Arthrobacter* spp. are an abundant population of the microbial community [unpublished data, 114].

One kilogram of contaminated sediment collected from the Coeur d'Alene River was incubated in a flow reactor system with medium designed to simulate fluvial conditions. The medium contained a final concentration (mg/L) of the following: 2.1, $MgCl_2 \cdot 6H_2O$; 16, NH_4Cl; 5.5, $CaCl_2 \cdot 2H_2O$; 246.1, CH_3COONa; 60, Na_2SO_4; and 1,732, $C_8H_{16.5}N_2Na_{1.5}O_6S_2$ (piperazine-N,N'-bis(ethanesulfonic acid); 1,4-piperazinediethanesulfonic acid, PIPES). Trace elements were added from concentrated stock solutions to final concentrations of (μg/L) of the following: 357, $C_6H_6NO_6Na_3$; 0.59, $NiCl_2 \cdot 6H_2O$; 30, $CoCl_2 \cdot 6H_2O$; 174.2, $Na_2MoO_4 \cdot 2H_2O$; 80, H_3BO_3; 6480, NaH_2PO_4; 0.75, $CuCl_2 \cdot 2H_2O$; 3.2, $PbCl_2$; 160, $ZnCl_2$; and 19,000, $NaHCO_3$. Medium components were obtained from Fisher (Phillipsburg, NJ) with the exception of CH_3COONa (Aldrich, St Louis, MO), $C_8H_{16.5}N_2Na_{1.5}O_6S_2$ (Aldrich, St Louis, MO), and $C_6H_6NO_6Na_3$ (Sigma, St Louis, MO). Thauers vitamin solution was used at a final concentration of (mg/L): 0.1, biotin; 0.01, folic acid; 0.05, pyridoxine HCl; 1, choline chloride; 0.005, vitamin B_{12}; and

0.025, each of thiamine HCl, riboflavin, nicotinic acid, pantothenic acid, p-aminobenzioic acid, and lipoic acid [115].

Liquid samples were taken above the sediment-water interface, at the sediment-water interface, and every 1.25 cm to a depth of 5 cm within the flow reactor after four weeks operation, and were spread directly onto agar plates containing 40 g tryptic soy agar (Difco) and 0.41 g CH_3COONa per liter. Plates were incubated at room temperature (23 ± 3^oC). Single colonies were picked and transferred to serum bottles containing 30 g/L Difco tryptic soy broth (TSB). Once growth was observed in the serum bottle cultures this process was repeated and single colonies from the second plating were taken as pure and transferred into serum bottles containing TSB.

Genomic DNA of isolates was extracted using Promega Wizard® Genomic DNA purification kit as per kit instructions. The presence of extracted DNA was confirmed using gel electrophoresis. DNA extracts were amplified using polymerase chain reaction (PCR) using universal bacterial primers (Invitrogen) BAC8F (5'-AGAGTTTGATCCTGGCTCAG-3') and BAC1492R (5'-GGTTACCTTGTTACGACTT-3') targeting the 16S rDNA gene. PCR products were verified using gel electrophoresis. Amplified PCR products were purified using gel filtration cartridges (Performa® DTR Edge Biosystems) as per BigDye™ protocol and amplified using a single forward primer BAC8F and the BigDye™ reagents. Products from the fluorescent labeled BigDye™ protocol were again purified using gel filtration cartridges and analyzed using an ABI 373 automated DNA sequencer at Washington State University's DNA sequencing facility. Bacterial sequences were analyzed using National Center for Biotechnology

Information and Ribosomal Database Project databases using Basic Local Alignment Search Tool (BLAST) and Sequence Match tools for comparison [116].

Media Development

After isolation, the *Arthrobacter* isolate was grown on a modified formulation of metal toxicity medium (MTM) to decrease metal complexation and precipitation [117]. Each liter of basal medium was composed of (g/L) 0.246, CH_3COONa; 0.06, Na_2SO_4; 0.02, $NaHCO_3$; 0.004, NaH_2PO_4; 0.016, NH_4Cl; and 0.02, yeast extract. For all pH values selected in this study, 1.73 g/L of PIPES buffer was added for an effective buffering range of 6.1-7.5. For experiments that required organic phosphate, filter sterilized (0.2 μm) solutions of glycerol-3-phosphate (33 μM) were amended to autoclaved medium in place of inorganic phosphate sources.

Stock solutions of 10 mM Zn chloride were prepared and acidified to pH 1.5 with hydrochloric acid and filter sterilized (0.2 μm) into autoclaved serum bottles to minimize complexation or precipitation at high temperature. Zn addition did not substantially influence pH (-0.2 units maximum at 250 μM Zn).

Thermodynamic Modeling

Aqueous speciation of the medium was calculated using Visual MINTEQ (version 2.52) to estimate complexation between medium components and Zn under the conditions tested. Batch experiments were designed using information predicted by Visual MINTEQ. Modeling was performed using the Davies equation for activity corrections and under the assumption that precipitates did not form during mixing. The

saturation indices of solid phases were monitored after simulations to verify this assumption. Visual and spectrophotometric (595nm) observations of abiotic controls also confirmed no precipitates formed under the conditions tested. All medium components except PIPES and yeast extract were used in modeling, as these components were not present in the database.

Pearson's correlation on Zn species predicted by Visual MINTEQ, pH, and specific growth rates were calculated in R [118]. Principle component analysis was used to identify significant Zn species for further investigation. Non-parametric Spearman's rho test was also performed on the dataset identifying those species which were most significantly correlated with growth inhibition.

Batch Experiments

Zn concentrations were monitored using the U.S. Environmental Protection Agency approved spectrophotometric ZincoVer5® reagent method (620nm) (Hach Method 8009; Sani *et al.* 2003) modified to utilize small sample volumes. Calibration standards were prepared from serially diluted stock solutions of 10 mM $ZnCl_2$. Growth of *Arthrobacter* sp. JM018 was monitored using absorbance measuremants at 595 nm.

Results and Discussion

Response of *Arthrobacter* sp. JM018 to Zn

In these experiments, pH was used to control aqueous speciation of medium components at a fixed total Zn concentration. *Arthrobacter* sp. JM018 was exposed to combinations of pH 6-8 and Zn concentrations of 0-250 μM. The Zn species predicted

by Visual MINTEQ under these experimental conditions are presented in Table 1. As shown in Table 1, the free ion, Zn^{2+}, decreases with increasing pH from approximately 89% of the total Zn at pH 6 to 75% at pH 8. The free metal ion (Zn^{2+}) is thought to contribute to the majority of toxic effects [80]. If the free metal ion controls the toxicity, then a decrease in toxicity should be observed with increasing pH as compared to metal-free controls at each corresponding pH.

Table 1: Zn speciation (%) at 50 μM Zn as predicted by visual MINTEQ

	pH 6	pH 7	pH 8
Zn^{+2}	88.73	86.82	74.49
$ZnOH^{+}$	0.05	0.48	4.07
$Zn(OH)_2$ (aq)	0.00	0.08	7.02
$ZnCl^{+}$	0.07	0.07	0.06
$ZnSO_4$ (aq)	4.20	4.08	3.50
$Zn(SO_4)_2^{-2}$	0.02	0.02	0.01
$ZnNH_3^{+2}$	0.00	0.02	0.14
$ZnHPO_4$ (aq)	0.19	1.11	1.87
$ZnCO_3$ (aq)	0.01	0.27	2.69
$ZnHCO_3^{+}$	0.13	0.34	0.34
Zn-Acetate^{+}	6.56	6.70	5.77
Zn-$(Acetate)_2$ (aq)	0.03	0.03	0.03

Zn affects the growth of *Arthrobacter* sp. JM018. At pH 7, cell yields and specific growth rates decreased and the length of the lag phase increased with increasing Zn concentration (Figure 1) with no observable growth at 175 μM. Figure 2A and 2B show the cell yields and specific growth rate, respectively, of *Arthrobacter* sp. JM018 in response to increasing Zn concentrations at pH 6, 7, and 8. With the exception of a small stimulatory effect at pH 6 and 10 μM Zn, Figure 2 illustrates that increases in both pH and Zn concentrations negatively affect specific growth rate and cell yield. No growth was observed at 175 μM Zn at all pH conditions tested.

Our observations of increasing Zn toxicity with increasing pH warranted inspection of the other Zn species with changing pH to determine the toxic Zn species responsible. At a given pH, the ratios of aqueous Zn species change very little with increasing total Zn concentrations. However, as shown in Table 1, at a fixed Zn concentration, Zn speciation can vary significantly with changes in pH. For a fixed concentration of total Zn, Zn^{2+}, $ZnSO_4$(aq), and Zn-$(acetate)^+$ decrease in concentration with increasing pH, whereas $ZnCl^+$, $Zn(SO4)_2^{2-}$, and Zn-$(acetate)_2$(aq) change very little with pH. $ZnHCO_3^+$ increases from pH 6 to 7, but shows no further increase from pH 7 to 8. The Zn species which showed significant increases with increasing pH are $ZnOH^+$, $Zn(OH)_2$(aq), $ZnNH_3^{2+}$, $ZnHPO_4$(aq), and $ZnCO_3$(aq). The concentration of hydrolysis products, $ZnOH^+$ and $Zn(OH)_2$(aq), increase with increasing pH at a fixed total soluble Zn concentration. However, $ZnNH_3^{2+}$, $ZnHPO_4$(aq), and $ZnCO_3$(aq) are more complex as they rely not only on soluble Zn, but also on other medium constituents that vary with pH. Further analysis of Zn species using principle component analysis and non-parametric Spearman's rho tests suggested $ZnHCO_3^+$, $ZnHPO_4^0$, $Zn(OH)_2^0$ were highly correlated with growth inhibition under the conditions tested. Of these Zn species, phosphate is known to play an additional role in cellular processes and was selected as a focus for further study.

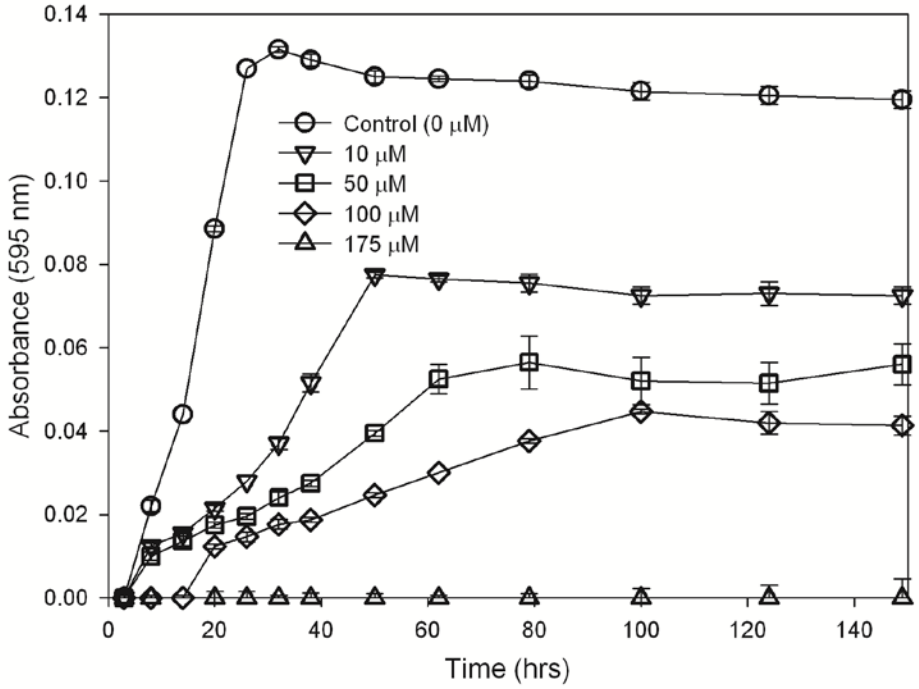

Figure 1: Growth of *Arthrobacter* sp JM018 in the presence of Zn at pH 7 and supplied with inorganic phosphate. Legend shows increasing treatments of total zinc (as $ZnCl_2$)

Inorganic phosphate can be transported via two systems: 1) the *pit* transport system which is thought to be constitutively expressed [119-120] though expression has been disputed [121], and 2) the *pst* transport system, a high affinity ABC-transporter expressed at low phosphate levels [122]. Organic phosphate can also be utilized as a phosphate source and systems have been identified to transport glycerol 3-phosphate (*GlpT*) and glucose-6-phosphate (*UhpT*) [122]. For inorganic phosphate transport, the *pit* transport system requires a neutral metal phosphate complex ($MeHPO_4^0$(aq)) [120, 122] and transport occurs via symport of the H^+ ion ($MeHPO_4$:H^+) [122]. The *pit* system has been shown to transport $ZnHPO_4^0$(aq) into the cytoplasm and *pit* deficient mutants confer a Zn resistant phenotype in *E. coli* [119]. Additionally, expression of *pitA* is upregulated by increases in extracellular Zn and by decreases in phosphate concentrations [121].

From an analysis of published *Arthrobacter* genomes from the National Center for Biotechnology Information (NCBI), it appears that the phosphate transporters, *pit*, *pst*, and *GlpT* are present in all *Arthrobacter* genomes available (August 2009), suggesting universal deployment in the genus *Arthrobacter* [116].

The *pit* system transports neutral metal phosphates, thus all neutral metal phosphates were examined. Table 2 presents the contribution of $MeHPO_4^0(aq)$ species as a fraction of all aqueous phosphate species and the fraction $ZnHPO_4^0(aq)$ in the $MeHPO_4^0(aq)$ pool. As is seen in Table 2, $ZnHPO_4^0(aq)$ accounts for less than 2% of the aqueous Zn species, but makes up between 9 to 92% of the $MeHPO_4^0(aq)$ pool. It can also be seen in Table 2 that increases in soluble Zn concentration at a fixed pH increases $ZnHPO4^0(aq)$, and additionally, increasing pH values at a fixed soluble Zn concentration also increase $ZnHPO4^0(aq)$. Figure 3A and 3B show the fraction of $ZnHPO_4^0(aq)$ to all other neutral metal phosphates overlaid onto a bar chart of growth inhibition (as cell yields and specific growth rates respectively) of JM018. Increases in either pH or soluble Zn significantly increase $ZnHPO_4^0(aq)$ which correlated with the inhibition of JM018. These results suggest that $ZnHPO_4^0(aq)$ is entering the cell via the *pit* system resulting in the increased toxicity with increased pH. The *pit* inorganic phosphate transport system requires neutral metal phosphates to uptake phosphate (and consequently Zn); to test this hypothesis we used an organic phosphate source to circumvent the inhibitory uptake of Zn via the *pit* inorganic phosphate transport system.

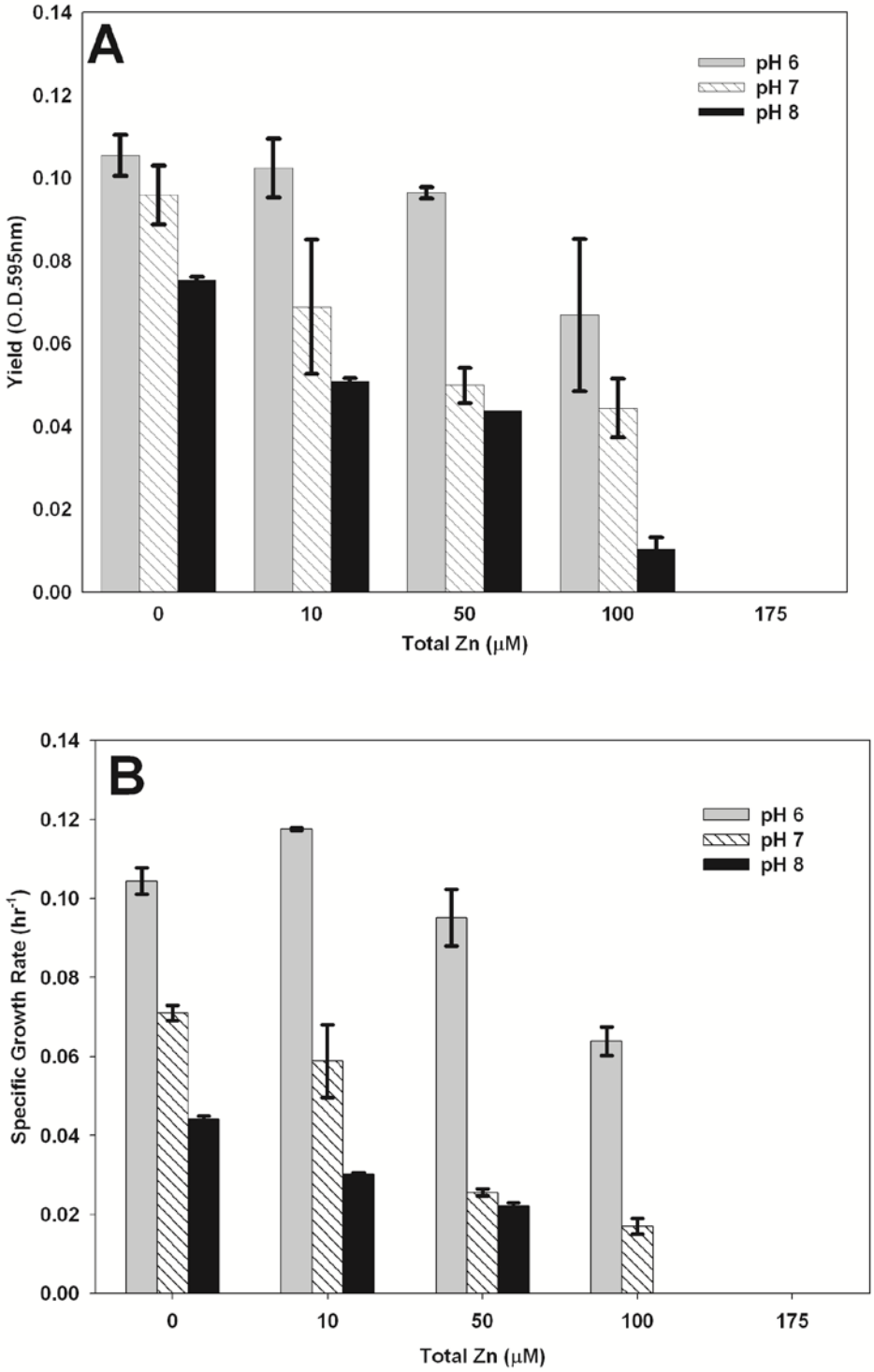

Figure 2: A) Response of yield of *Arthrobacter* sp. JM018 to pH and total Zn B) Response of specific growth rate (hr^{-1}) of *Arthrobacter* sp. JM018 to pH and total Zn

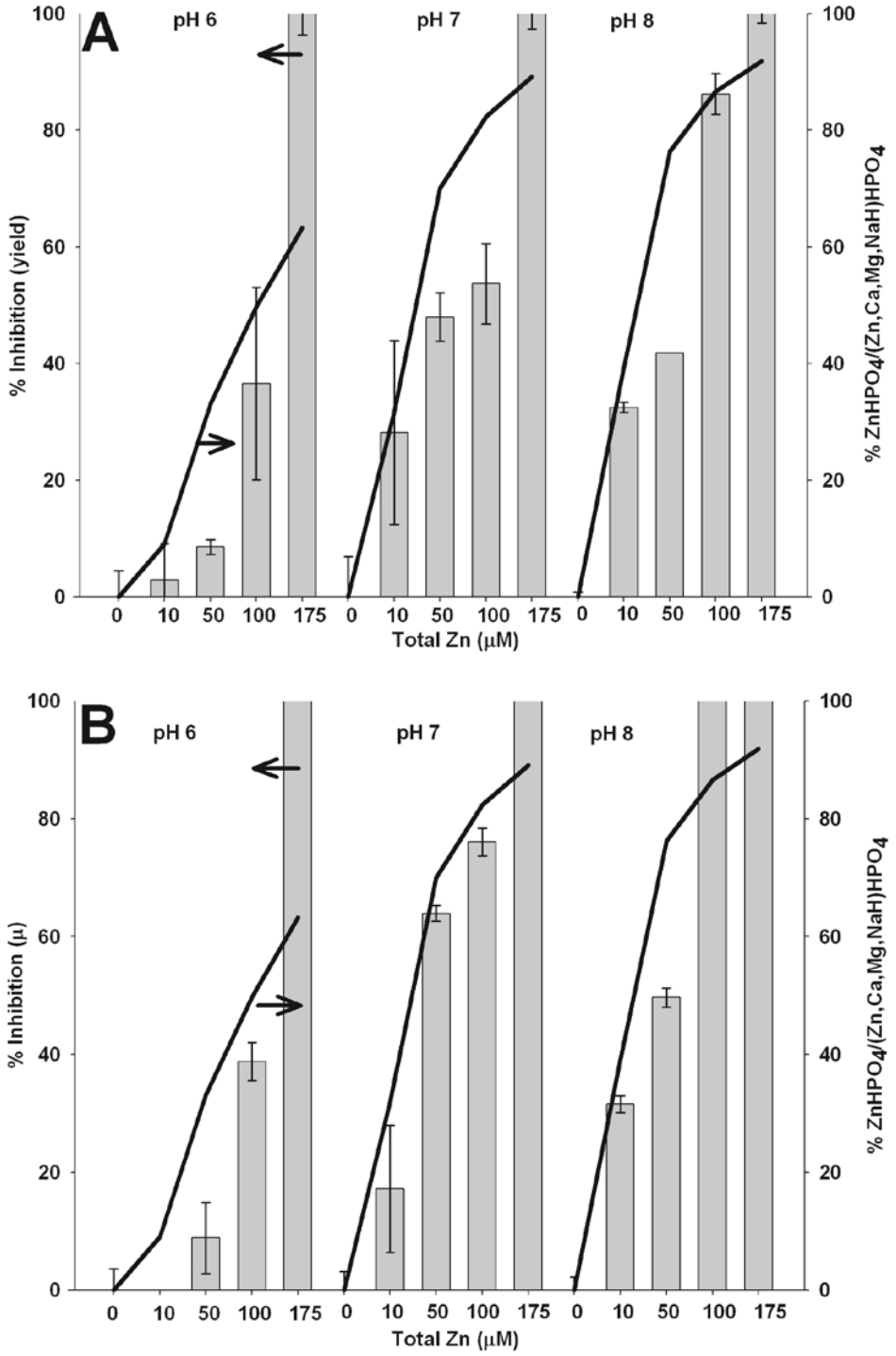

Figure 3: Percent inhibition (bars) of A) yield and B) specific growth rate (μ, hr^{-1}) of *Arthrobacter* sp. JM018 with 95% confidence intervals and percent of $ZnHPO_4$ to neutral metal phosphates (lines) at different Zn and pH conditions

Table 2: Neutral metal phosphate species (% aqueous phosphate) as predicted by Visual MINTEQ

pH	6			7			8		
Zn (μM)	10	100	175	10	100	175	10	100	175
% $MgHPO_4$ (aq)	0.024	0.024	0.024	0.141	0.135	0.13	0.274	0.257	0.244
% $CaHPO_4$ (aq)	0.063	0.062	0.062	0.368	0.353	0.341	0.716	0.671	0.638
% NaH_2PO_4 (aq)	0.648	0.642	0.637	0.382	0.367	0.355	0.075	0.07	0.067
% $ZnHPO_4$ (aq)	0.073	0.719	1.247	0.416	3.995	6.764	0.686	6.44	10.723
% $ZnHPO_4$ (aq)/$MeHPO_4$(aq)	9.03	49.69	63.30	31.83	82.37	89.12	39.18	86.58	91.87

Phosphate Transport Linked to Zn Toxicity

Growth of *Arthrobacter* sp. JM018 on glycerol-3-phosphate (an organic phosphate source), was performed to isolate Zn inhibition from the *pit* inorganic phosphate transport system. Glycerol-3-phosphate is transported into the cytoplasm via the *GlpT* transport system [122-123] with the electroneutral antiport of inorganic phosphate, organic phosphate anions, or both [124]. *Arthrobacter* sp. JM018 is capable of utilizing glycerol as a carbon and energy source (yield 0.06±0.01 O.D. (595nm)/mmol glycerol) and it is likely that *Arthrobacter* sp. can directly utilize glycerol-3-phosphate via glycerol-3-phosphate dehydrogenases (E.C. 1.1.1.94, 1.1.5.3) in the electron transport chain to produce reducing equivalents [125].

Figure 4 shows pH dependence of normalized (inhibited to metal-free) cell yields in Zn treated (50 μM) inorganic and organic phosphate media. Linear models of these yields show inhibition of JM018 is significantly ($p=9.45e-7$) dependent on pH when grown on inorganic phosphate, but when supplied with glycerol-3-phosphate JM018 shows an approximately 20% decrease in yield compared to metal free treatments but pH has no significant effect ($p=0.197$). This supports the hypothesis that Zn enters through

the *pit* inorganic phosphate transport system and results in additional toxicity to that already present from Zn entering into the cell through other means (e.g., non-specific divalent cation transport). These findings suggest that a pH dependent effect of Zn toxicity depends on the source of phosphate available for growth and supports the hypothesis that $ZnHPO_4^0(aq)$ is responsible for increased toxicity with increasing pH.

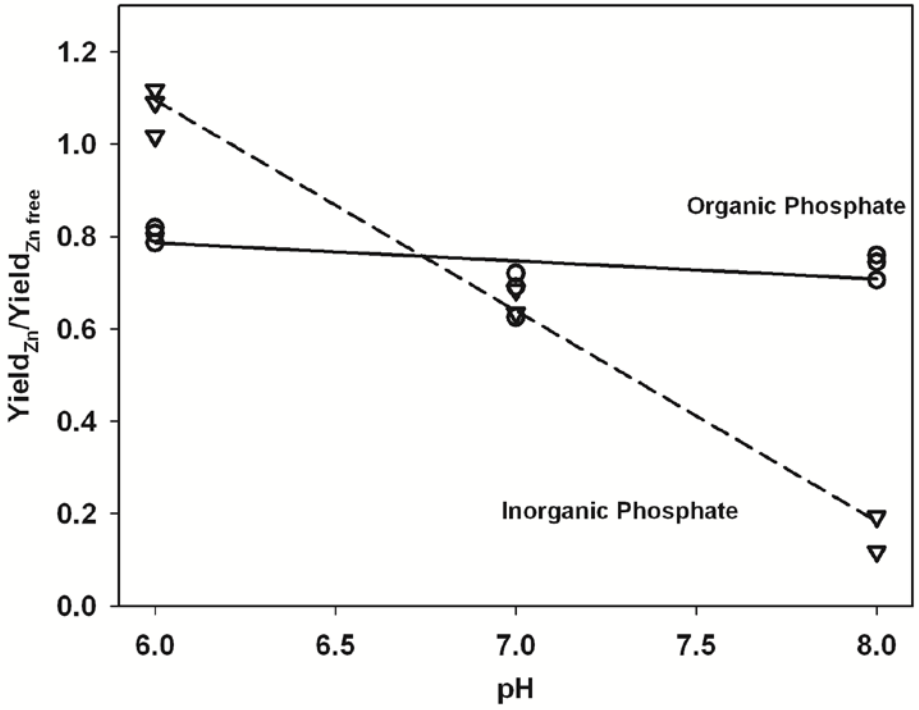

Figure 4: Plot of normalized cell yields of *Arthrobacter* sp. JM018 versus pH for 50 μM Zn treatments in inorganic phosphate (open triangles) and glycerol-3-phosphate (open circles) treatments. Cultures supplied with glycerol-3-phosphate show approximately 20% decrease in yield compared to metal free treatments with no significant response to pH (p=0.20) while inhibition in inorganic phosphate supplemented cultures whose neutral metal phosphate are increasingly dominated by $ZnHPO_4^0(aq)$ show significant pH dependence (p=9.5e-7).

Zinc and Phosphate Cycling

As shown in Figure 5 mechanism 2, the divalent form of Zn can enter the cell through non-specific divalent cation transporters (e.g., MgT), or Zn specific transporters

(e.g., ZnuABC, ZntA) [121, 126]. Figure 5 mechanism 1 shows transport of neutral metal phosphates into the cell via the *pit* transport system. It is unclear whether the toxicity of Zn entering through the *pit* transport system adds to 1) the total metal burden (Zn^{2+} pool) and thus ATP cost to efflux Zn or 2) causes the co-transported phosphate to become less bioavailable. Cellular depletion of free phosphate via efflux of neutral metal phosphates by *pit* is unlikely as this would also be present (and perhaps more pronounced) in an organic phosphate containing medium. *Arthrobacter* sp. JM018 grown on glycerol-3-phosphate do not exhibit the same level of toxicity to Zn, suggesting that Zn transport into the cell is affected. Phosphate entering the cell through the *GlpT* organic phosphate transport system does not increase the total metal burden on the cell. This does not negate the inhibitory effect of Zn entering through other transport mechanisms (# 2) since an overall decrease in yields of approximately 20% was observed when cells were treated with 50 μM Zn with glycerol-3-phosphate. These findings suggest that Zn toxicity for *Arthrobacter* sp. JM018 can be best predicted by the ratio of $ZnHPO_4^0$(aq) concentrations to other neutral metal phosphates in an inorganic phosphate containing medium.

These findings may have wider implications, such as a better understanding and control of transport of toxic heavy metals via the widely distributed *pit* inorganic phosphate transport system (e.g., bacteria, archaea, and eukaryotes) [127]. Additionally, these findings demonstrate that “minor” constituents of heavy metal species can play an important role in inhibition of microorganisms. Future evaluation of toxicological models should incorporate influences of heavy metal constituents based on speciation

changes coupled to known biological transport pathways for a more comprehensive predictive tool.

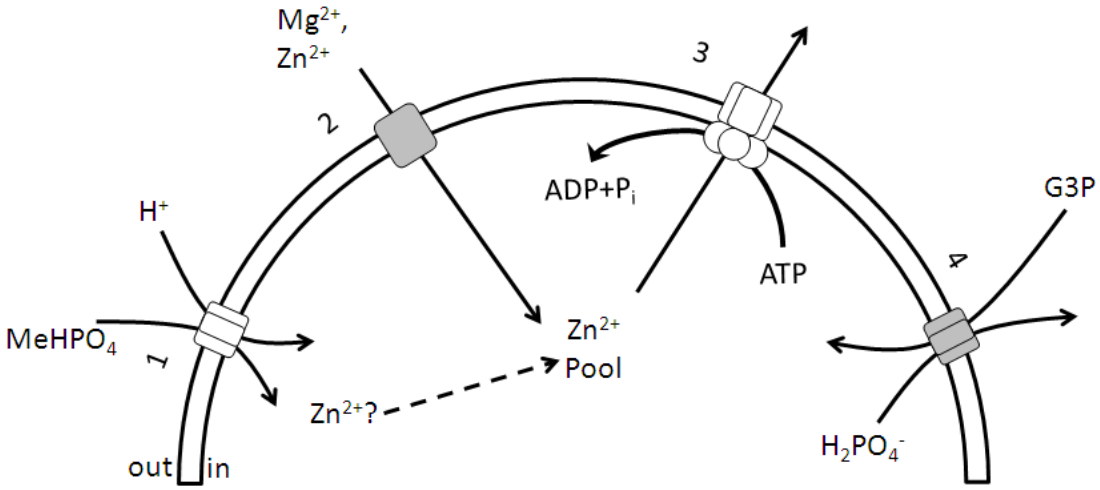

Figure 5: Schematic presentation of modes of cellular transport of Zn and phosphate 1. MeHPO4:H^+ symport using pit inorganic phosphate transport system where "Me" can be a divalent cation such as Mg^{2+} or Zn^{2+}; 2. non-specific divalent cation transport (e.g., *MgT*); 3. divalent cation efflux via P-type ATPase with the consumption of ATP to ADP + P_i; 4. electroneutral uptake of organic phosphate via *GlpT* with antiport of inorganic phosphate

Acknowledgements

The authors gratefully acknowledge financial support provided by the National Science Foundation (Grant # EAR-0420374). Any opinions, findings, and conclusions or recommendations expressed in this material are those of the author(s) and do not necessarily reflect the views of the National Science Foundation. Additional thanks to Al Parker (MSU) for invaluable statistical help and counsel.

CHAPTER 3

MICROBIAL COMMUNITY SIGNATURE IN LAKE COEUR D'ALENE: EFFECT OF ENVIRONMENTAL VARIABLES AND OPERATIONALLY DEFINED HEAVY METAL PHASES

Abstract

The waters and sediments of Lake Coeur d'Alene in northern Idaho have been impacted by decades of mining operations within the Coeur d'Alene Mining district. Using a multivariate statistical approach, correlations between the microbial community (via 16S rDNA microarray) in sediment cores and operationally defined heavy metal phases (via continuous sequential extractions) were explored. Candidate phyla *NC10, OP8* and *LD1PA* were only present in metal contaminated cores and diversity doubled among *Natronoanaerobium* in metal contaminated cores compared to the uncontaminated control site which may suggest some increased fitness of these phyla in contaminated sediments. In contrast, diversity within the phyla *Aquificae, Coprothermobacteria,* and *Synergistes* was at least double in the uncontaminated control site. From the presumed sulfate reducing lineages detected in this study, orders *Desulfobacterales, Desulfuromonadales, Desulfotomaculum,* and *Syntrophobacterales* correlated with the ratio of Zn to Pb in the operationally defined residual fraction, and most taxa within orders from *Desulfovibrionales* and *Bdellovibrionales* correlated with the ratio of Pb in the exchangeable/carbonate to oxyhydroxide phases. Diversity within families from metal reducing bacterial lineages *Shewanellaceae, Geobacteraceae,* and *Rhodocyclaceae*

showed correlation with the ratio of Pb in the exchangeable/carbonate to oxyhydroxide phases. This is the first time these techniques have been used in combination to describe a contaminated system. These correlations suggest the microbial community diversity is controlled by partitioning of heavy metals into Mn and Fe sulfidic/organic, Pb and Zn residual phases, and greater than 50% of the diversity by labile Pb phases.

Introduction

The waters and sediments of LCDA in northern Idaho have been impacted by decades of mining operations within the Coeur d'Alene Mining district. In its history, the Coeur d'Alene Mining district has had 90 mines in operation producing Pb, Zn, Ag, and Sb [1, 3-4, 6]. Over 7 million tons of Pb, 3 million tons of Zn, and 34 thousand tons of Ag have been mined from the Coeur d'Alene Mining district, stretching from Coeur d'Alene, Idaho to Superior, Montana [7].

The history of this district as well as the type of ore deposits and mineralogy has been summarized by Leach and others [7-11]. Briefly, the mineralogy of the Coeur d'Alene Mining District consists primarily of quartz [SiO_2] and siderite [$FeCO_3$] veins containing deposits of galena [PbS], sphalerite [ZnS], and tetrahedrite [$Cu_{12}Sb_4S_{13}$] [7]. Pyrite [FeS_2], chalcopyrite [$CuFeS_2$], and pyrrhotite [Fe_xS x=0.8,1] are also locally abundant [7]. Fe minerals including siderite, magnetite, pyrite, pyrrhotite, goethite, hematite, and ferrihydrite have been reported in the sediments of LCDA and the Mining district [12-14].

Horowitz *et al*. [3] found the CDAR and delta region to be heavily contaminated. Heavy metals in the delta region of LCDA appear to be associated with an operationally defined sulfidic phase [18], while those elsewhere in LCDA appear to be predominantly associated with the more mobile hydroxides [3, 24], though there is some controversy as to the solid phase partitioning [35]. Additionally, studies of mixing and neutralization experiments of acidic and metal contaminated water with uncontaminated surface waters [68, 128] and surface complexation of metals onto oxyhydroxides [6, 31] have been performed to predict metal fate and transport in this contaminated system. More recently Sengör *et al.* [39] developed models that incorporated microbial influences with surface complexation and chemical species changes during neutralization.

The microbial ecology of LCDA has been studied through culture dependent [12, 17, 62, 92, 94] and independent techniques [60, 93, 95]. Novel organisms have been cultivated, including *Ferribacterium limneticum* [92], *Desulfovibrio idahonensis* [94], and *Geobacter sp*. [12]. Using taxa specific primers for real-time polymerase chain reaction (rt-PCR) and denaturing gradient gel electrophoresis (DGGE), Cummings *et al.* [60] reported that, across metal contaminated and uncontaminated sites sampled, *Geobacteraceae* were abundant and diverse in LCDA. Similarly, Ramamoorthy *et al*. [93] used most probable numbers and quantitative PCR of the a-adenosine 5'-phosphosulfate reductase to estimate SRB populations in LCDA, and reported non-culture based estimates of SRB populations were higher in contaminated site than pristine sites. Utilizing clone libraries of *rpoB* and 16S rDNA genes, Rastogi *et al.* [95] found β-*Proteobacteria* and *Crenarchaeota* to be the dominant bacterial and archaeal

communities in CDAR, respectively. However, with advancements in microbial community analysis, larger scale, community level analyses have yet to be reported in the LCDA system.

Microbes are known to catalyze reactions that alter their environment resulting in detoxification (e.g., precipitation, reduction, (de)methylation, production of metal-binding proteins, cell surface complexation) and adaptation (e.g., horizontal gene transfer, gene expression, mutation) [56]. Additionally, metal toxicity has been shown to depend on chemical speciation and geochemical factors, such as surface area for adsorption and redox active phases (e.g., hematite, goethite, and ferrihydrite) [46, 49, 51-52]. A combined simultaneous characterization of both heavy metal speciation and microbial community is important to begin to understand the impact of geochemical conditions on microbial communities. Effects of anthropogenic heavy metal contamination on microbial community structure have been studied in other systems, but are lacking in the LCDA system [129-132]. In this study, we explore correlations between microbial community diversity at the phylum and family levels, and operationally defined heavy metal phases.

Methods

Sediment Sampling

Core samples were collected in July 2008 from the LCDA delta region reported to be most heavily contaminated with heavy metals [1]. As a comparison site with similar geochemistry, samples were also collected from the relatively uncontaminated St. Joe

River delta, also in LCDA. Core sleeves were disinfected with ethanol prior to sampling. Sealed sediment cores were flash frozen immediately after removal from the lake bed by submersion in a mixture of dry ice and ethanol. Cores were transported on dry ice to Montana State University and frozen at -25^{o}C for approximately two days until sectioning. Samples were sectioned into sub-cores while frozen according to visible stratification (probable redox zones) and divided for geochemical and molecular analyses. Samples for molecular analyses were taken with sterile spatula from the inner diameter of the core to avoid contamination from both sample handling and from organisms transported laterally along the core while sampling. Samples destined for geochemical analysis were sealed in serum bottles under nitrogen and frozen (-25°C) until analysis.

Microbial Community Characterization

Genomic DNA was extracted from approximately 0.5 g of sediment from each stratified sub-core using a PowerSoil DNA extraction kit (Molecular Biosciences). Extracted DNA was divided between 16S rDNA micro-array analysis (PhyloChip) [133] and, as a comparative tool, clone libraries to provide another means of microbial community comparison that includes relative abundance. DNA for PhyloChip analysis was prepared as previously described by Brodie *et al.* [133]. Clone libraries were produced using TOPO-TA (Invitrogen, Carlsbad, CA).

As previously described by Brodie *et al.* [133], the PhyloChip uses 25 mer oligonucleotides with central 17 mers as perfect match probes with mismatched probes at the 13th base. There are at least 11 single base mismatches in the 13th position of

mismatched probes. A positive score must meet two criteria: 1) intensity of perfect match probes was 1.3 times higher than mismatched controls, 2) the differences of intensity between perfect match and mismatched was 500 times greater than the square of the noise value. Positive fraction (pf) is the number of positive probe pairs divided by the total number of probe pairs in the set. An OTU was considered present when pf >0.92. OTU detections were combined at each of the taxonomic levels.

Statistical Comparative Tools

Information on community structure obtained from PhyloChips was initially analyzed using the ARB software package and the resulting distance matrix was combined with geochemical data in UniFrac [134], R [118], and Matlab (v2008b) to statistically analyze differences between communities and correlate community structure with geochemical variables. Pearson's correlations were used for comparison of linear correlation between responses and predictors. Pearson's correlation between two variables is given by the covariance of the variables divided by their standard deviations and has direct interpretability. The range of the Pearson's correlation is -1 to 1. For linear model selection, a false positive discovery rate (p-value) of 0.05 was selected.

Geochemical Characterization

Sub-cores from each site were analyzed using continuous sequential extractions (CSE) designed to identify operationally defined phase associations of heavy metals in these sediments. The CSE techniques used here follow Shiowatana [86] except that extractions employed the revised Community of Bureau of Reference (BCR) extraction

methods, as outlined by Mossop [135] and van Hullebusch [87]. The benefit of CSE is that transient metals are less likely to redistribute during flow extractions than in equilibrium batch processes [85-86, 88]. Metals selected for analysis were Fe, Mn, Zn, and Pb. Fe and Mn were selected for their ability to absorb heavy metals, compete with other heavy metals for reactive sulfides in the anaerobic water column, and for their potential as a terminal electron acceptor for IRB. Zn and Pb were selected for their abundance in LCDA, and toxicity to microorganisms. Sediment samples were thawed, weighed, and loaded into the extraction vessel under anaerobic conditions. Anaerobic conditions were maintained during extraction via ultrapure nitrogen bubbling into the solvent phases and extractant chamber. Chemicals for extraction were as follows: concentrated hydrochloric acid (Fisher, trace metal grade), concentrated nitric acid (Fisher, trace metal grade), 30% hydrogen peroxide (Fisher, ACS grade), glacial acetic acid (Spectrum, USP), hydroxylamine hydrochloride (Acros, ACS grade), and ammonium acetate (MP Biomedicals). Briefly, 0.1 g of solids were initially contacted with 0.11 M acetic acid (pH 2.85) to remove exchangeable and water/weak acid soluble phases (e.g., carbonates). This was followed by extraction using 0.5 M hydroxylamine hydrochloride (pH 1.5) to remove Fe and Mn (hydr)oxides phases. The solids were then washed in water adjusted to pH 2 with nitric acid to reduce the reactivity for the next step of the extraction. A 30% hydrogen peroxide and 1 M ammonium acetate solution (pH 2) was then used to extract elements associated with organic and sulfidic phases. The residual solids from these sequential extractions were dried and digested in *aqua regia* (3 HCl:1 HNO_3) under batch conditions to remove remaining phases. As a comparative tool

for extraction efficiency, a parallel sample of 0.1 g was directly digested using *aqua regia* digestion under batch conditions to determine *aqua regia* soluble fraction. Each digested fraction collected was stabilized in 0.5% HCl-1% HNO_3 and analyzed using inductively coupled plasma mass spectrometry (ICP-MS).

Results and Discussion

Phase Association and Geochemistry

Total elemental concentrations (Table 3) compare well with previously reported literature from the CDAR and St. Joe River delta (STJOE) as the control site [18]. Decreases in Pb and Zn concentrations were observed with increased distance from the CDAR channel. Additionally, there were higher concentrations of all metals in the CDAR samples compared to STJOE control site (Pb_{CDAR}/Pb_{STJOE} =94, Mn_{CDAR}/Mn_{STJOE} = 60, Zn_{CDAR}/Zn_{STJOE}= 22, Fe_{CDAR}/Fe_{STJOE}=8). pH and dissolved O_2 varied very little between the four sites.

Table 3: Sample sites characterization from July 2008

	Coeur d'Alene River Delta			St. Joe River Delta
	CDAR-1	**CDAR-2**	**CDAR-3**	**STJOE-5**
pH	6.04	6.00	6.02	5.97
Water Depth (cm)	150	90	170	100
Dissolved Oxygen (mg/L)	8.7	8.6	8.9	9.2
Water Temperature (^oC)	19.4	19.8	20.1	18.7
Perpendicular Distance from CDAR Channel Center (km)	0.04	0.130	0.200	11.400
GPS Coordinates (Lat)	N 47^o 27.612'	N 47^o 27.594'	N 47^o 27.517'	N 47^o 21.972'
GPS Coordinates (Long)	W 116^o 47.878'	W 116^o 47.877'	W 116^o 47.834'	W 116^o 44.336'
Total Average Fe (mg/kg)	86,089	125,156	94,577	12,839
Total Average Mn (mg/kg)	9,638	12,198	9,897	176
Total Average Zn (mg/kg)	6,029	5,224	2,199	207
Total Average Pb (mg/kg)	3,422	3,180	1,514	29

Figure 6 shows an example of the phase association of sub-samples from CDAR and STJOE sites. Figure 6 A and B show redox active elements (Fe, Mn) with similar profiles between contaminated and uncontaminated sites, however the concentrations between contaminated and control sites differ substantially. Approximately 60% of the totals of both Fe and Mn were primarily associated with oxyhydroxide phases. The greater prevalence of sulfidic/organic phases in CDAR compared to STJOE reflects the primary mineralogy and deposition of sulfidic host material from the Mining district upstream. Greater than 50% of the total Zn was primarily associated with the sulfidic/organic fraction (Figure 6-C) while greater than 70% of Pb was associated with the exchangeable/carbonate phase (Figure 6-D). The exchangeable/carbonate fraction is thought to be the most bioavailable fraction as heavy metals in this fraction are easily released with changes in pH [136].

Comparing this study to previous studies by Horowitz *et al.* [1] and Harrington *et al.* [18] suggests that Pb undergoes significant phase association changes. In studies of surface sediments from Coeur d'Alene, Horowitz *et al.* [1] reported that 95% of Pb and 80% of Zn were associated with the reducible oxide/oxyhydroxide phases, while Harrington *et al*. [18] reported Pb and Zn to be primarily associated with the sulfidic phase. Our study shows Pb to be primarily associated with the more bioavailable exchangeable/carbonate fraction. These differences in phase partitioning between this and other studies may be due to the method of extraction (batch vs. continuous) to identify phase association, extractant scheme (BCR, Tessier), sample handling and treatment, or seasonal/depositional effects.

Table 4: Heavy metal phase association, depth from sediment water interface, and OTU presence from samples taken July 2008

Metal (mg/kg dry wt.)	Coeur d'Alene River Delta							St. Joe River Delta		
	CDAR-1A	CDAR-1B	CDAR-1C	CDAR-2A	CDAR-2B	CDAR-3A	CDAR-3B	STJOE-5A	STJOE-5B	STJOE-5C
Core Depth(cm)	0-7	7-31	31-52	0-27	27-45	0-21	21-45	0-30	30-41.5	41.5-60
OTU Presence (#)	18	909	235	1048	365	73	124	583	146	737
Mn-Exchangeable/CO3	1,700	2,892	2,082	1,038	2,452	1,028	1,500	10	27	NQ
Mn-(Oxy)hydroxides	5,700	4,169	7,722	6,783	9,162	5,963	7,324	151	99	172
Mn-Sulfidic/Organic	1,057	274	2,177	1,106	3,078	1,495	1,709	NQ	ND	ND
Mn-Residual	330	536	275	157	620	466	308	9	15	26
Fe-Exchangeable/CO3	7,801	14,314	9,584	5,910	13,067	5,386	6,563	ND	ND	NQ
Fe-(Oxy)hydroxides	52,774	31,733	69,502	65,205	90,848	54,600	75,062	5,142	5,603	6,920
Fe-Sulfidic/Organic	9,233	2,548	21,651	13,509	34,454	11,885	17,930	ND	ND	1,582
Fe-Residual	17,421	13,724	7,981	8,251	19,068	10,146	7,581	1,967	3,609	10,530
Zn-Exchangeable/CO3	1,091	1,179	625	1,080	1,388	564	684	62	173	NQ
Zn-(Oxy)hydroxides	650	596	171	741	305	146	140	NQ	NQ	ND
Zn-Sulfidic/Organic	4,616	3,575	4,307	4,662	2,038	1,329	1,162	NQ	ND	NQ
Zn-Residual	558	560	158	82	151	121	252	ND	89	ND
Pb-Exchangeable/CO3	2,789	1,588	3,625	1,744	3,515	906	1,674	3	3	2
Pb-(Oxy)hydroxides	273	303	331	286	304	111	120	10	12	8
Pb-Sulfidic/Organic	177	157	797	155	318	71	112	17	12	16
Pb-Residual	50	156	21	14	23	17	16	<1	1	1

OTU: Operational Taxanomic Unit; ND: Not Detected; NQ: Detected But Not Quantifiable; Theoretical Detection Limits-3σ (mg/kg dry wt.) Mn(8), Fe(500), Zn(80), Pb(0.2);

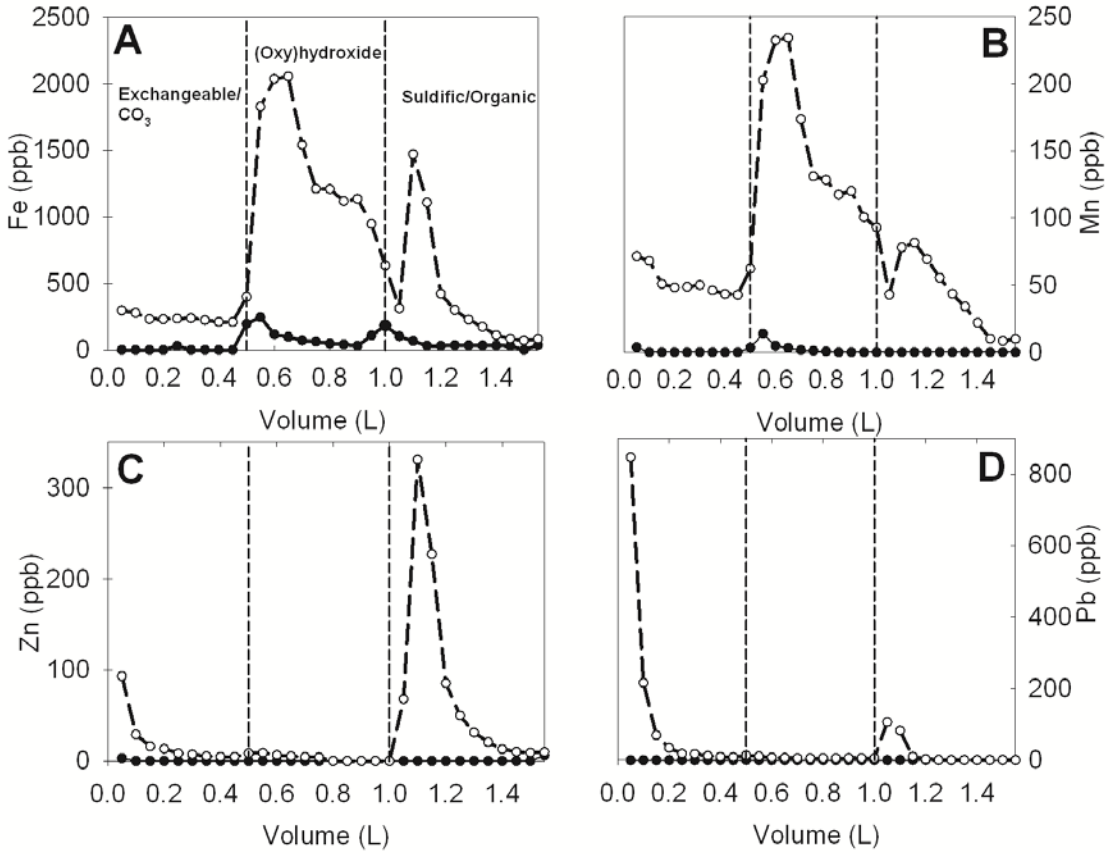

Figure 6: Extractogram of (A) Fe, (B) Mn, (C) Zn, and (D) Pb phases from CDAR 1-C (o) and STJOE 5-C (•). Extractogram shows heavy metal phases as defined by chemical extraction.

Table 4 provides the complete CSE data set for all core samples. Comparison of CSE to batch *aqua regia* digests show CSE underestimated Fe by about 10% and Pb by approximately 30% while overestimating Zn by 10%. While variability exists between *aqua regia* and CSE data, this has been noted by others using the revised BCR extraction technique [135]. Additionally, an important factor that may have contributed to differences in phase partitioning for this study was that the samples were collected soon after a sizeable seasonal flooding event. Monthly discharge rates were approximately 3.5

times the previous three years mean monthly discharge rate for June and greater than 4.5 times the previous three years mean monthly discharge rate for July (http://waterdata.usgs.gov/id/nwis/) which presumably transported, mixed, and deposited new sediments from riparian zones, stream beds, and surrounding soils into these river deltas. In the lateral lakes surrounding the CDAR, Bostick *et al.* [26] found that seasonal changes affected the partitioning of Zn with sulfidic and carbonate phases predominating in flooded areas, while oxyhydroxides were found in oxic, drier soils and sediments. The metal oxyhydroxides species were transformed to carbonate and sulfidic species during submersion due to reducing conditions, however a small portion remained as metal oxyhydroxides [26]. In LCDA, La Force *et al*. [19] found that Zn and Pb increased in the operational carbonate and exchangeable phases during oxygenation. As our sampling occurred after a significant high flow event, transport and oxygenation from the riparian zone, riverbed, and lateral lakes most likely occurred to deposit additional sediments onto the CDAR delta and may explain the predominance of Pb exchangeable/carbonate.

Microbial Communities and Heavy Metal Phases

Out of 121 demarcated phyla, 40 phyla and 246 unique families were detected in core samples. Nineteen of the 246 families were eliminated from further analysis either due to single OTU detections or uniform detections across all samples. Due to a very simple community, duplicate PhyloChips were performed on site 1A and compared to clone libraries. Both techniques supported repeatable, low diversity in this sample. Unclassified members of orders of *Bacteroidetes KSA1* and *marine group A mgA-2* were

present as single detections in every sample and 17 families were only present as single detections; 12 in CDAR and 5 in STJOE. Phyla of these single detections were represented as follows with OTU quantities in parenthesis: *Actinobacteria* (6), *Firmicutes* (3), *Proteobacteria* (3), *Acidobacteria* (2), and single detections of *Aquaficae*, *Cyanobacteria*, and candidate phyla *LD1PA* group.

In an effort to visually examine the partitioning of taxa between the uncontaminated and contaminated sites, environment affinity was developed in this study to rapidly compare taxa across environments. In this system positive scores denote affinity to STJOE site and negative scores show affinity to CDAR. The affinity score gives a numerical magnitude, but cannot be used to compare between different taxonomies (e.g., phylum vs. family). Environment affinity is defined as the logarithm (base 2) of $[\#\text{ of taxa/gram wet sediment}]_{STJOE}/[\#\text{ of taxa/gram wet sediment}]_{CDAR}$. Thus an increase of one environment affinity unit indicates a doubling of diversity of the taxa of interest with respect to its environment and equal distribution of taxa diversity between environments are zeros.

Microbial signatures changed with metal content. Figure 7 shows the phyla environment affinity. Candidate phyla *NC10*, *OP8* and *LD1PA* were only present in metal contaminated cores and the diversity of *Natronoanaerobium* appear to double in metal contaminated cores compared to the control site. This may suggest some increased fitness for these phyla in contaminated sediments. In contrast, the diversity of phyla *Aquificae*, *Coprothermobacteria*, and *Synergistes* were at least two times greater in the control site.

Figure 8 shows environment affinity at the family level. Taxa must have been detected in at least 2 sub-cores to be considered for analysis. Those taxa at the axis extremes are only detected in their respective environments; negative has affinity for CDAR samples and positive for STJOE samples. Lineages from *Pseudomonadaceae* and *Ralstoniaceae* show affinity for the STJOE site. *Pseudomonadaceae* did not correlate well with the environmental variables, which may suggest other factors more strongly influence this family's distribution in LCDA. Linear models for *Ralstoniaceae* did not correlate well with any of the environmental variables measured. This family is known to be substantially metal tolerant, but its distribution also must depend on other factors.

Metal Microbe Interactions

A "G+GE" biplot is a graphical representation of the correlations between environmental variables and responses. G+GE biplots have been used for examining single and multiple variable predictor correlations on responses, as well as "which-won-where" analyses in multi-environment datasets in plant ecology [137-138]. The axes in G+GE biplots are similar to those used in principle component analysis, and are calculated by taking a singular value decomposition of the correlation matrix between the environmental factors and microbial responses [138-139]. These biplots can be used to show correlation and association between multiple variables in one plot. Moving outward along the variable axis shows more correlation (either positive or negative), while moving off of the axis shows more variability with respect to the variable of interest. Figures 9 and 10 show "mean performance vs. stability" G+GE biplots [138] of

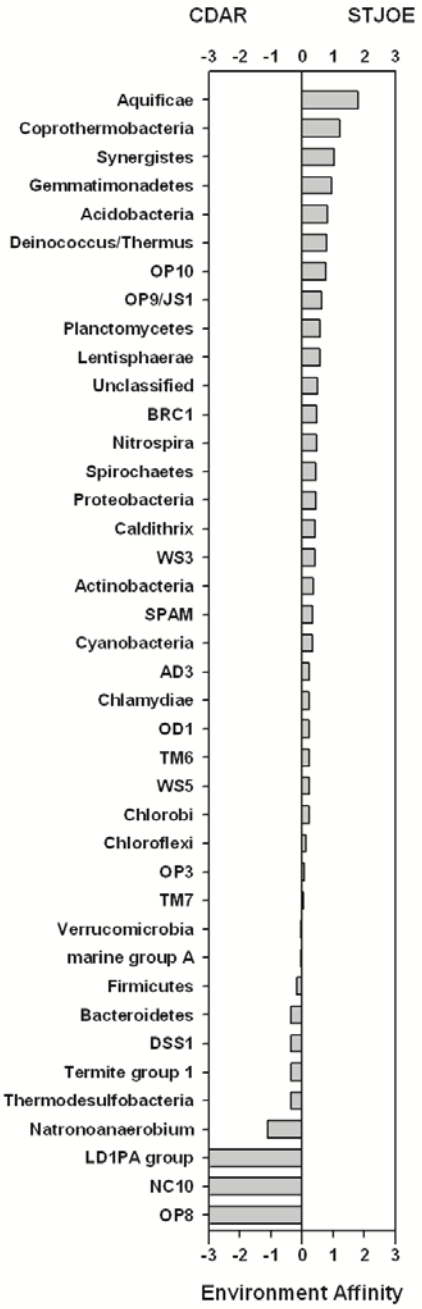

Figure 7: Environment affinity $\log_2$([# taxa detected/g wet sediment] STJOE /[# taxa detected / g wet sediment] CDAR) comparison of phyla between CDAR and STJOE sites

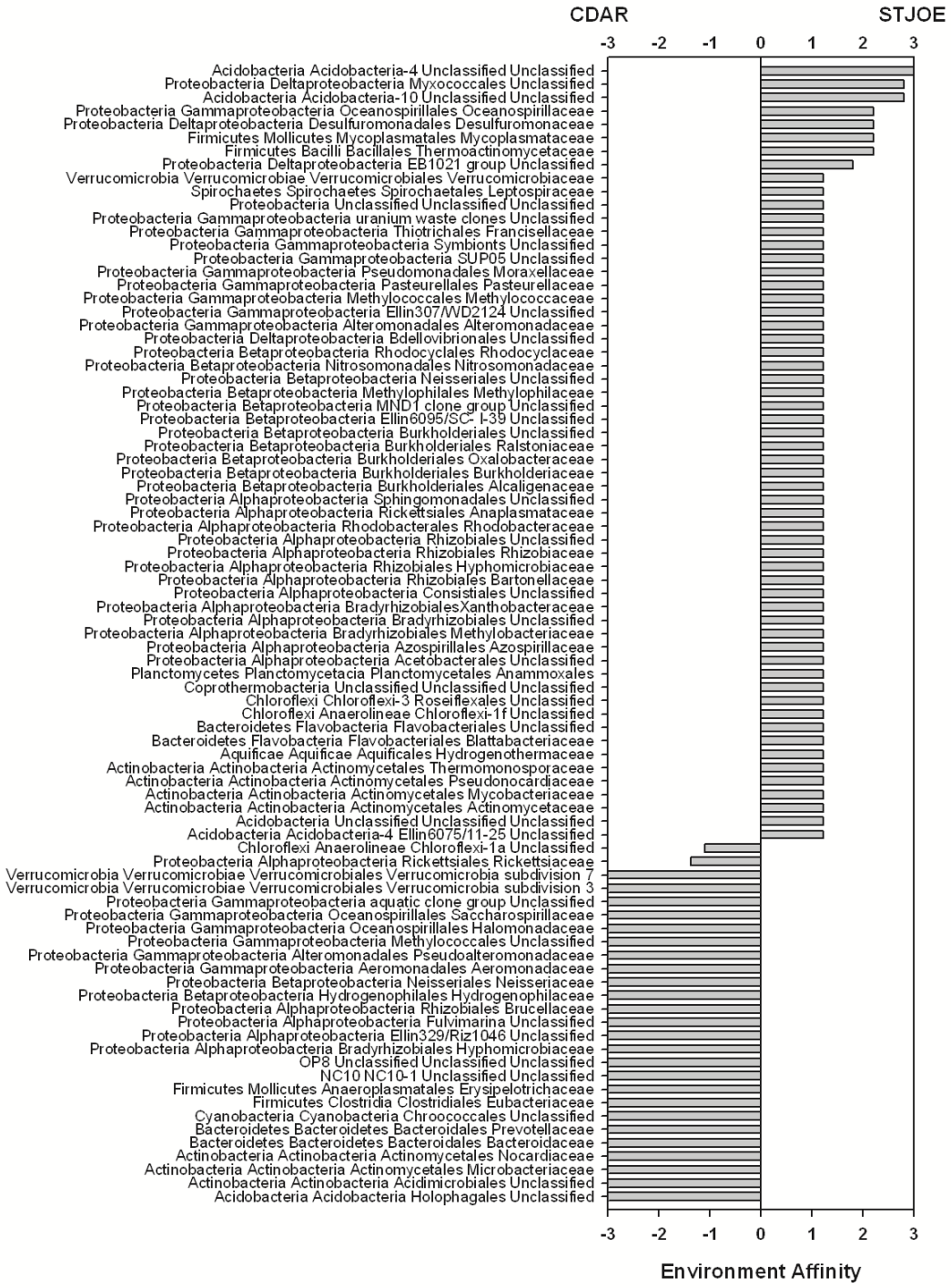

Figure 8: Environment affinity $\log_2$([# taxa detected/ g wet sediment] $_{STJOE}$ /[# taxa detected / g wet sediment] $_{CDAR}$) comparison of families with affinity at least two times greater between CDAR or STJOE sites

phyla to the dominant phases for Zn and Pb, respectively. The two principle axes in Figures 9 and 10 capture 89.7% of the variability in the correlations. Figure 9 shows that diversity of candidate phyla *OP8* (Pearson's 0.64) is most positively correlated with focus variable Zn in the sulfidic/organic fraction, while diversity of *OP10* (Pearson's -0.48) is most negatively correlated.

Stability is a measure of variance with respect to a variable; those closest to the environment axis show high stability (low variance) with respect to that environmental variable. The phylum *Firmicutes* shows the most stability (least variance) within those phyla positively correlated with Zn sulfidic/organic and *OP10* shows the most stability with those negatively correlated. This may indicate that candidate phylum *OP10* requires low concentrations of Zn in the sulfidic/organic fraction for growth and *Firmicutes* are more Zn tolerant.

Similarly in Figure 10, *Aquificae* (Pearson's -0.52) and *Synergistes* (Pearson's -0.49) are most negatively correlated with Pb in the exchangeable/carbonate fraction, while candidate phylum *LD1PA* (Pearson's 0.49) is most positively correlated. Few phyla from the extreme regions of the environment axis in Figure 10 show substantial stability with respect to the Pb exchangeable/carbonate focus variable. Dominant phases from Fe and Mn (e.g., oxyhydroxides) lie approximately on the same ray from the origin as Pb exchangeable/carbonate and show very similar results and interpretation and were not included as additional figures. As these three variables lie closely along the first principle axis (x-axis), these variables account for a large part of the variability in the correlation dataset.

Linear models can be useful in better understanding correlations between predictors and responses. Table 5 presents the simplest linear models (least terms with a p-value <0.05) based on phyla level analysis. Phyla *Acidobacteria, Calithrix, Coprothermobacteria, Cyanobacteria, Firmicutes, Gemmatimonadetes, Lentisphaerae, Spirochaetes, Thermodesulfobacteria, Verrucomicrobia,* unclassified phyla, and candidate phyla from *AD3, BRC1, DSS1, marine group A, OP3, OP9/JS1, and WS3* detected in this study did not correlate well with any model containing two or less environmental variables. Figure 11 presents the fraction of models represented by a given model (Figure 11-A) and the fraction of OTUs represented by a given model (Figure 11-B). As can be seen from Figure 11, some models were more prominent than others in predicting multiple phyla. Approximately a third of the OTU diversity could not be decribed by two or less component models (Figure 11-B). The linear model Mn and Fe-sulfidic/organic and model Zn and Pb-residual each described approximately 6% of the OTUs measured in this study while the Pb-exchangeable/carbonate and Pb-oxyhydroxide model accounts for over 50% (Figure 11-B). This highlights the importance of Pb partitioning in predicting diversity.

The operationally defined Mn and Fe sulfidic/organic phases appear to be important in multiple linear models. In all of the linear models that contain Mn and Fe sulfidic/organic, the coefficients from Mn sulfidic/organic phases were always negative while the coefficients for the Fe sulfidic/organic phases were always positive. Additionally, when present in the same model, coefficients of Mn sulfidic/organic phases were an order of magnitude higher than Fe sulfidic/organic phases. Thus the ratio of Fe

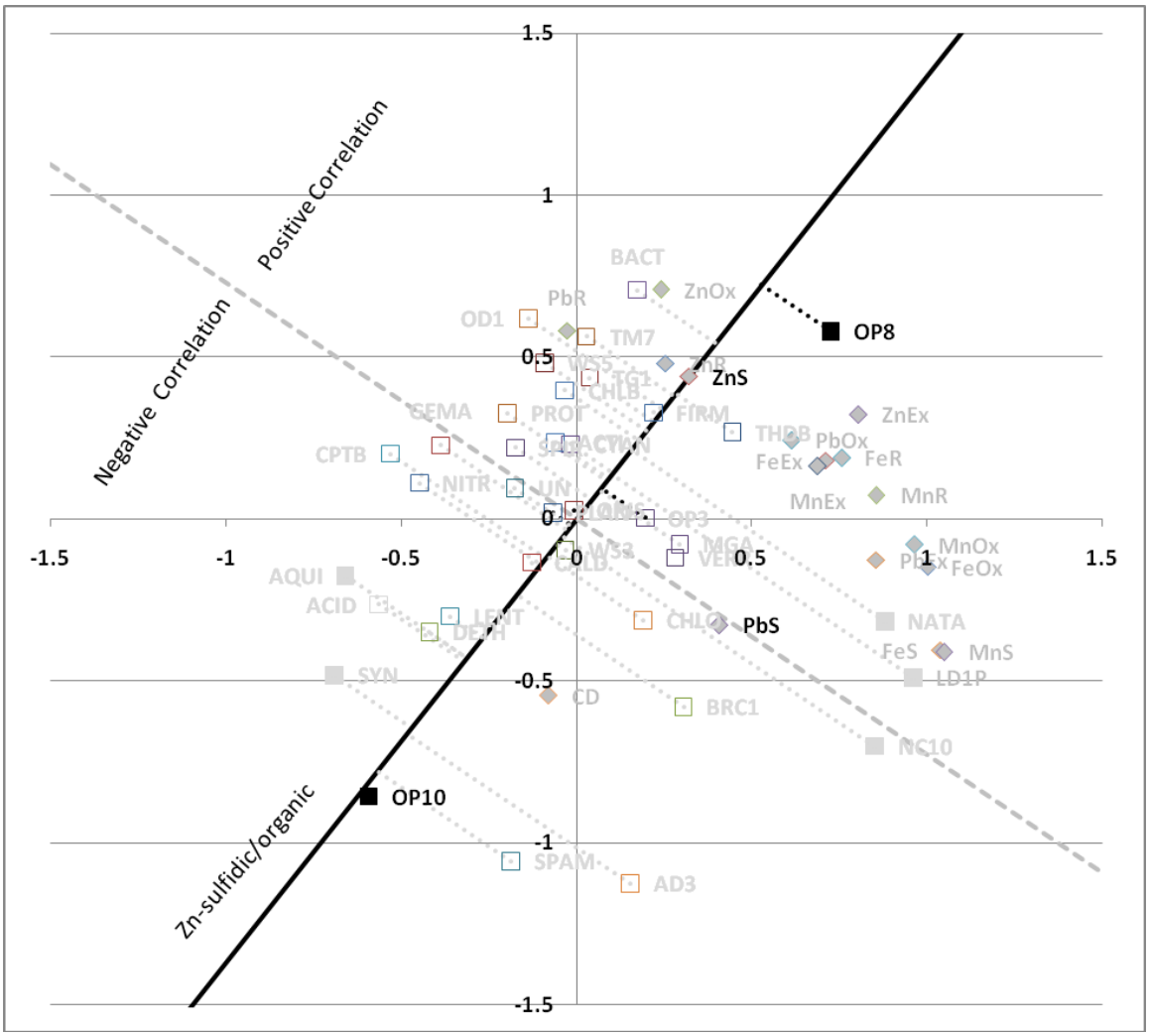

Figure 9: Mean subtracted and standard deviation normalized "mean performance vs. stability" G+GE biplot of Zn sulfidic/organic phase. X and Y axes account for 89.7% of the variance. Markers for phyla (boxes) and environmental variables (diamonds) with abbreviations as follows: Acidobacteria (ACID), Actinobacteria (ACTI), AD3 (AD3), Bacteriodetes (BACT), BRC1 (BRC1), Caldithrix (CALD), Chlorobi (CHLB), Chloroflexi (CHLO), Coprothermobacteria (CPTB), Cyanobacteria (CYAN), Deinococcus/Thermus (DETH), Firmicutes (FIRM), Gemmatimonadetes (GEMA), LD1PA group (LD1P), Lentisphaerae (LENT), marine group A (MGA), Natronoanaerobium (NATA), NC10 (NC10), Nitrospira (NITR), OD1 (OD1), OP10 (OP10), OP3 (OP3), OP8 (OP8), OP9/JS1 (OPJS), Planctomycetes (PLAN), Proteobacteria (PROT), SPAM (SPAM), Spirochaetes (SPIR), Synergistes (SYN), termite group 1 (TG1), Thermodesulfobacteria (THDB), TM7 (TM7), Unclassified (UN), Verrucomicrobia (VERR), WS3 (WS3), WS5 (WS5), Fe exchangeable/carbonate (FeEx), Mn exchangeable/carbonate (MnEx), Pb exchangeable/carbonate (PbEx), Zn exchangeable/carbonate (ZnEx), Fe oxyhydroxides (FeOx), Mn oxyhydroxides (MnOx), Pb oxyhydroxides (PbOx), Zn oxyhydroxides (ZnOx), Fe sulfidic/organic (FeS), Mn sulfidic/organic (MnS), Pb sulfidic/organic (PbS), Zn sulfidic/organic (ZnS), Fe residual (FeR), Mn residual (MnR), Pb residual (PbR), and Zn residual (ZnR).

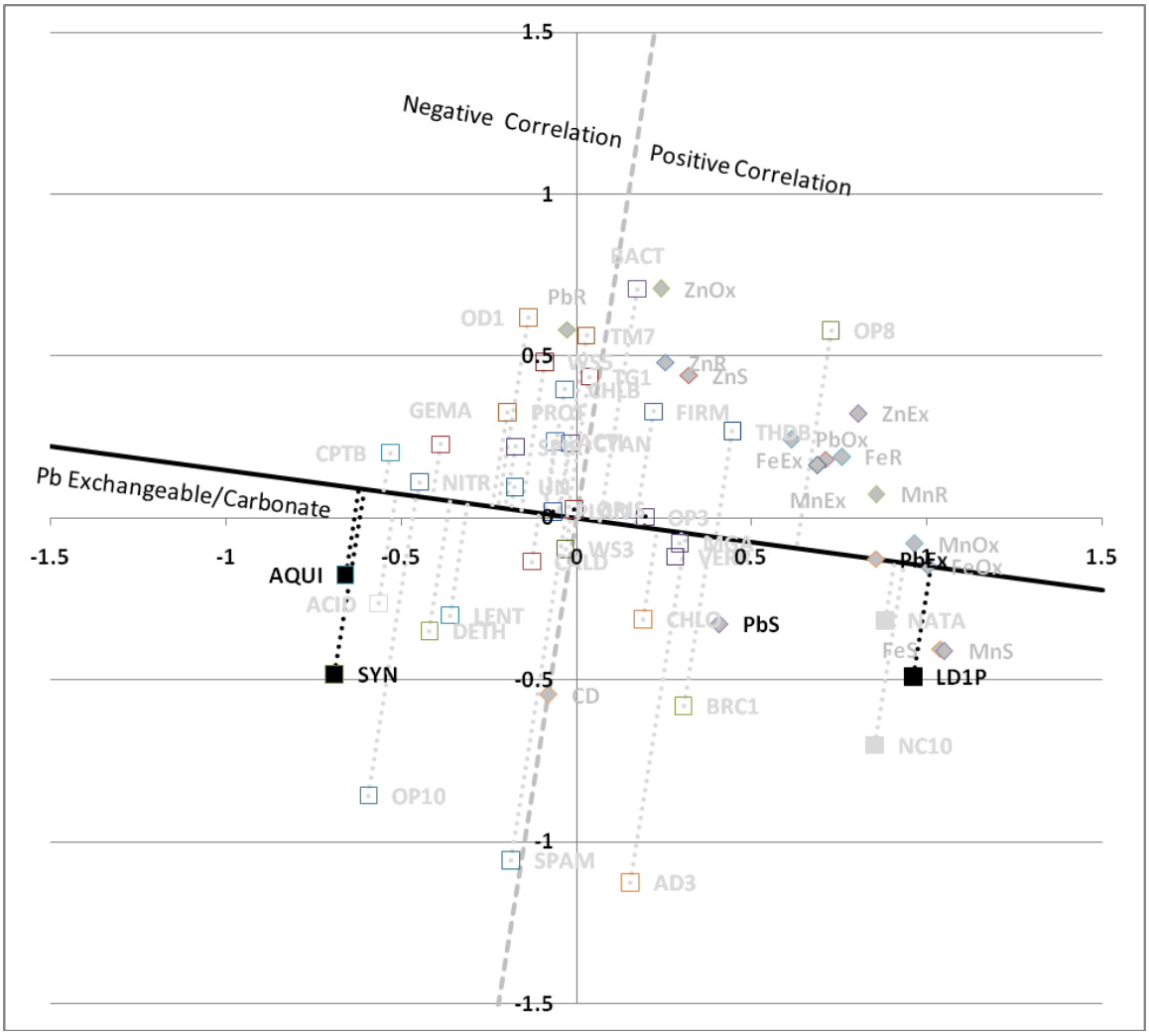

Figure 10: Mean subtracted and standard deviation normalized "mean performance vs. stability" G+GE biplot of Pb exchangeable/carbonate phase. X and Y axes account for 89.7% of the variance. Markers for phyla (boxes) and environmental variables (diamonds) with abbreviations as follows: Acidobacteria (ACID), Actinobacteria (ACTI), AD3 (AD3), Bacteriodetes (BACT), BRC1 (BRC1), Caldithrix (CALD), Chlorobi (CHLB), Chloroflexi (CHLO), Coprothermobacteria (CPTB), Cyanobacteria (CYAN), Deinococcus/Thermus (DETH), Firmicutes (FIRM), Gemmatimonadetes (GEMA), LD1PA group (LD1P), Lentisphaerae (LENT), marine group A (MGA), Natronoanaerobium (NATA), NC10 (NC10), Nitrospira (NITR), OD1 (OD1), OP10 (OP10), OP3 (OP3), OP8 (OP8), OP9/JS1 (OPJS), Planctomycetes (PLAN), Proteobacteria (PROT), SPAM (SPAM), Spirochaetes (SPIR), Synergistes (SYN), termite group 1 (TG1), Thermodesulfobacteria (THDB), TM7 (TM7), Unclassified (UN), Verrucomicrobia (VERR), WS3 (WS3), WS5 (WS5), Fe exchangeable/carbonate (FeEx), Mn exchangeable/carbonate (MnEx), Pb exchangeable/carbonate (PbEx), Zn exchangeable/carbonate (ZnEx), Fe oxyhydroxides (FeOx), Mn oxyhydroxides (MnOx), Pb oxyhydroxides (PbOx), Zn oxyhydroxides (ZnOx), Fe sulfidic/organic (FeS), Mn sulfidic/organic (MnS), Pb sulfidic/organic (PbS), Zn sulfidic/organic (ZnS), Fe residual (FeR), Mn residual (MnR), Pb residual (PbR), and Zn residual (ZnR).

Table 5: Simplest linear model for phyla with p-value<0.05						
Phyla	# of OTUs detected	Terms in model	Model terms	p-value	R^2	intercept
SPAM	17	2	Core Depth (cm)	0.0105	0.5799	0.53
LD1PA group	1	2	Fe-Sulfidic/Organic	0.0168	0.5313	-0.13
NC10	2	2	Fe-Sulfidic/Organic	0.0232	0.4950	-0.10
LD1PA group	1	2	Mn-Sulfidic/Organic	0.0356	0.4434	-0.12
NC10	2	2	Mn-Sulfidic/Organic	0.0399	0.4289	-0.09
OP8	4	2	Zn-Exchangeable/CO3	0.0463	0.4095	-0.22
OP8	4	2	Zn-Oxyhydroxides	0.0196	0.5142	-0.12
Synergistes	32	3	Core Depth (cm) Fe-Oxyhydroxides	0.0498	0.5756	3.02
Synergistes	32	3	Core Depth (cm) Mn-Sulfidic/Organic	0.0499	0.5753	2.11
Natronoanaerobium	24	2	Fe-Exchangeable/CO3 Zn-Residual	0.0313	0.6283	1.66
Natronoanaerobium	24	2	Mn-Exchangeable/CO3 Zn-Residual	0.0304	0.6314	1.65
Acidobacteria	210	3	Mn-Sulfidic/Organic Fe-Sulfidic/Organic	0.0168	0.6890	29.74
Aquificae	5	3	Mn-Sulfidic/Organic Fe-Sulfidic/Organic	0.0409	0.5987	2.79
Deinococcus\Thermus	21	3	Mn-Sulfidic/Organic Fe-Sulfidic/Organic	0.0285	0.6383	4.41
Synergistes	32	3	Mn-Sulfidic/Organic Fe-Sulfidic/Organic	0.0319	0.6262	0.98
Chlorobi	27	3	Pb-Exchangeable/CO3 Pb-Oxyhydroxides	0.0486	0.5786	14.60
Bacteroidetes	263	3	Pb-Exchangeable/CO3 Pb-Oxyhydroxides	0.0056	0.7727	0.86
Chlamydiae	3	3	Pb-Exchangeable/CO3 Pb-Oxyhydroxides	0.0422	0.5953	2.18
Nitrospira	16	3	Pb-Exchangeable/CO3 Pb-Oxyhydroxides	0.0129	0.7113	177.74
OD1	3	3	Pb-Exchangeable/CO3 Pb-Oxyhydroxides	0.0422	0.5953	0.22
Proteobacteria	1965	3	Pb-Exchangeable/CO3 Pb-Oxyhydroxides	0.0418	0.5964	0.22
Termite group 1	4	3	Pb-Exchangeable/CO3 Pb-Oxyhydroxides	0.0452	0.5872	0.22
TM6	3	3	Pb-Exchangeable/CO3 Pb-Oxyhydroxides	0.0451	0.5873	0.22
TM7	13	3	Pb-Exchangeable/CO3 Pb-Oxyhydroxides	0.0260	0.6474	0.21
WS5	3	3	Pb-Exchangeable/CO3 Pb-Oxyhydroxides	0.0451	0.5873	2.09
Natronoanaerobium	24	3	Zn-Residual Pb-Oxyhydroxides	0.0271	0.6431	1.47
Nitrospira	16	2	Zn-Residual Pb-Residual	0.0256	0.6492	1.98
Chlorobi	27	2	Zn-Residual Pb-Residual	0.0371	0.6099	2.67
Chloroflexi	156	2	Zn-Residual Pb-Residual	0.0478	0.5805	3.16
OP10	19	2	Zn-Residual Pb-Residual	0.0364	0.6118	20.30
Planctomycetes	41	1	Zn-Residual Pb-Residual	0.0481	0.5797	5.45

sulfidic/organic to Mn sulfidic/organic may be an important predictor of diversity for some taxa. It could be that the measurements of the ratio of these phases predict redox zones, and thus distribution of microorganism in these zones, or that Mn and Fe associated organic matter changes with pH or redox are predicted by this ratio. Mn sulfides are not likely to form in this system due to competition from carbonate ions [140], thus Mn is most likely present as the organically associated form. These sulfidic/organic phases were present almost solely in CDAR samples as compared with STJOE samples.

Pb (positive coefficient) and Zn (negative coefficient) in the residual fraction also appear to be an important model for multiple phyla. Though the biological availability of the residual fraction is not well defined in terms of chemistry, it may suggest that the ratio of Pb residual to Zn residual is important in increasing diversity or that Zn in the residual fraction somehow offsets the selective pressure of Pb in the residual fraction.

Pb exchangeable/carbonate and Pb oxyhydroxide appeared in multiple models with Pb exchangeable/carbonate phase coefficients consistently negative and an order of magnitude less when present in the same linear model with Pb oxyhydroxide phases. It may be that the partitioning of Pb into more bioavailable phases was responsible for a decrease in diversity (as # OTU detected), while greater Pb partitioning into the oxyhydroxide phases increases diversity. This suggests that the presence of Pb in more bioavailable phases drives selection for more metal tolerant organisms, while Pb in less bioavailable phases does not exert the same selective pressure.

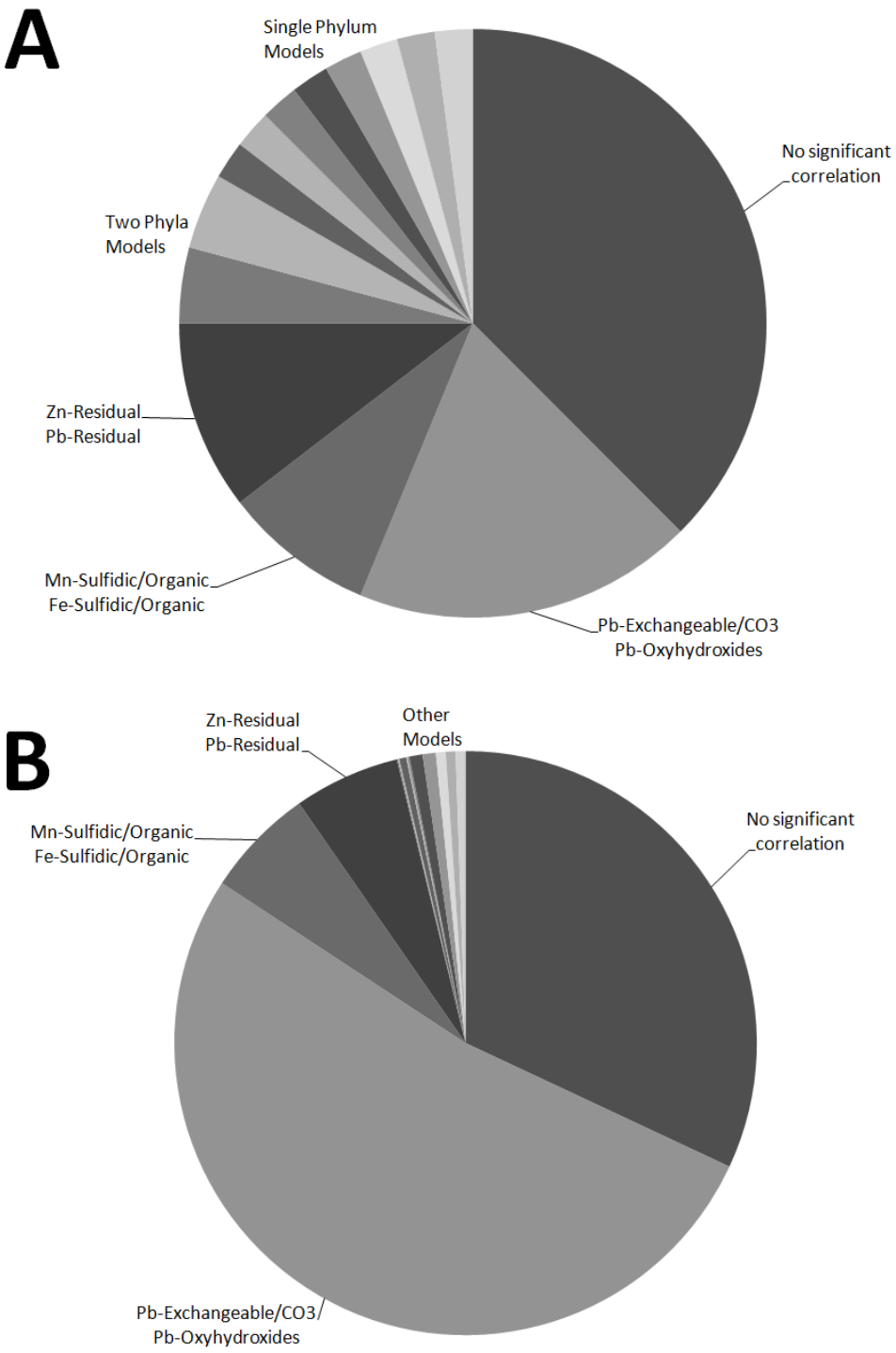

Figure 11: A) Fraction of linear models represented by a given model B) fraction of OTUs represented by a given model

Because IRB can release heavy metals through reductive dissolution and SRB can precipitate heavy metals as insoluble metal sulfides, IRB [12, 60, 92] and SRB [93-94] have been the focus of multiple studies in LCDA. The interplay between IRB and SRB may influence the fate and transport of heavy metals in LCDA [39, 78]. From the presumed SRB lineages detected in this study, most members of orders *Desulfobacterales* ($p=0.007$), *Desulfuromonadales* ($p=0.094$), *Desulfotomaculum* ($p=0.039$), and *Syntrophobacterales* ($p=0.038$) correlate with Pb and Zn in the residual fraction. Orders from most *Desulfovibrionales* ($p=0.078$) and *Bdellovibrionales* ($p=0.06$) correlate with Pb in the exchangeable/carbonate and oxyhydroxide phases. Some exceptions which influence the overall p-value of their respective orders are families from unclassified members of the order *Myxococcales* (Zn sulfidic/organic; $p=0.017$) and families *Desulfuromonaceae* (Mn oxyhydroxide, Fe sulfidic/organic; $p=0.032$), *Desulfomicrobiaceae* (Pb sulfidic/organic; $p=0.032$) and *Thermodesulfobacteriaceae* (Mn sulfidic organic, Fe sulfidic/organic, Mn residual; $p=0.022$). The "environment affinity" presented in Figure 10 shows *Desulfuromonaceae* was detected in greater diversity in STJOE samples. With the exception of the model for *Desulfohalobiaceae*, coefficients for Pb exchangeable/carbonate are consistently negative while oxyhydroxides coefficents are consistently positive. Models for SRB lineages are negative for Zn residual and positive for Pb residual phases. Families from IRB lineages *Shewanellaceae*, *Geobacteraceae*, and *Rhodocyclaceae* show correlation to Pb in the exchangeable/carbonate and oxyhydroxide phases with decreases in diversity predicted by increases in phase partitioning to the more bioavailable Pb exchangeable/carbonate.

Conclusions

Metal contamination from decades of upstream mining has impacted LCDA in both sediment and aqueous chemistries. This study reflects the complexity of natural systems and interactions between microbes and their environment. Total metal concentrations measured in this study compare well with previous studies [1, 18], although phase association differs, specifically in this study with respect to Pb. Microbial signatures appear to change with sediment metal content. Candidate phyla *NC10, OP8* and *LD1PA* were only detected in metal contaminated cores and diversity among the *Natronoanaerobium* was double that found in the uncontaminated control site. In contrast, diversity within the phyla *Aquificae*, *Coprothermobacteria*, and *Synergistes* appeared to be at least twice as high in the uncontaminated control site. Partitioning of Pb into more bioavailable phases appeared to drive decreases in diversity (as # OTU detected), while greater partitioning of Pb into the oxyhydroxide phases correlated with increased diversity for multiple lineages for approximately 50% of the OTUs detected in this study. This emphasizes the importance of Pb speciation in the LCDA system.

CHAPTER 4

CONCLUSIONS AND FUTURE WORK

Microbial growth, metal detoxification, and biogeochemical cycling of metals can be linked to mineral phases in environmental settings. Although total metal content is important, the mobility, reactivity, and bioavailability of heavy metals is dictated by crystallinity, particle size, mineral phase, and associated chemistry in which these metals reside [42]. In the LCDA system, there has been little research on integrated investigations of the effects of heavy metal speciation on indigenous microbes from LCDA, especially large scale community analysis. This research was focused on determining the effects of heavy metal speciation on microorganisms in community and single genus studies. The following are areas for further investigation into chemical speciation and its effects on microorganisms.

Chapter two focused on species specific Zn toxicity to *Arthrobacter* sp JM018. A relatively large increase in toxicity was observed from a relatively small shift in pH (6-8). $ZnHPO_4^0$(aq) species makes up less than 2% of the aqueous Zn species, but contribute approximately 60% of the inhibition at pH 8. This highlights the importance of Zn speciation in microbial toxic response. Further work in this area could focus on other well characterized microorganisms, such as *E. coli*, to verify the findings demonstrated in *Arthrobacter* sp. JM018. Zn also may behave differently than other divalent heavy metal cations and further investigation with other heavy metals would be desirable. Speciation may also be dynamic in systems that contain bacteria, as bacteria consume and produce

ligands that complex heavy metals and metal speciation in different phases of their growth cycle. Monitoring these changes may yield important pieces of information on the interaction of metals and microorganism.

Chapter three introduced the use of microarrays and continuous sequential extractions to study the effect of heavy metals phase partitioning on microbial community signatures. Microbial signatures appear to change with metal content. Candidate phyla *NC10, OP8* and *LD1PA* were only present in metal contaminated cores and *Natronoanaerobium* appear twice as frequently in metal contaminated cores compared to control site. In contrast, phyla *Aquificae, Coprothermobacteria*, and *Synergistes* appear at least twice as frequently in the control site. Partitioning of Pb into more bioavailable phases appears to drive decreases in diversity (as # OTU detected) while greater partitioning into the oxyhydroxide phases increases diversity for multiple lineages (~50% OTUs). Additionally, Fe and Mn in the sulfidic/organic phases, and Pb and Zn in the residual fraction appear to be an important model for multiple taxa, though the bioavailability of the residual fraction is not well defined in terms of chemistry and warrants further study.

Future work in the LCDA system could begin by verifying these linear models with laboratory and environmental isolate strains from identified taxa with mineral identified in the LCDA system. Studies in the CDAR have identified the most likely Pb and Zn-bearing mineral phases of dundasite, coronadite, stolzite, mattheddleite, bindheimite, and smithsonite [33]. Chemical extractions on these minerals should be verified before further investigation, but could be used as a starting point for hypothesis

testing. Core samples taken from LCDA in July 2008 show greatest variation within core samples and not between core samples, so future work in the LCDA system should not only focus on additional core samples, especially the STJOE site, but increase sectioning within a core sample. Presumed metabolic functions based on families for exploratory analysis were used in this study, but further work in this area should quantify metabolic functions of active populations using meta-genomic analyses, for example 454 sequencing [96], functional gene microarrays [97] and/or employ live/dead extraction procedures [98] for more complete picture of the environment. Additionally, only Pb, Zn, Mn, and Fe were studied, but further work could examine other factors including, but not limited to, Hg, Cu, As, and Cd.

Chemical speciation and phase association of heavy metals is essential in determining bioavailability and toxicity as well as reactivity, environmental stability, and fate and transport. Advancements in determining heavy metal chemical species in either aqueous or solid phases would improve understanding of how these constituents interact with microorganisms, especially in natural systems where these organisms reside. Electrochemistry has shown promise in the ability to determine transient molecular states that may not have been detected by other techniques [75]. Additionally, advances in biosensors may provide valuable information about bioavailability to a wide range of organisms and systems [141].

APPENDICES

APPENDIX A

ROLE OF SULFATE REDUCING AND IRON REDUCING BACTERIA IN METAL MOBILITY AND BIOAVAILABLILITY

Abstract

Fe and sulfate reducing bacteria are important in the global cycling of Fe and S. Previous work by Sengor *et al*. [39] in the Coeur d'Alene Mining district, (northern Idaho, USA) suggests that the interaction between these two functional bacterial groups affects the fate and transport of heavy metals in this contaminated environment. Batch systems of ferrihydrite and quartz where exposed to 1 mM Zn and inoculated with an Fe reducing bacterium (*Geobacter* sp. CDA-2) and a sulfate reducing bacterium (*Desulfovibrio vulgaris* Hildenborough) to simulate anaerobic metal contaminated sediments. Primers designed for the 16S rDNA region of *Geobacter* sp. CDA-2 show gene copy numbers for this organism decreased in a mixed community samples compared to *Geobacter* sp CDA-2 only cultures. Zinc concentrations did not significantly increase in the aqueous phase in mixed species systems, though Fe increased compared to other treatments.

Introduction

IRB are important in the global Fe cycling, reductive dissolution and release of trace elements, and play an important role in anaerobic carbon cycling. SRB are capable of catalyzing reactions which detoxify their environment through production of sulfides and direct enzymatic reduction as well as anaerobic carbon cycling and hydrogen production.

LCDA has been contaminated with heavy metals from decades of mining. Studies in LCDA have detected the presence of Fe(III) reducing bacteria [60] and SRB [17, 93], including *Geobacteracea* and *Desulfovibrio* species. Due to the capacity for IRB to release heavy metals through reductive dissolution of poorly crystalline (oxy)hydroxides and SRB to precipitate heavy metals as insoluble metal sulfides, IRB [12, 60, 92] and SRB [93-94] have been a focus for study in LCDA and elsewhere. The predominant activity of either IRB and SRB may significantly influence the fate and transport of heavy metals in LCDA [39, 78] and thus warrant investigation. In this study the IRB *Geobacter* sp CDA-2, isolated from LCDA [12] and the SRB *Desulfovibrio vulgaris* Hildenborough were co-cultured to examine the ability of *Desulfovibrio* to shield *Geobacter* from Zn toxicity and examine the fate of Zn in the co-culture.

Methods

Experimental Design

Table 6 contains the experimental design matrix. Each sampling period of the experiment was performed in triplicate and employed destructive sampling to minimize changes in mineral phase due to alterations in the micro-environment introduced by sampling. This also allows measurements of cell concentrations associated with the solid phase. Metals of interest in the Coeur d'Alene system are Pb and Zn, due to their high concentration and toxicity. Zn was selected for these experiments due to its increased solubility under environmental conditions when compared to Pb.

Table 6: Experimental Matrix of Batch Experiments

Experiment	IRB	SRB	Sulfate	Experimental Conditions
1	+	+	H	Dual-species
2	+	+	L	
3	-	+	H	No IRB
4	-	+	L	
5	+	-	H	No SRB
6	+	-	L	
7	-	-	H	Abiotic Control
8	-	-	L	
+ =present - =absence	H=High L=Low	IRB =Iron Reducing Bacteria SRB=Sulfate Reducing Bacteria		

A basal medium consisting of (g/L) sodium phosphate dihydrate 0.6, ammonium chloride 0.75, potassium chloride 0.1, sodium acetate 0.82, sodium lactate 0.75, piperazine-1,4-bis(2-ethanesulphonic acid) (PIPES) 1.73, and yeast extract 0.05 was used in these experiments. Stock solutions were prepared as follows; calcium chloride solution consist of (g/L) calcium chloride dihydrate 0.001, Wolfe's vitamin solution (mg/L) pyridoxine-HCl 10, thiamine-HCl dihydrate 5, riboflavin 5, nicotinic acid 5, D-Ca-pantothenate 5, p-aminobenzoic acid 5, lipoic acid 5, biotin 2, folic acid 2, vitamin B_{12}, 0.1, selenate/tungstate solution (mg/L), sodium hydroxide 500, disodium selenite pentahydrate 3, disodium tungstate dehydrate 4. SL-10 trace element solution was prepared as follows, 1.5 g ferrous chloride tetrahydrate was dissolved in 10 mL of 7.7M HCl and diluted to a final volume of 990 mL with DI water. Remaining salts were added to SL-10 as follows (mg/L) zinc chloride 70, manganous chloride tetrahydrate 100, boric acid 6, cobalt chloride hexahydrate 190, copper chloride dihydrate 2, and disodium

molybdate dihydrate 36. Additionally, a sterilized anaerobic stock solution of sodium sulfate was added after autoclaving to vary the sulfate concentration in these experiments.

Four liters of basal medium was boiled under flowing N_2-gas and autoclaved. In an anaerobic chamber, filter sterilized anaerobic stock solutions of calcium chloride (4 mL), Wolfe's vitamin solution (40 mL), selenate/tungstate solution (4 mL), SL-10 trace element solution (4 mL), 400 mL of Zn (as $ZnCl_2$) from a 10 mM stock solution were added to room temperature autoclaved basal medium to minimize high temperature complexation and precipitation just prior to inoculation with cells. The medium was divided in half and 40 mL for high and 20 μL for low treatments of 1 M sodium sulfate was added to the high and low sulfate experiments, respectively. The medium was divided in half again into screw-top 1 L flasks and inoculated with cells for each experiment. A sterilized, autoclaveable, re-pipette was used to consistently aliquot 10 mL of this medium into 15 mL Balch tubes. Balch tubes were sealed with sterilized anaerobic butyl-rubber stoppers and aluminum seals and stored in the dark to mimic anaerobic sediments.

Experimental Parameters

Initial inoculum of bacteria was $5x10^7$ cells/mL total ($2.5x10^7$ cell/mL for each species), determined by direct counts. Two-line ferrihydrite was used in the ratio of 1:9 by mass (ferrihydrite:quartz) which is representative of the total Fe concentrations in the LCDA system. The ferrihydrite was derived from titration of ferric nitrate with potassium hydroxide to a pH of between 7 and 8 according to Schwertmann and Cornell [142]. Due to the potential for phase modifications during autoclaving [143], washed

ferrihydrite was instead baked at 80^{o}C for 18 hours to prevent microbial growth [63]. A total of 5 g of solids were added to 10 mL of media in Balch tubes sealed under nitrogen. For Zn containing experiments, Zn concentrations (~20 μM) were selected from a nine year average (1999-2008) of non-sequential measurements from the CDAR at Harrison, ID and was introduced (as aqueous $ZnCl_2$) into the batch mixtures until this concentration was reached in the aqueous phase, approximately 1 mM. In order to control the activity of sulfate reducing bacteria, sulfate concentrations were moderated. The high and low sulfate concentration for the batch experiments were approximately twice and 1/1000th that of the electron equivalent of Fe in the solid phase or 20 mM and 0.01 mM respectively.

Batch Characterization

Cell Enumeration: Genomic DNA was extracted from supernatant/solids using a PowerSoil DNA extraction kit (MoBio) as per manufacturer instructions. Cell numbers were quantified using extracted DNA for quantitative polymerase chain reaction (qPCR). Two separate PCR conditions employing SYBR Green which binds to double stranded DNA was used with unique primer sets tailored to each genus. This enabled independent enumeration of both *Geobacter* sp. CDA-2 and *Desulfovibrio vulgaris* Hildenborough. Two primers (Geo494a 5'-CHY AAA GGA AGC GGC TAA CTC-3' and Geo768R 5'-CGT CTG AGC GTC AAT AT-'3) were developed for this study based on genus specific regions of the 16S rDNA gene for *Geobacter* spp. For detection of sulfate reducing populations, primers based on the dissimilatory (bi)sulfite reductase gene (*dsr*)

(dsrF1 5'-ACS CAS TGG AAG CAC G-3' and RH3-dsr-R 5'-GGT GGA GCC GTG CAT GGT-3') [144] which appears to be conserved among all SRB were used. PCR reaction mixtures for *Geobacter* sp. CDA-2 consisted of (for 1 reaction of 12.5 μL) in μL:0.1 *Taq* polymerase (Invitrogen), 1.25 10X PCR buffer (Invitrogen), 0.375 $MgCl_2$ (50 mM) (Invitrogen), 0.25 dNTPs (Promega), 0.25 forward primer, 0.25 reverse primer, 0.05 SYBR® Green (Invitrogen). Template DNA and DNAse/RNase free water were varied to a final reaction volume of 12.5 μL. qPCR employed a cycling gradient of 95°C for 1 minute followed by 30 cycles of 95°C for 1 minute, 55°C for 1 minute, and 72°C for 30 seconds in a Corbett Rotor-Gene® 6000. qPCR data was analyzed using Rotor-Gene real-time rotary analyzer software (v1.7).

Aqueous Characterization: Inductively coupled plasma-mass spectrometry (Agilent 7500 ICP-MS) was used to analyze for total metal concentrations of aqueous metals Fe and Zn. For the speciation of aqueous Fe(II), Fe(III), and detection of sulfide, colorimetric assays ferrozine [145] and methylene blue method (HACH) were used, respectively. To measure organic acids, a high pressure liquid chromatography (HPLC) 1200 series Agilent HPLC with Bio-Rad Aminex HPX-87H column was used with an isocratic sulfuric acid (0.005 M) eluent. Both refractive index and a variable wavelength detector set at 280 nm were employed. Due to the potential for the HPLC column to be damaged from high metal concentrations, Chelex 100 resin (Sigma Aldrich, St. Louis, MO) was added to each sample prior to analysis to remove metals. Anions were determined by ion chromatography using an isocratic sodium carbonate (9 mM) eluent with a Dionex AS9-HC column and AG9-HC guard. Suppression of the CD20 detector

was set at 50 mA. Samples and standards were filter sterilized (0.2 μm) and diluted 10 fold before analysis in >17.6 MΩ de-ionized water.

Solids Characterization: Representative solids samples were subject to mineralogical analysis using a Scintag XDS 2000 X-ray diffractometer (XRD) for mineral phase identification. Typical detection limits for XRD are between 1-3 weight percent. Field emission scanning electron microscopy-energy dispersive x-ray spectroscopy (FESEM-EDS) was used for bulk elemental analysis and imaging at the Image and Chemical Analysis Laboratory (ICAL) at Montana State University.

Results and Discussion

Zinc Free Treatments

Geobacter sp. CDA-2 Treatments: Treatments containing *Geobacter* sp. CDA-2 showed initial decrease in Fe(II) concentrations, probably explained by a combination of ferrihydrite absorption and degradation of pyrophosphate ligands to phosphate, thus decreasing Fe solubility (Figure 12). A soluble Fe source was used for the inoculum of CDA-2 (Fe(III)-pyrophosphate) in order to make it possible for cell counting prior to inoculation. A portion of these pyrophosphates were carried over in the aqueous fraction upon inoculation to this experiment. Using ion chromatography to monitor sulfate showed little decrease in sulfate in CDA-2 treatments (Figure 14). DNA concentrations appeared to stabilize after 14 days incubation (Figure 13).

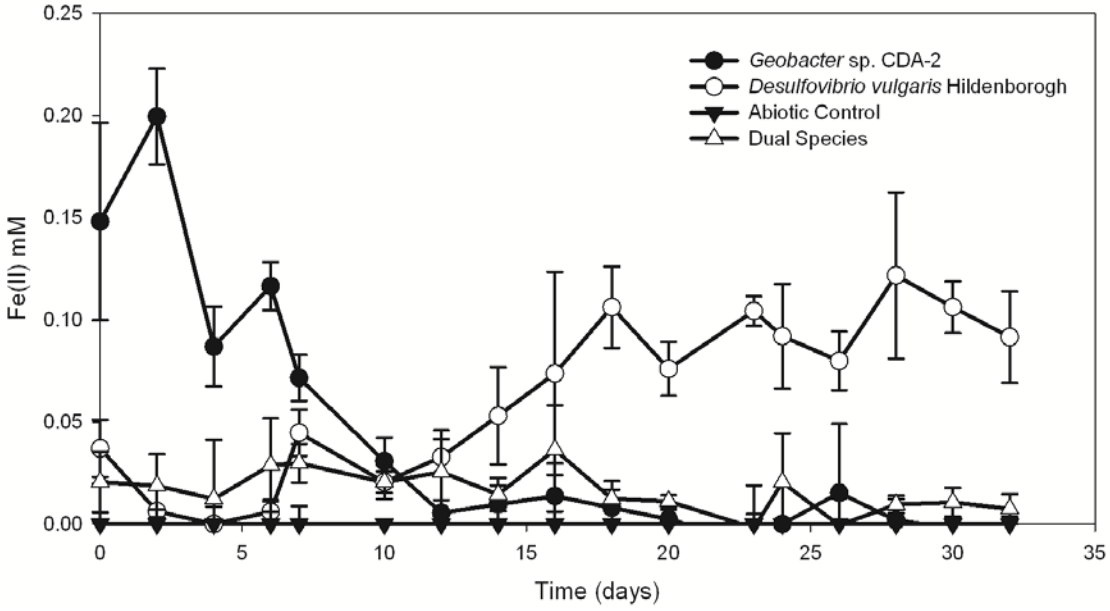

Figure 12: Fe(II) concentrations from zinc free experiments of *Geobacter* sp. CDA-2, *Desulfovibrio vulgaris* Hildenborough, abiotic, and dual species treatments with 95% confidence intervals

Desulfovibrio vulgaris Hildenborough Treatments: Fe(II) increased over time in *D. vulgaris* treatments to approximately 0.1 mM (Figure 12). Park *et al.* [146] reported *D. vulgaris* to have Fe reduction levels of approximately 0.1 mM when grown on ferrihydrite, which compares well with what is observed in this study. Total DNA increased with time, greater than *Geobacter* sp. CDA-2 treatments, but not statistically different from dual species treatments (Figure 13). Sulfate concentrations decreased with time from about 40 to 30 mM, as expected (Figure 14).

Dual Species Treatments: The concentration of Fe(II) appeared to be stable, though higher than abiotic controls, throughout the dual species treatment experiment (Figure 12). Sulfate concentrations decreased at a similar rate when compared to *D. vulgaris* treatments (Figure 14). Total DNA also appeared to be very similar to *D. vulgaris* treatments (Figure 13).

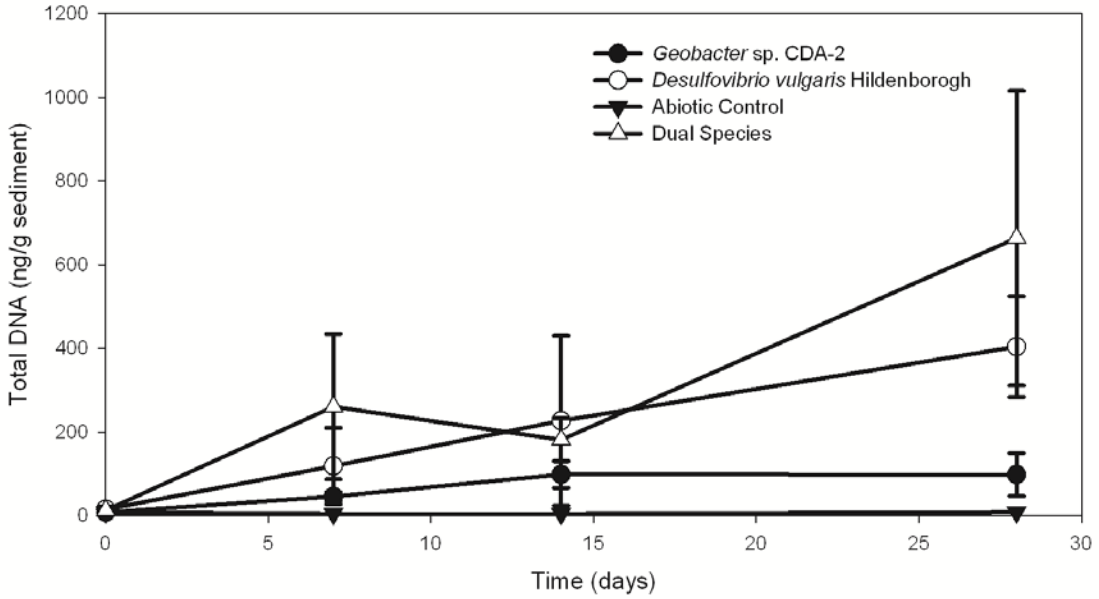

Figure 13: Total DNA concentrations from zinc free experiments of *Geobacter* sp. CDA-2, *Desulfovibrio vulgaris* Hildenborough, abiotic, and dual species treatments with 95% confidence intervals

Zinc Containing Treatments

Abiotic Treatments: The results for the abiotic low and high sulfate controls were presented in Figures 15 and 16 A-G, respectively. The slightly lower pH combined with the lower ionic strength of the low sulfate treatments may have contributed to increasing the Zn concentrations (Figure 15 B). In fact the abiotic low sulfate treatments showed the highest dissolved Zn concentrations of all experiments. In studies of Zn sorption to ferrihydrite, Dyer *et al*. [147] found sorption to be strongly influenced by pH and that sorption onto ferrihydrite began to plateau around pH 6.

Slight contamination from, presumably, sulfate reducing bacteria in samples from week three could explain the increases in total DNA and acetate concentrations with a decrease in lactate concentrations, while nitrate concentrations were relatively stable. Efforts were made to maintain sterile conditions throughout experimental setup, however,

conditions in the anaerobic glove bag were disinfected, but not sterile and could explain the contamination in some of the samples from the low sulfate treatments. There were no visible transformations of the mineral phases in the abiotic controls within the sampling time.

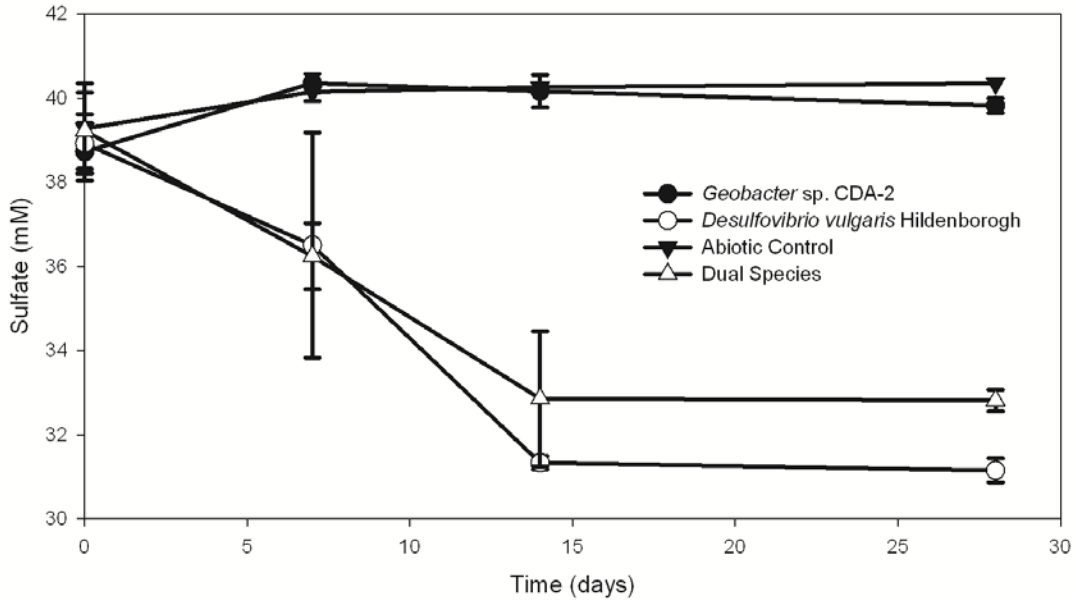

Figure 14: Sulfate concentrations from zinc free experiments of *Geobacter* sp. CDA-2, *Desulfovibrio vulgaris* Hildenborough, abiotic, and dual species treatments with 95% confidence intervals

Geobacter sp. CDA-2 Treatments: *Geobacter* sp CDA-2 had been reported to reduce nitrate previously [12], which is supported in this data (Figure 17 and 18 D). Nitrate in this system stems from residual nitrate, from the preparation of ferrihydrite, liberated from ferrihydrite during reductive dissolution. Increases in pH were observed in CDA-2 treatments though it is unclear whether this stems from nitrate or Fe reduction (Figure 17 and 18 C). Very little Fe was liberated to the aqueous phase; however, ferrihydrite is known to adsorb significant amounts of cations (Figure 17 and 18 A). Sulfate concentrations in all high sulfate treatments were initially approximately half of

the total sulfate added to the system, probably due to adsorption to ferrihydrite. Sulfate in CDA-2 treatments increased in both high and low sulfate treatments presumably due to release of surface adsorbed sulfate following reductive dissolution of ferrihydrite (Figure 17 and 18 E) [148]. Growth of CDA-2 in both low and high sulfate treatments were approximately the same with 10^8 gene copies/g sediment (Figure 17 and 18 H).

Desulfovibrio vulgaris Hildenborough Treatments: Figure 19 and 20 C showed pH increase to approximately 6.5 potentially driven by sulfate reduction. Nitrate appeared to have been stable throughout SRB treatments, suggesting no nitrate reduction. Lactate was consumed and acetate produced under SRB treatments, though much less in low sulfate treatments. Total DNA extracted in SRB treatments was low compared to IRB treatments. This could mean that SRB were less active in these treatments or SRB catalyzed reactions under non-growth conditions, such that little cell division occured. Figures 19 and 20 A show Fe levels in SRB treatments. Fe levels in both low and high sulfate treatments increased with time. *Desulfovibrio vulgaris* Hildenborough and other sulfate reducing bacteria are known to catalyze Fe dissolution through indirect attack by sulfide production and/or direct enzymatic reduction of aqueous Fe(III) [146, 149]. *Desulfovibrio vulgaris* Hildenborough is capable of catalyzing non-growth reactions that reduce soluble Fe directly via a cytochrome-c_3 complex [150], however in studies by Park *et al*. [146], *D. vulgaris* was incapable of growth using Fe reduction on solid Fe substrates, though some Fe was liberated. Carbon and sulfate (and possibly Fe) analysis suggests that SRB were active in SRB treatments. Additionally, if Zn and/or Fe was inhibiting growth, but not activity, such that SRB must consume energy to detoxify their

environment, this may explain the observed lack of DNA. In Zn-free high sulfate treatments, recovered DNA concentrations were not substantially different from Zn-containing treatments.

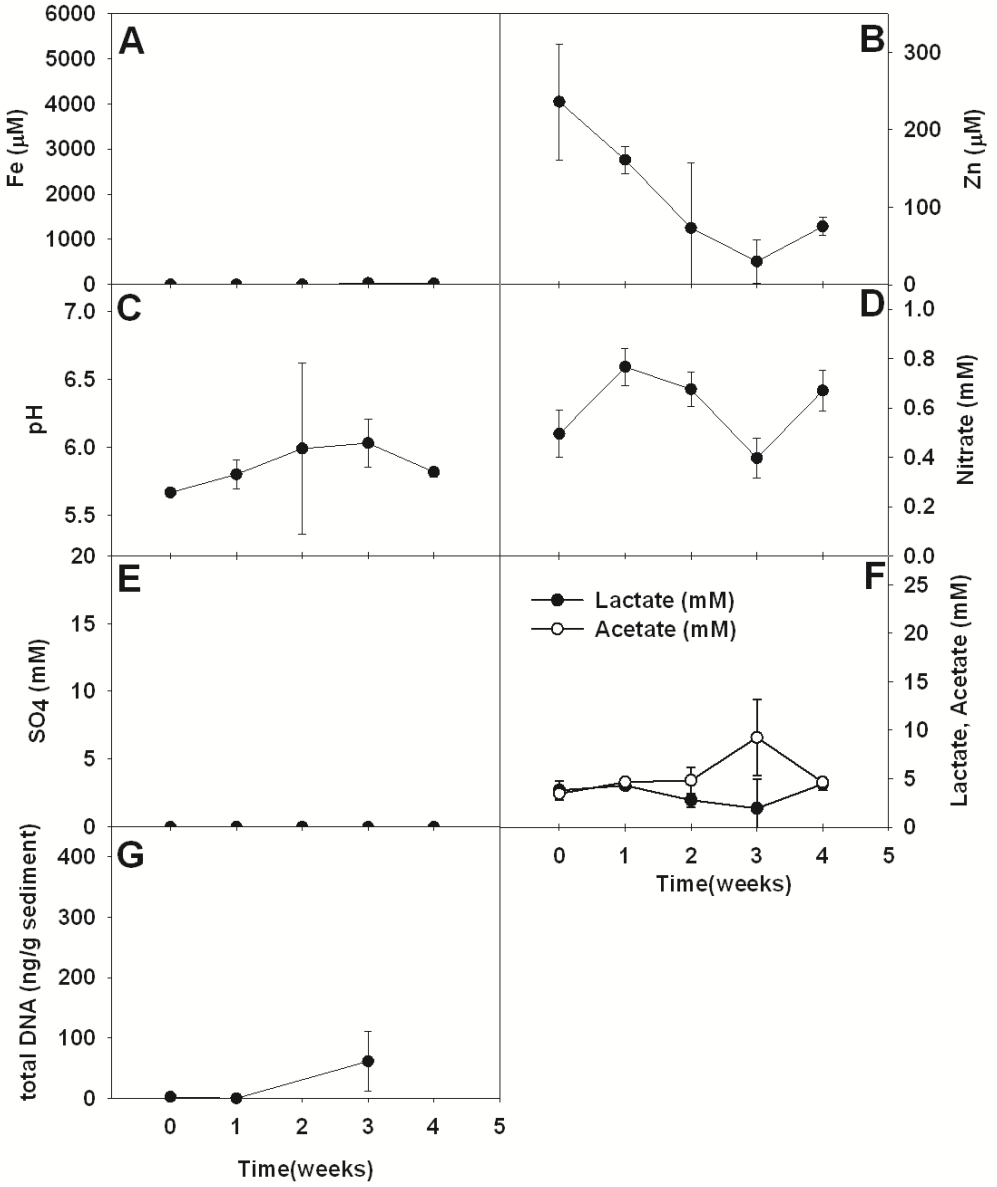

Figure 15: Abiotic low sulfate treatments showing A) total aqueous iron, B) total aqueous zinc, C) pH, D) aqueous nitrate, E) aqueous sulfate, F) lactate (closed circles) and acetate (open circles), and G) total DNA per gram sediment

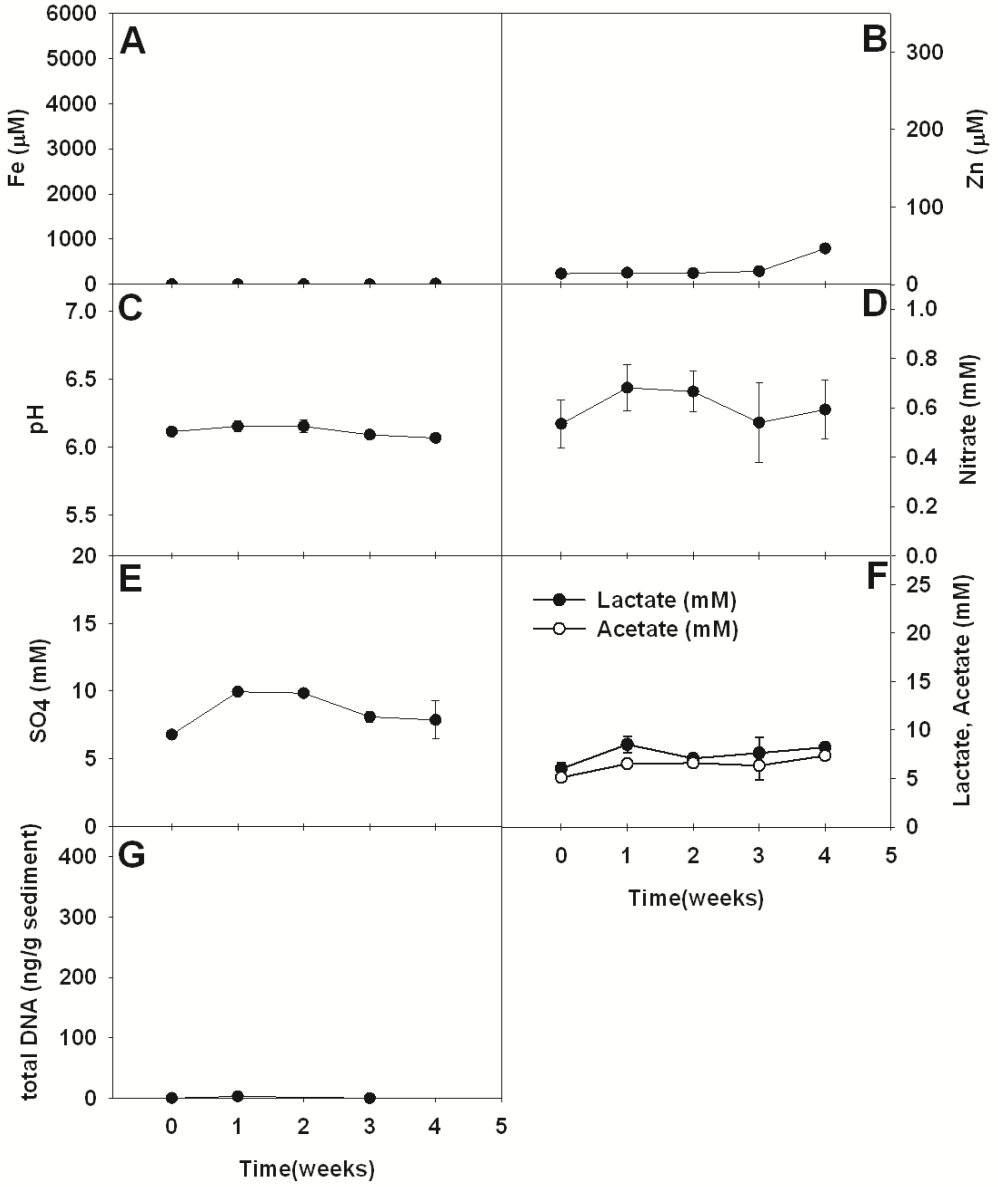

Figure 16: Abiotic high sulfate treatments showing A) total aqueous iron, B) total aqueous zinc, C) pH, D) aqueous nitrate, E) aqueous sulfate, F) lactate (closed circles) and acetate (open circles), and G) total DNA per gram sediment

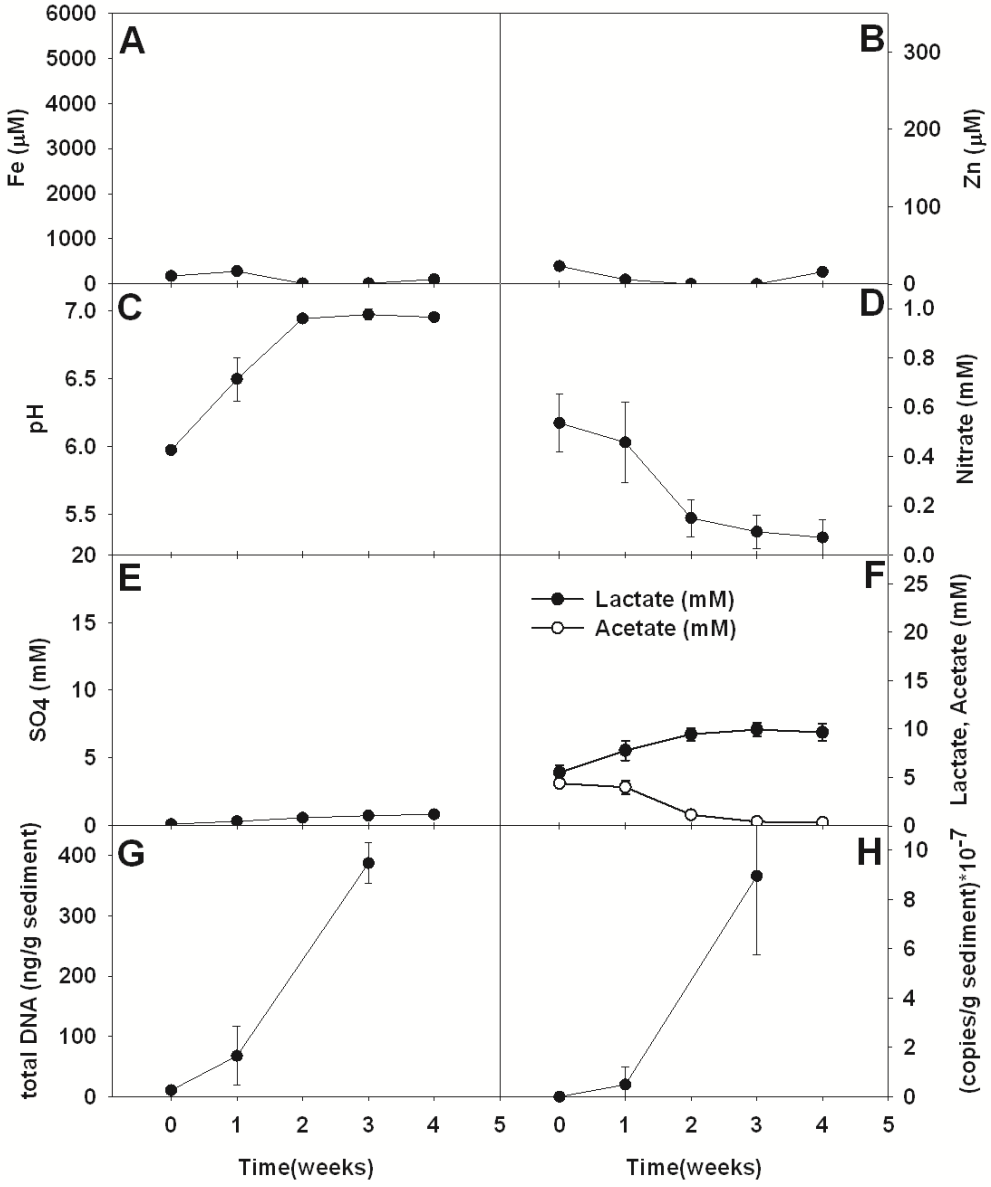

Figure 17: *Geobacter* sp. CDA-2 low sulfate treatments showing A) total aqueous iron, B) total aqueous zinc, C) pH, D) aqueous nitrate, E) aqueous sulfate, F) lactate (closed circles) and acetate (open circles), G) total DNA per gram sediment, H) CDA-2 16SrDNA gene copies/gram sediment.

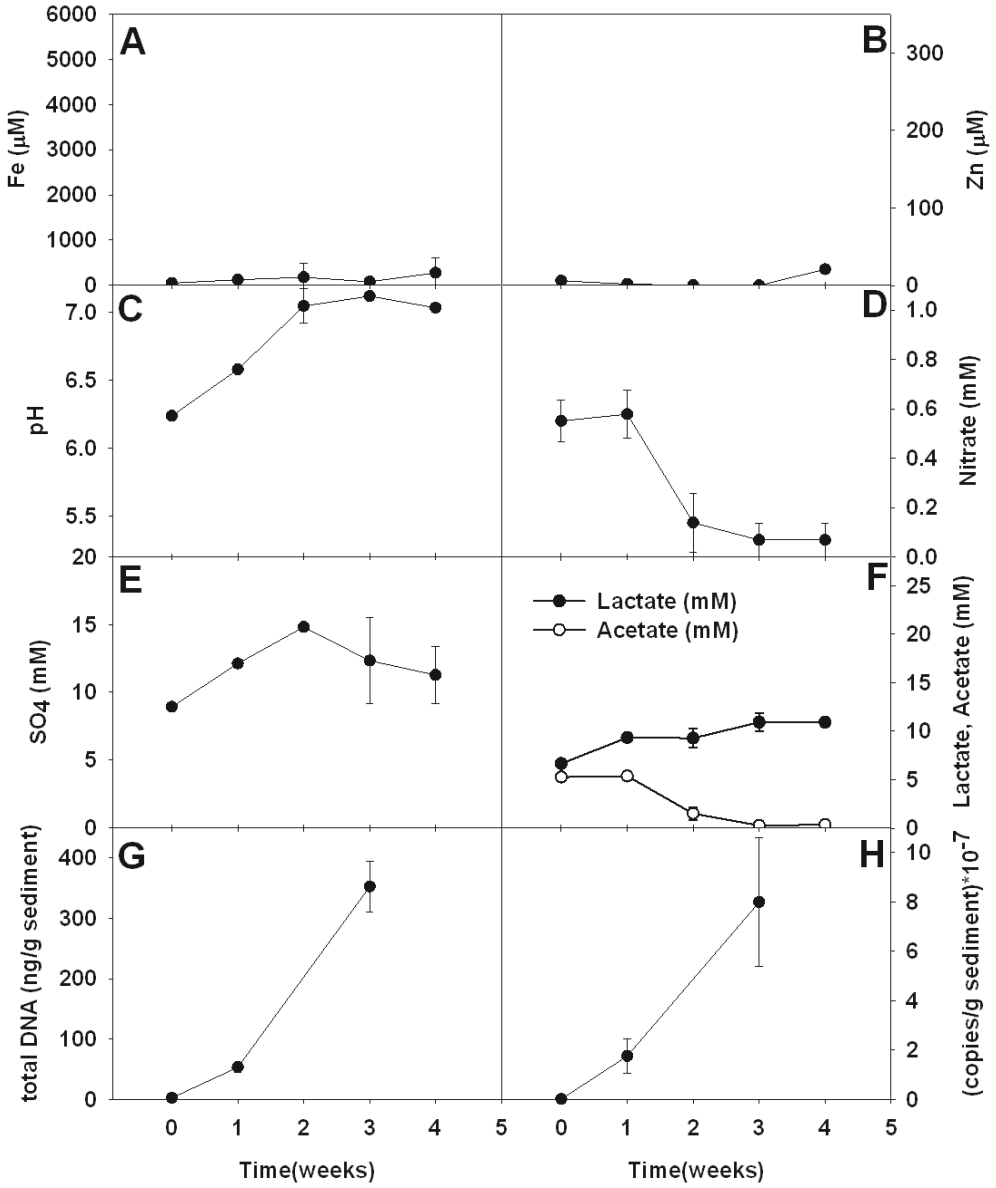

Figure 18: *Geobacter* sp CDA-2 high sulfate treatments showing A) total aqueous iron, B) total aqueous zinc, C) pH, D) aqueous nitrate, E) aqueous sulfate, F) lactate (closed circles) and acetate (open circles), G) total DNA per gram sediment, H) CDA-2 16SrDNA gene copies/gram sediment.

Both cultures show visible sulfide precipitates, though lower quantities in low sulfate conditions due to sulfate limitations. Iron sulfides, greigite (Fe_3S_4), mackinawite ($Fe_{1+X}S$, X=0 to 1.1), and pyrrhotite (Fe_7S_8) have been observed under biological sulfate-reduction, though achieving a crystalline structure can require long incubation times (>2

years) [151-152]. Additionally, Fe minerals in both *Desulfovibrio* and mixed species samples show transformation over time of ferrihydrite to other mineral phases (Figure 21). X-ray diffractograms of high and low SRB treatments show formation of hematite, a thermodynamically stable end-product (Figure 24 A and B). While no magnetite is detected via XRD (Figure 24 A and B), applying a magnetic field to SRB treatments show a small portion of magnetic particles greater than abiotic controls and increasing in high sulfate treatments. This could be magnetite (Fe_3O_4), a magnetic mineral know to be a product of ferrihydrite transformation during Fe^{2+} reduction [153], or greigite, a magnetic Fe sulfide mineral. Figure 25 show field emission scanning electron microscopy of mineral formations adjacent to bacteria under high sulfate conditions. Phenotypically, the mineral resembles schwertmannite ($Fe^{(III)}_{16}O_{16}(SO_4)_2(OH)_{12} \bullet 10H_2O$) or hematite ($Fe_2O_3$), however, in the case of schwertmannite, sulfur peaks were only intermittently detected in different samples via energy dispersive spectroscopy (EDS). This could be because of the depth of penetration as EDS may detect parent Fe minerals from which the unknown mineral is formed. EDS shows that the mineral is composed of mainly Fe (~20-25%) and oxygen (~75-80%) with traces of sulfur and chloride, consistent with hematite.

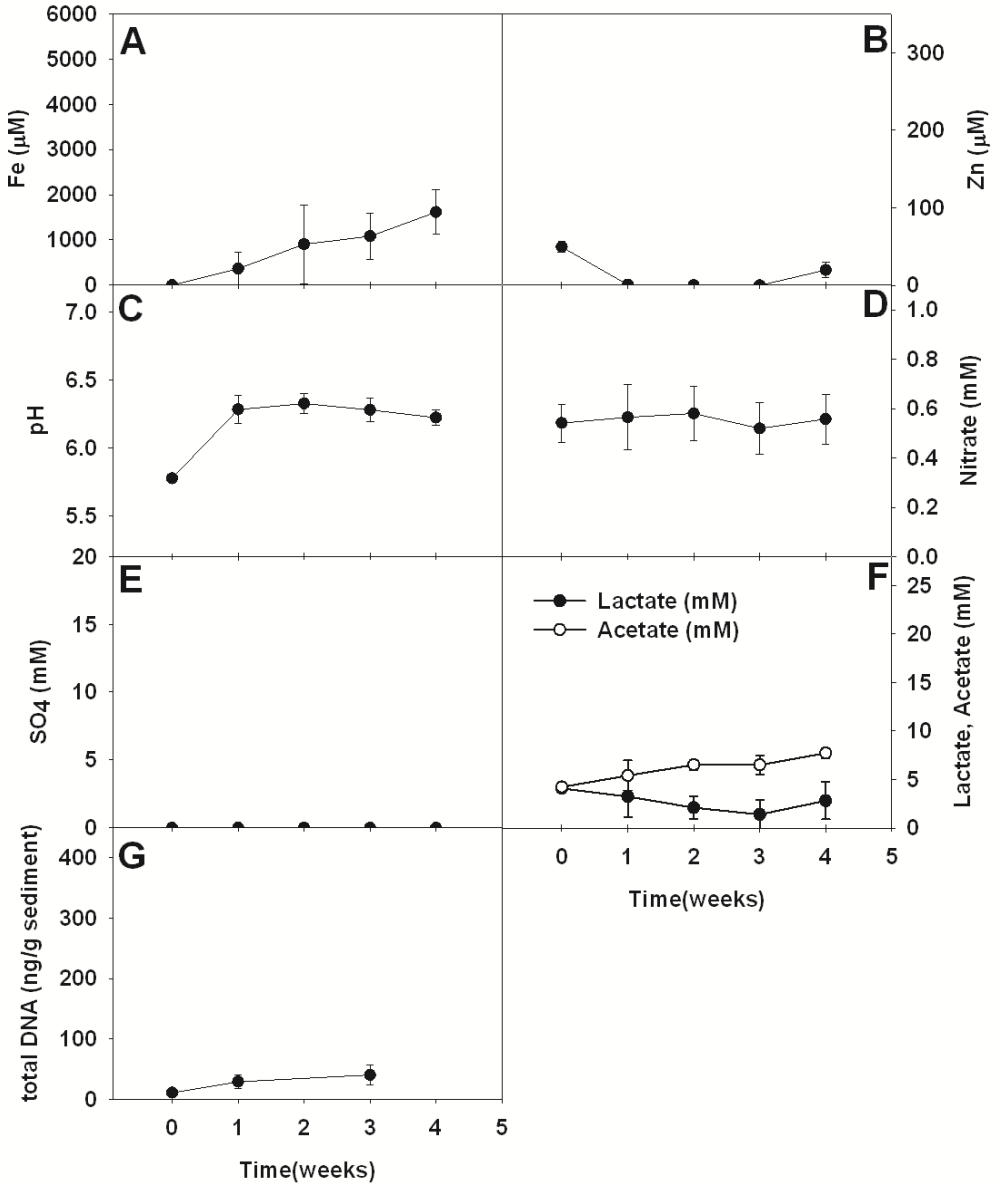

Figure 19: *Desulfovibrio vulgaris* Hildenborough low sulfate treatments showing A) total aqueous iron, B) total aqueous zinc, C) pH, D) aqueous nitrate, E) aqueous sulfate, F) lactate (closed circles) and acetate (open circles), and G) total DNA per gram sediment.

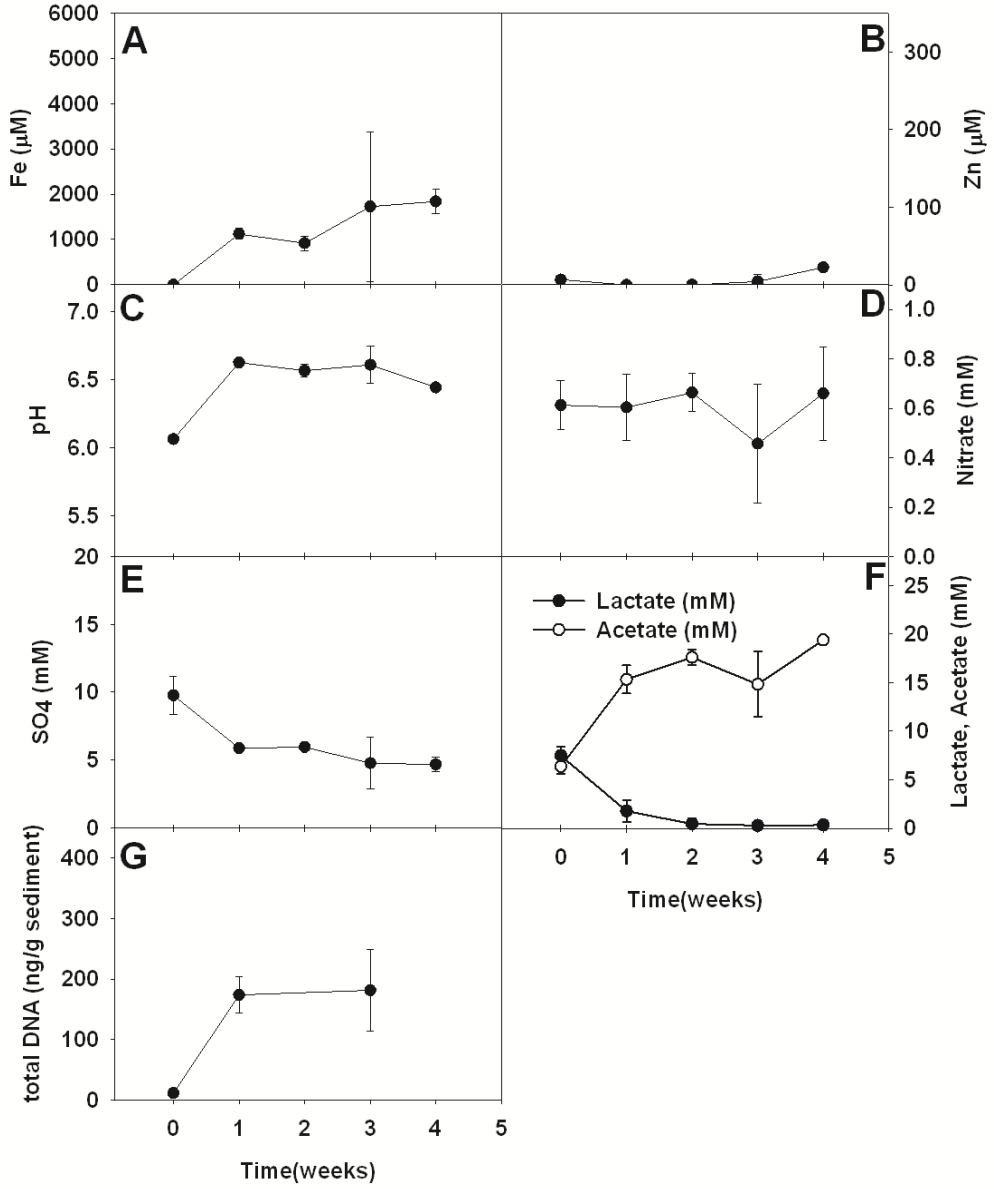

Figure 20: *Desulfovibrio vulgaris* Hildenborough high sulfate treatments showing A) total aqueous iron, B) total aqueous zinc, C) pH, D) aqueous nitrate, E) aqueous sulfate, F) lactate (closed circles) and acetate (open circles), and G) total DNA per gram sediment

Dual Species Treatments: Increases in soluble Fe concentrations and pH are observed in the mixed species system with time (Figure 22-23 A). The pH increase in mixed species treatments is not as pronounced as in IRB treatments. Slight decreases in nitrate concentrations are observed in mixed high and low SO_4^{2-} treatments suggesting

nitrate reduction by *Geobacter* sp. CDA-2, though much less than in *Geobacter* sp. CDA-2 only treatments suggesting inhibition of CDA-2.. In high sulfate treatments, sulfate concentrations decrease at a comparable rate to SRB only treatments. DNA concentrations in mixed species systems however, are approximately the same as in SRB treatments and lower than in IRB treatments. Copies of *Geobacter* sp. CDA-2 are much lower in mixed species treatments which may either stem from low activity. It may be that there is an antagonistic effect between *Geobacter* sp. CDA-2 and *Desulfovibrio vulgaris* Hildenborough as DNA concentrations and gene copy number are lower in mixed treatments, especially in high sulfate treatments were presumably SRB are most active. Transformation of ferrihydrite to hematite occurs in both high and low treatments of mixed species (Figure 24), however, magnetite is detected in the XRD of high sulfate treatments (Figure 24-D). Application of a magnetic field to high sulfate treatments shows substantial development of magnetite and minor development in low sulfate treatments.

Conclusions

It appears that the addition of the sulfate reducing bacteria *Desulfovibrio vulgaris* Hildenborough did not benefit,and in fact inhibited growth of *Geobacter* sp. CDA-2 (as nitrate and qPCR data would suggest) by decreasing Zn bioavailability in the presence of ferrihydrite. Reduced Fe and sulfur species are highly reactive and sulfide is known to be toxic to bacteria which may have contributed to the inhibition of *Geobacter* sp. CDA-2 in mixed species systems. The major metal sink in this system was ferrihydrite which

appears to adsorb the majority of Zn added to the system; however, as is demonstrated in the abiotic low sulfate system, small changes in pH are capable of releasing significantly more Zn. Identification of hematite and magnetite is not unexpected due to ligands which facilitate transformations and the presence of reduced Fe in these systems.

Future work in this area should focus on other SRB and IRB populations, organism quantification as DNA concentrations may not accurately represent the community activity, and kinetics of mineral transformations especially small scale analyses to trace the fate of Zn.

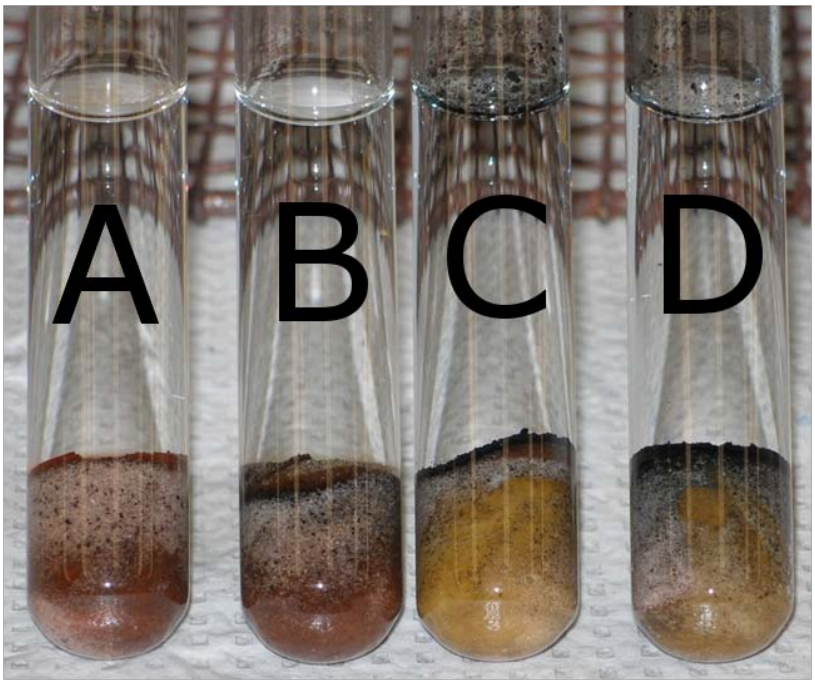

Figure 21: Image of high sulfate treatments for experiments A) abiotic, B) *Geobacter* sp. CDA-2 only, C) *Desulfovibrio vulgaris* Hildenborough only, D) both *Geobacter* sp. CDA-2 and *Desulfovibrio vulgaris* Hildenborough dual species system

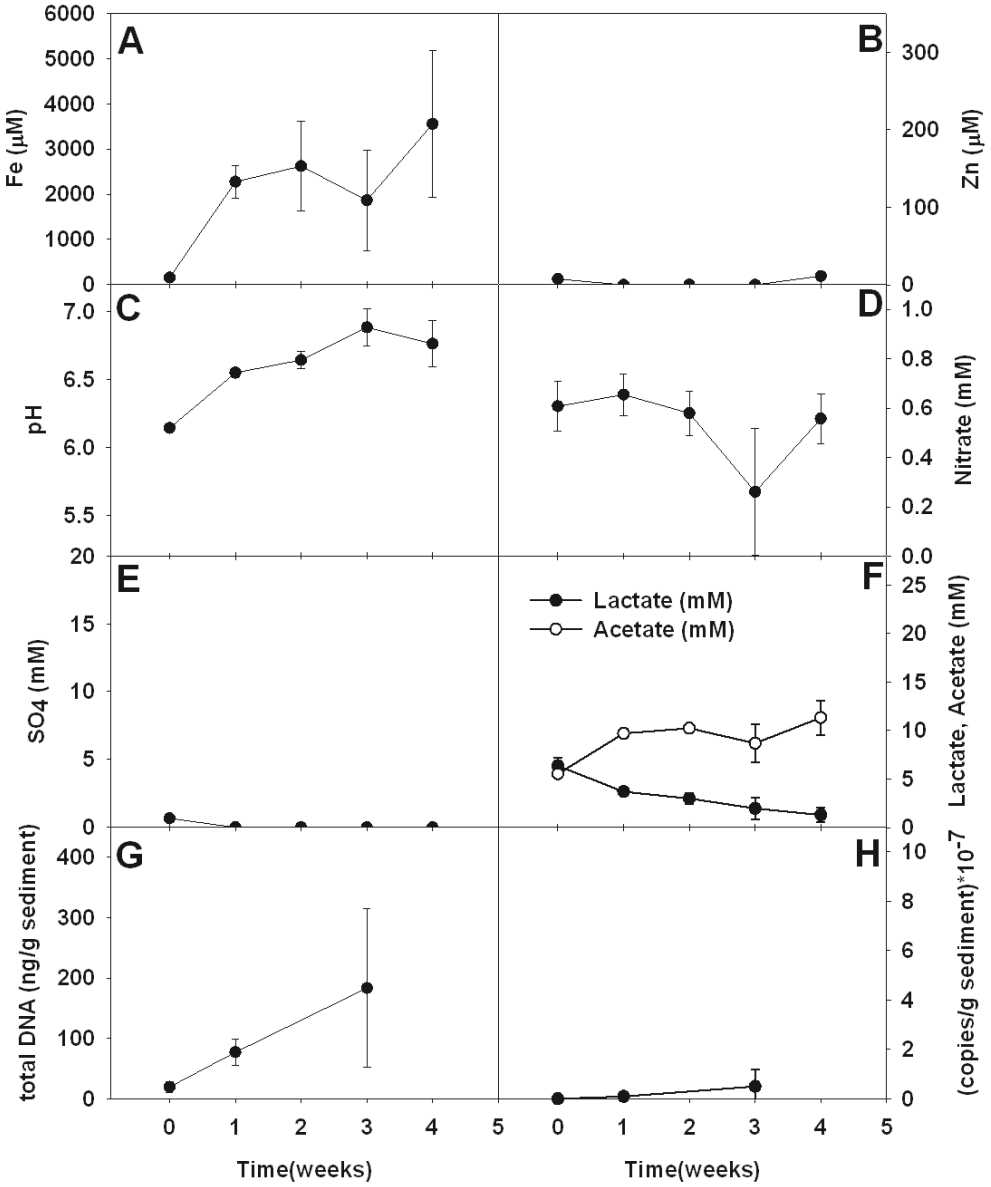

Figure 22: Dual species low sulfate treatments showing A) total aqueous Fe, B) total aqueous zinc, C) pH, D) aqueous nitrate, E) aqueous sulfate, F) lactate (closed circles) and acetate (open circles), G) total DNA per gram sediment, H) gene copies/gram sediment *Geobacter* sp. CDA-2

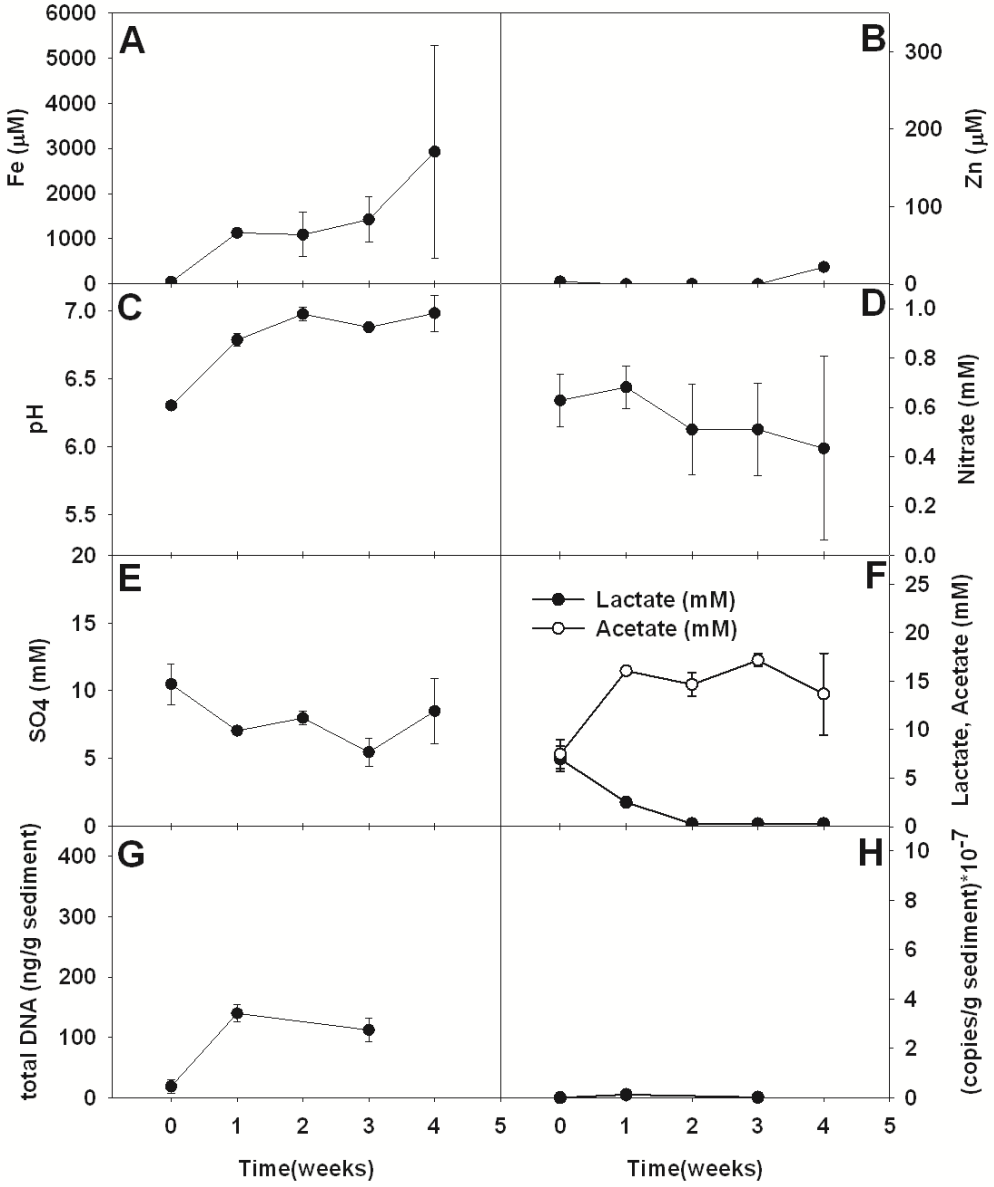

Figure 23: Dual species high sulfate treatments showing A) total aqueous Fe, B) total aqueous zinc, C) pH, D) aqueous nitrate, E) aqueous sulfate, F) lactate (closed circles) and acetate (open circles), G) total DNA per gram sediment, H) gene copies/gram sediment *Geobacter* sp. CDA-2

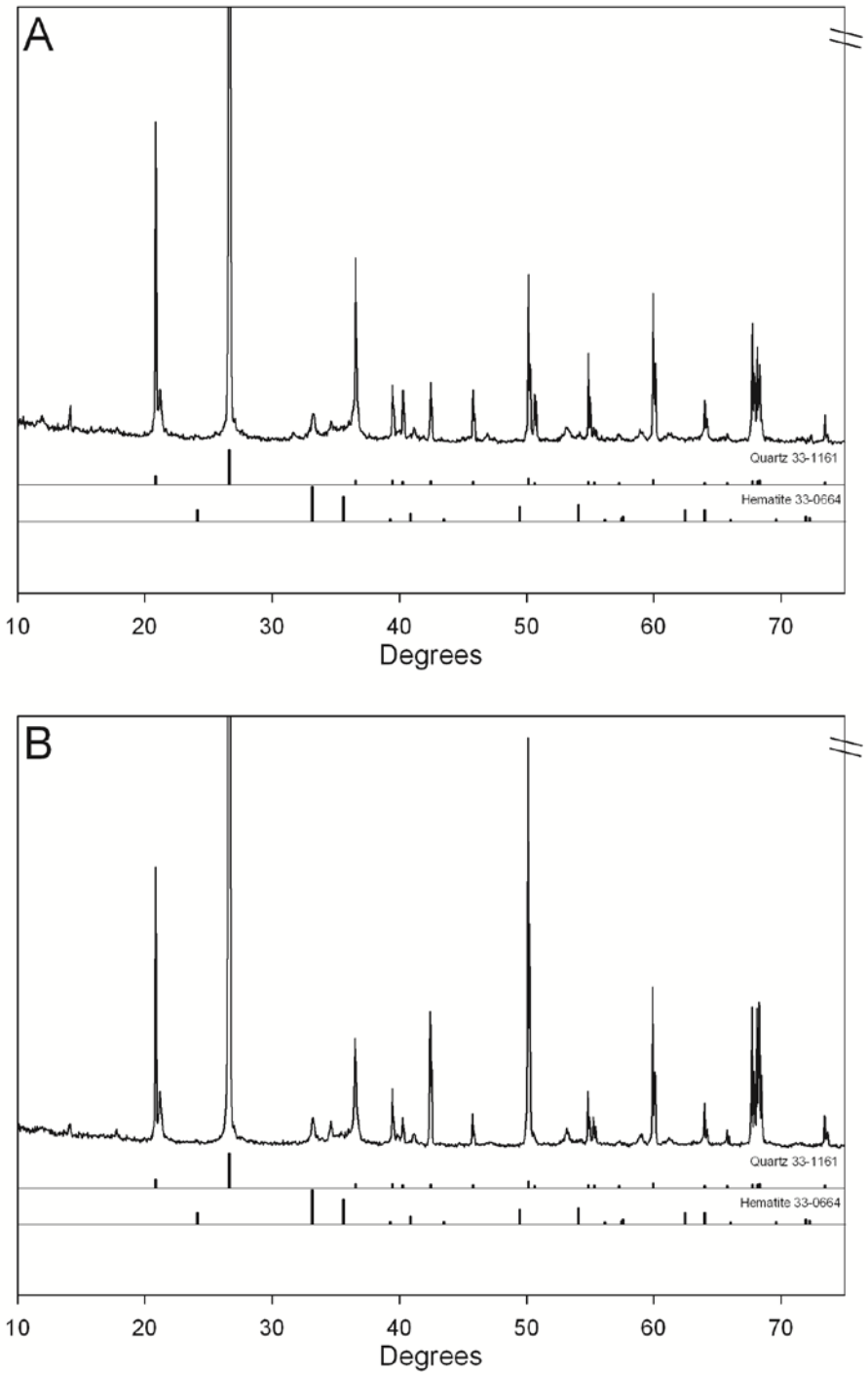
A
Quartz 33-1161
Hematite 33-0664
10
20
30
40
50
60
70
Degrees
B
Quartz 33-1161
Hematite 33-0664
10
20
30
40
50
60
70
Degrees

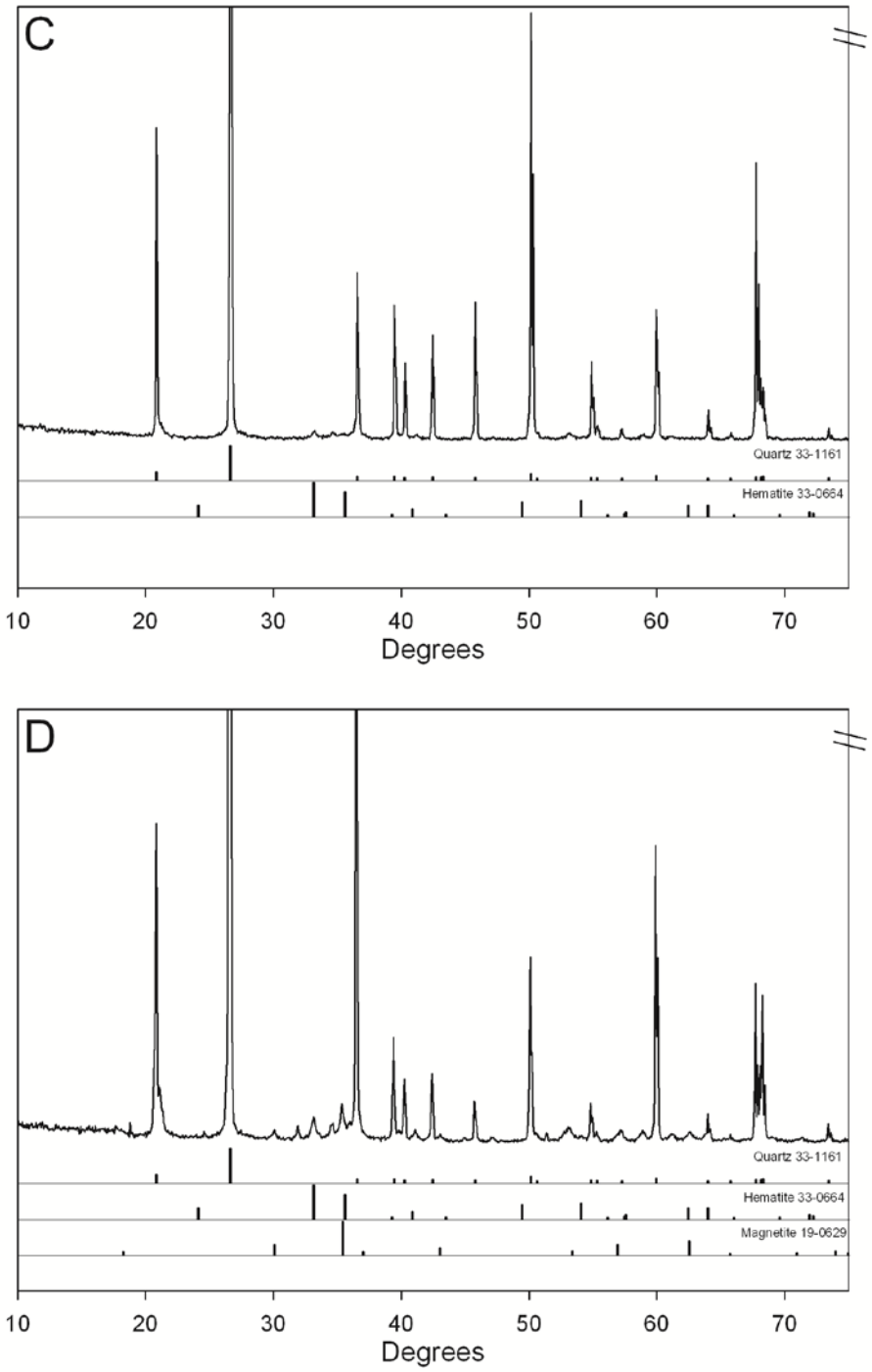

Figure 24: X-ray diffraction analyses of sediments in A) *Desulfovibrio vulgaris* Hildenborough low sulfate treatment, B) *Desulfovibrio vulgaris* Hildenborough high sulfate treatment, C) *Desulfovibrio vulgaris* Hildenborough and *Geobacter* sp. CDA-2 low sulfate treatment, D) *Desulfovibrio vulgaris* Hildenborough and *Geobacter* sp. CDA-2 high sulfate treatment after 26 weeks incubation. Note: Y-axis is arbitrary and has been scaled to show smaller peaks.

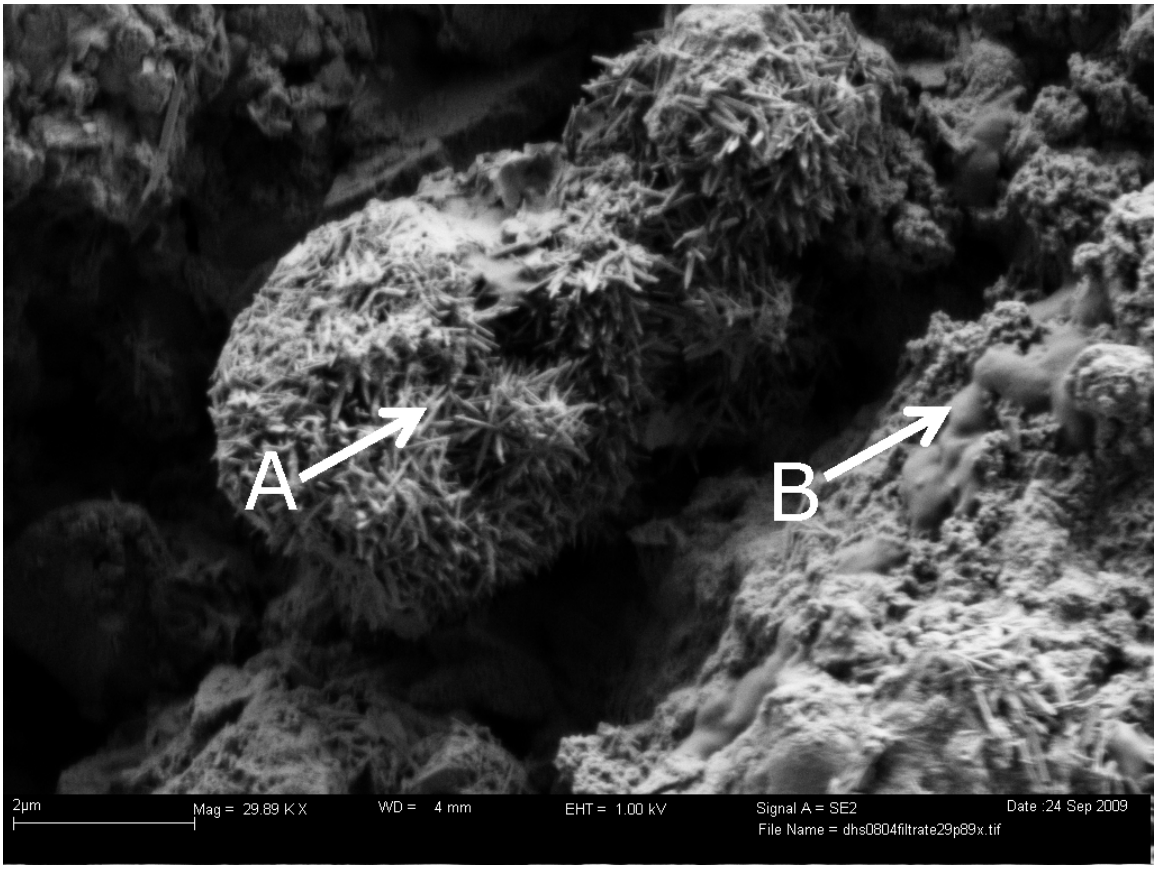

Figure 25: FESEM image of *Desulfovibrio vulgaris Hildenborough* only high sulfate treatment after 6 weeks of incubation. A) unknown mineral (presumably hematite) formed only under *Desulfovibrio vulgaris Hildenborough* treated cultures and B) *Desulfovibrio vulgaris Hildenborough* cells

APPENDIX B

EXPERIMENTAL DATA FOR ZINC FREE AND ZINC CONTAINING TREATMENTS, BATCH EXPERIMENTS

Table 7: Zinc Free Batch Treatments								
	DNA				95% confidence			
Time	CDA-2	DSV	AB	FESRB	CDA-2	DSV	AB	FESRB
0	7.709816	14.98361	7.62133	12.44084	3.535917	7.174362	2.87045	9.080168
7	45.47209	118.1644	4.158399	260.0458	10.27452	90.92782	1.189692	173.7452
14	98.20319	226.4608	4.066543	180.9755	32.26093	203.0403	0	51.36956
28	97.7974	403.4239	7.991632	663.0483	51.21186	120.1105	0	352.289
	SO4				95% confidence			
Time	CDA-2	DSV	AB	FESRB	CDA-2	DSV	AB	FESRB
0	38.72	38.92	39.27	39.22	0.6849	0.6951	1.075	0.9092
7	40.35	36.50	40.14	36.24	0.2207	2.676	0.2213	0.7834
14	40.16	31.33	40.25	32.85	0.388	0.158	0	1.6037
28	39.82	31.15	40.35	32.81	0.1745	0.2878	0	0.2517
	Fe(II)				95% confidence			
Time	CDA-2	DSV	Abiotic	Fe/SRB	CDA-2	DSV	Abiotic	Fe/SRB
0	0.148	0.037	ND	0.021	0.048	0.014	0.020	0.015
2	0.200	0.006	ND	0.019	0.023	0.000	0.007	0.015
4	0.087	ND	ND	0.012	0.020	0.008	0.000	0.029
6	0.116	0.006	ND	0.029	0.012	0.006	0.011	0.023
7	0.072	0.045	ND	0.030	0.011	0.011	0.009	0.010
10	0.031	0.020	ND	0.020	0.012	0.008	0.000	0.005
12	0.005	0.033	ND	0.025	0.006	0.009	0.000	0.020
14	0.010	0.053	ND	0.014	0.000	0.024	0.019	0.008
16	0.014	0.074	ND	0.036	0.016	0.050	0.006	0.022
18	0.008	0.106	ND	0.012	0.013	0.020	0.010	0.004
20	0.002	0.076	ND	0.011	0.005	0.013	0.000	0.003
23	ND	0.104	ND	ND	0.000	0.007	0.019	0.007
24	ND	0.092	ND	0.020	0.000	0.026	0.000	0.024
26	0.015	0.080	ND	ND	0.034	0.014	0.013	0.002
28	0.002	0.122	ND	0.010	0.011	0.041	0.007	0.004
30	ND	0.106	ND	0.011	0.000	0.013	0.004	0.007
32	ND	0.092	ND	0.007	0.007	0.022	0.000	0.007
	HS-				95% confidence			
Time	CDA-2	DSV	Abiotic	Fe/SRB	CDA-2	DSV	Abiotic	Fe/SRB
0	ND	ND	ND	ND	0.000357	0.000618	0.002162	0.002083
2	ND	0.000475	ND	0.000264	0	0.000878	0.000311	0.000262
4	0.000501	0.000834	ND	0.000779	0.000626	0.000626	0	0.001036
6	ND	0.016924	ND	0.020008	0.000386	0.007192	0.001823	0.006086
7	0.0002	0.100017	ND	0.114553	0.002744	0.072898	0.002352	0.047257
10	0.005165	0.028408	ND	0.051752	0.006188	0.00777	0.000595	0.018933
12	0.056441	0.004471	ND	0.080843	0.05862	0.001897	0	0.043238
14	0.15393	0.00074	ND	0.038811	0.025711	0.000483	0.000967	0.006799
16	0.045608	0.000204	ND	0.049137	0.047527	0.000399	0.000922	0.018609
18	0.107789	0.002104	ND	0.098982	0.090885	0.001153	0.000917	0.052565
20	0.043574	0.001644	ND	0.045327	0.041093	0.000617	0.000322	0.023869
23	0.0367	ND	ND	0.035718	0.015658	0	0.002335	0.028181
24	0.072175	ND	ND	0.004335	0.074809	0.000425	0.004248	0.002968
26	0.001347	0.000299	ND	0.049902	0.000293	0.000678	0.000339	0.03404
28	0.00484	0.001894	ND	0.028898	0.001409	0.001237	0.000825	0.010385
30	0.004109	ND	ND	0.019807	0.000715	0.000358	0.0008	0.005928
32	0.001933	0.000215	ND	0.026062	0.000421	0.000421	0.000842	0.007648

Table 9: Zinc Treated High Sulfate Batch Experiments

		Time (weeks)	Time (days)	Fe (μM)	95% Confidence Intervals Fe (μM)	Zn (μM)	95% Confidence Intervals Zn (μM)	SO4 (mM)	95% Confidence Interval SO4 (mM)	pH	Lactate (mM)	95% Confidence Interval Lactate	Acetate (mM)	95% Confidence Intervals Acetate	Total Extracted DNA (ng/ g sediment)	95% Confidence Interval Total Extracted DNA (ng/ g sediment)	CDA-2 (Gene Copy Number/g Sediment) *10^{-7}	95% Confidence Interval (Gene Copy Number/g Sediment)* 10^{-7}
	Abiotic Control	0	1	ND	N/A	13.9	1.9	6.8	0.3	6.1	6.02	0.58	5.10	0.46	ND	N/A	NM	NM
		1	8	ND	N/A	15.1	0.7	9.9	0.0	6.2	8.52	0.83	6.51	0.33	2.7	2.8	NM	NM
		2	15	ND	N/A	14.8	3.6	9.8	0.2	6.2	7.07	0.48	6.59	0.35	NM	NM	NM	NM
		3	22	ND	N/A	17.1	1.4	8.1	0.4	6.1	7.64	1.61	6.33	1.50	ND	N/A	NM	NM
		4	29	15	7	46.4	3.8	7.9	1.4	6.1	8.23	0.46	7.35	0.18	NM	NM	NM	NM
	Geobacter sp CDA-2	0	1	48	13	6.0	3.2	8.9	0.3	6.2	6.66	0.34	5.27	0.35	2.4	4.2	1.44E-02	1.90E-02
		1	8	126	53	1.7	0.4	12.1	0.2	6.6	9.35	0.34	5.37	0.43	53.1	8.8	1.7642	0.6988
		2	15	179	304	DQ	1.4	14.8	0.3	7.0	9.28	0.95	1.50	0.64	NM	NM	NM	NM
		3	22	81	13	ND	0.1	12.3	3.2	7.1	10.92	0.96	0.27	0.37	352.8	42.5	7.9981	2.602
		4	29	277	333	21.0	0.5	11.3	2.1	7.0	10.93	0.49	0.35	0.51	NM	NM	NM	NM
Desulfovibrio vulgaris Hildenborough		0	1	ND	ND	6.8	2.2	9.8	1.4	6.1	7.48	0.94	6.36	0.71	11.1	6.5	NM	NM
		1	8	1119	120	ND	0.1	5.9	0.0	6.6	1.77	1.10	15.33	1.46	173.7	29.4	NM	NM
		2	15	917	160	ND	0.3	6.0	0.1	6.6	0.46	0.58	17.59	0.77	NM	NM	NM	NM
		3	22	1725	1653	4.2	8.8	4.8	1.9	6.6	0.29	0.29	14.83	3.37	181.4	67.9	NM	NM
		4	29	1838	262	22.5	1.5	4.7	0.5	6.4	0.33	0.36	19.38	0.26	NM	NM	NM	NM
	Dual Species	0	1	45	21	3.2	1.9	10.5	1.5	6.3	6.98	1.29	7.46	1.51	18.5	11.5	2.87E-03	0.0026496
		1	8	1132	76	ND	0.0	7.1	0.2	6.8	2.50	0.37	16.07	0.35	139.8	14.7	0.1287	0.1091
		2	15	1089	492	ND	0.1	8.0	0.5	7.0	0.29	0.29	14.65	1.21	NM	NM	NM	NM
		3	22	1425	503	ND	0.4	5.5	1.0	6.9	0.29	0.29	17.15	0.66	112.2	19.4	0.0215	0.011
		4	29	2926	2350	22.0	1.0	8.5	2.4	7.0	0.29	0.29	13.68	4.21	NM	NM	NM	NM

NM-not measured, ND-not detected, DQ- Detectable but not quantifiable, N/A-not applicable, Theoretical Quantification Limits- Fe(μM) 1, Zn(μM) 0.7, SO4(mM) 0.3, Lactate(mM) 0.08, Acetate(mM) 0.16, Total DNA(ng/g sediment) 2

APPENDIX C

SCHEMATIC OF ANAEROBIC CONTINUOUS SEQUENTIAL EXTRACTOR

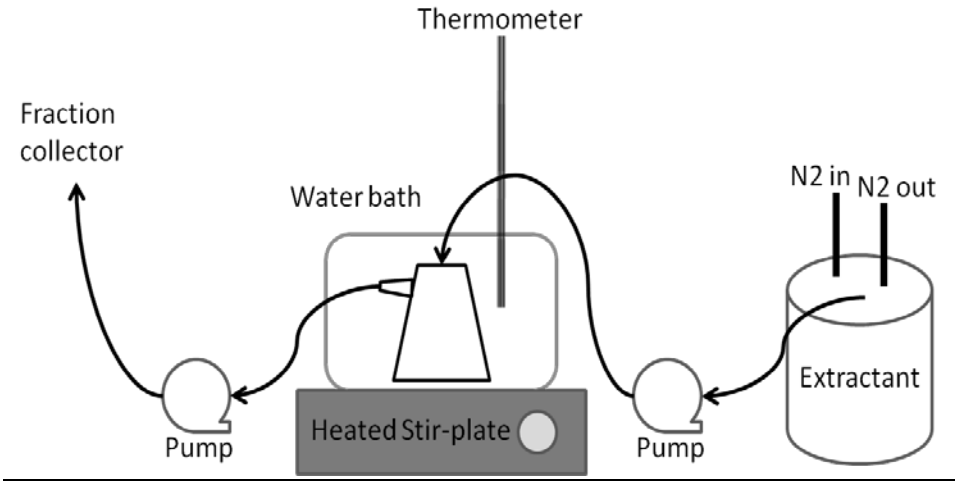

Figure 26: Experimental setup for continuous sequential extractions under anaerobic conditions

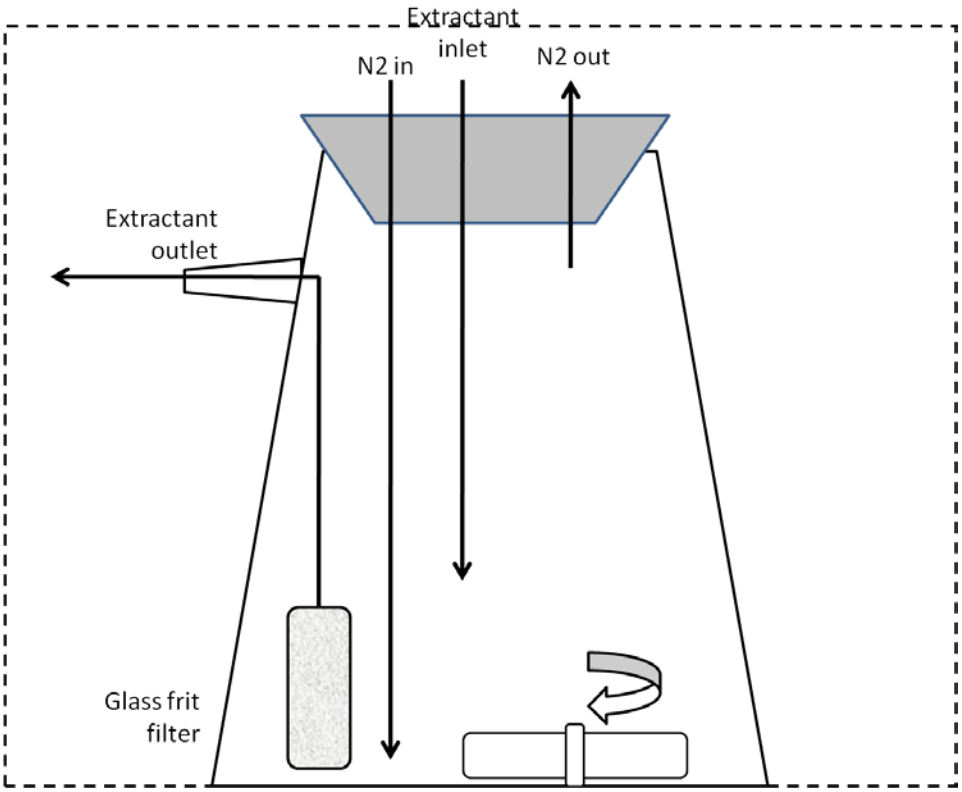

Figure 27: Schematic of extraction chamber showing anaerobic gassing setup

APPENDIX D

FIELD EMISSION SCANNING ELECTRON MICROSCOPY AND ENERGY DISPERSIVE X-RAY ANALYSIS OF BATCH CULTURES OF *GEOBACTER* SP. CDA-2 AND *DESULFOVIBRIO VULGARIS HILDENBOUGH*

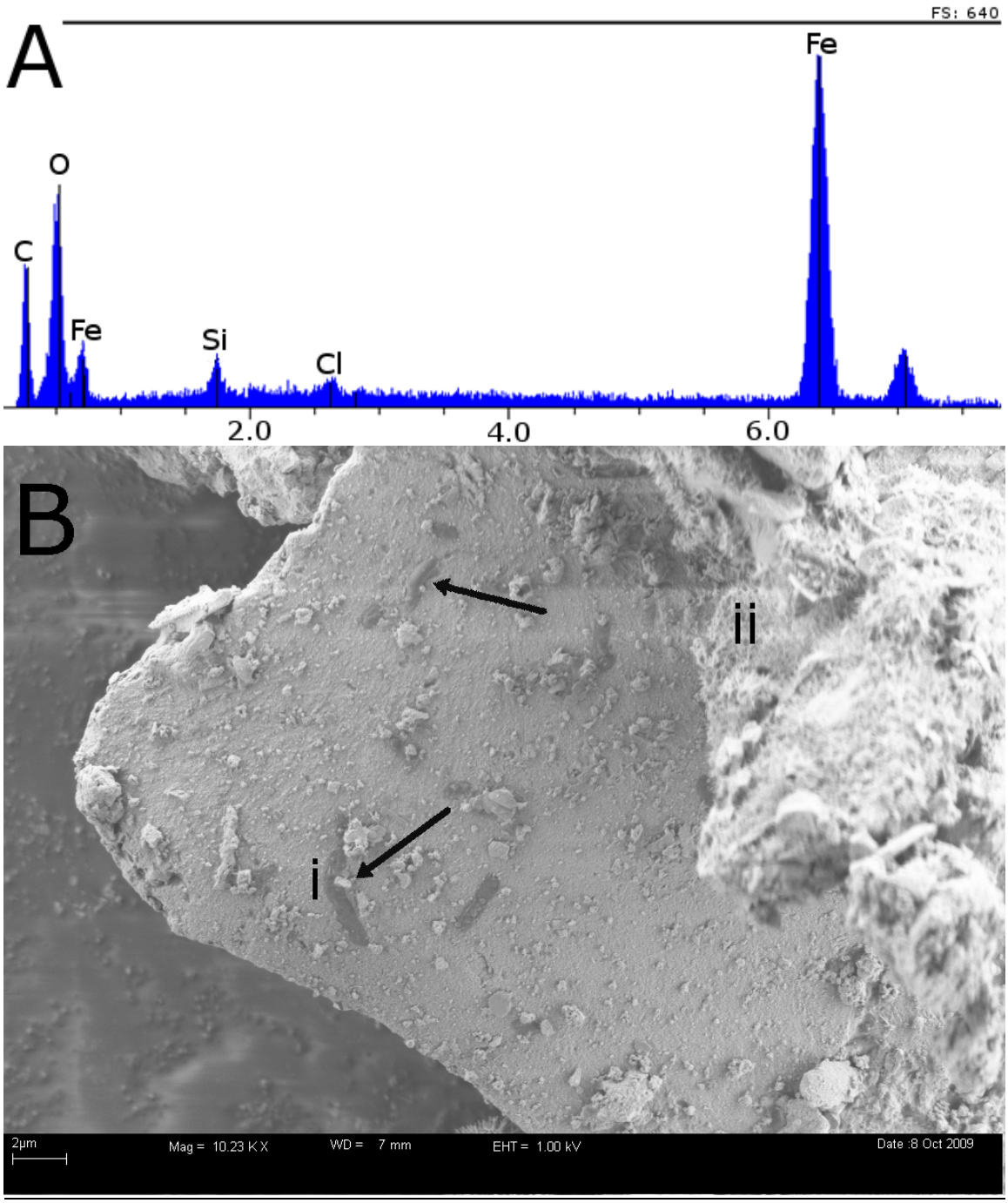

Figure 28: A) Energy dispersive X-Ray spectroscopy of *Geobacter* sp. CDA-2 high sulfate treatments B) Field emission scanning electron microscopy image of *Geobacter* sp. CDA-2 high sulfate treatments showing i) *Geobacter* sp. CDA-2 cells (arrows), ii) minor formation of unknown (probably hematite) secondary mineral

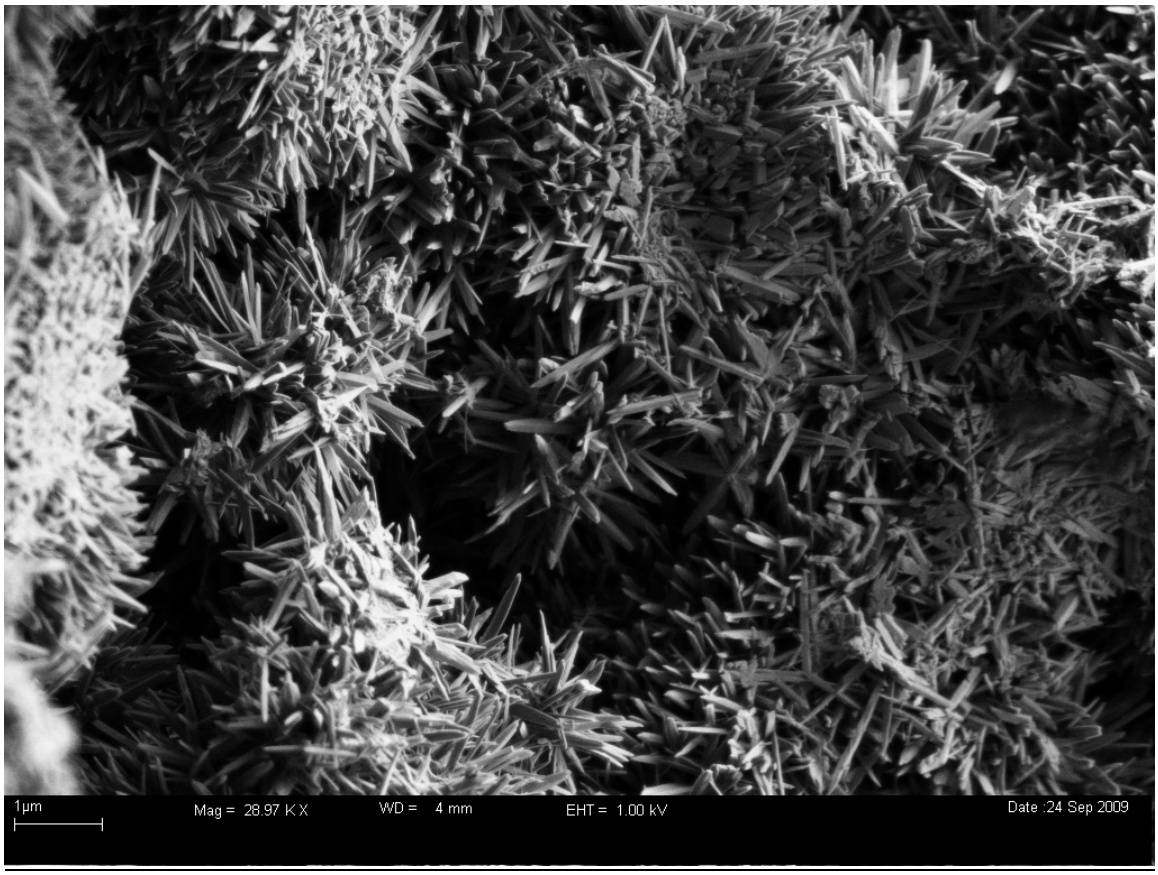

Figure 29: Field emission scanning electron microscopy image of mineral (probably hematite) formed under sulfate reducing bacteria treatments

APPENDIX E

EXPERIMENTAL DATA OF GROWTH OF *ARTHROBACTER* SP JM018 ON INORGANIC PHOSPHATE, PH 6-8, WITHOUT ZINC

Table 10: Growth of *Arthrobacter* sp JM018 on inorganic phosphate, pH 6, without zinc

Time (hrs)	O.D. (600nm)	O.D. (600nm)	O.D. (600nm)	Average	95% confidence intervals
0	0.012	0.011	0.012	0.012	0.001
8	0.036	0.037	0.036	0.036	0.001
16	0.072	0.089	0.068	0.076	0.013
24	0.095	0.115	0.089	0.100	0.015
32	0.104	0.122	0.1	0.109	0.013
40	0.109	0.119	0.105	0.111	0.008
48	0.108	0.115	0.104	0.109	0.006

Table 11: Growth of *Arthrobacter* sp JM018 on inorganic phosphate, pH 7, without zinc

Time (hrs)	O.D. (600nm)	O.D. (600nm)	O.D. (600nm)	Average	95% confidence intervals
0	0.01	0.009	0.01	0.010	0.001
8	0.034	0.03	0.038	0.034	0.005
16	0.057	0.039	0.047	0.048	0.010
24	0.077	0.047	0.061	0.062	0.017
32	0.094	0.055	0.072	0.074	0.022
40	0.105	0.063	0.086	0.085	0.024
48	0.111	0.083	0.1	0.098	0.016
56	0.108	0.085	0.105	0.099	0.014

Table 12: Growth of *Arthrobacter* sp JM018 on inorganic phosphate, pH 8, without zinc

Time (hrs)	O.D. (600nm)	O.D. (600nm)	O.D. (600nm)	Average	95% confidence intervals
0	0.012	0.014	0.013	0.013	0.001
8	0.036	0.033	0.027	0.032	0.005
16	0.056	0.05	0.039	0.048	0.010
24	0.075	0.069	0.048	0.064	0.016
32	0.091	0.082	0.056	0.076	0.021
40	0.1	0.092	0.067	0.086	0.019
48	0.103	0.096	0.078	0.092	0.015
56	0.102	0.092	0.085	0.093	0.010

Table 13: Growth of *Arthrobacter* sp JM018 on organic phosphate, pH 6, without zinc

Time (hrs)	O.D. (600nm)	O.D. (600nm)	O.D. (600nm)	Average	95% confidence intervals
0	0.012	0.012	0.013	0.012	0.001
8	0.046	0.042	0.048	0.045	0.003
16	0.117	0.115	0.127	0.120	0.007
24	0.136	0.141	0.157	0.145	0.012
32	0.144	0.151	0.153	0.149	0.005
40	0.152	0.147	0.155	0.151	0.005
48	-	0.145	0.148	0.147	0.003

Table 14: Growth of *Arthrobacter* sp JM018 on organic phosphate, pH 7, without zinc

Time (hrs)	O.D. (600nm)	O.D. (600nm)	Average	95% confidence intervals
0	0.013	0.012	0.0125	0.001
8	0.053	0.048	0.0505	0.005
16	0.119	0.099	0.109	0.020
24	0.147	0.121	0.134	0.025
32	0.144	0.13	0.137	0.014
40	0.141	0.134	0.1375	0.007
48	0.139	0.131	0.135	0.008

Table 15: Growth of *Arthrobacter* sp JM018 on organic phosphate, pH 8, without zinc

Time (hrs)	O.D. (600nm)	O.D. (600nm)	O.D. (600nm)	Average	95% confidence intervals
0	0.013	0.015	0.013	0.014	0.001
8	0.05	0.053	0.051	0.051	0.002
16	0.087	0.096	0.099	0.094	0.007
24	0.108	0.127	0.122	0.119	0.011
32	0.119	0.138	0.134	0.130	0.011
40	0.12	0.137	0.134	0.130	0.010
48	0.12	0.135	0.132	0.129	0.009

Table 16: Growth of *Arthrobacter* sp JM018 on inorganic phosphate, pH 6, with 50 μM zinc

Time (hrs)	O.D. (600nm)	O.D. (600nm)	O.D. (600nm)	Average	95% confidence intervals
0	0.006	0.009	0.009	0.008	0.002
8	0.012	0.015	0.015	0.014	0.002
16	0.021	0.03	0.026	0.026	0.005
24	0.041	0.062	0.039	0.047	0.014
32	0.073	0.093	0.063	0.076	0.017
40	0.106	0.12	0.086	0.104	0.019
48	0.125	0.126	0.106	0.119	0.013
56	0.124	0.121	0.113	0.119	0.006

Table 17: Growth of *Arthrobacter* sp JM018 on inorganic phosphate, pH 7, with 50 μM zinc

Time (hrs)	O.D. (600nm)	O.D. (600nm)	O.D. (600nm)	Average	95% confidence intervals
0	0.007	0.011	0.008	0.009	0.002
8	0.017	0.018	0.016	0.017	0.001
16	0.035	0.034	0.035	0.035	0.001
24	0.05	0.053	0.049	0.051	0.002
32	0.057	0.054	0.059	0.057	0.003
40	0.062	0.058	0.064	0.061	0.003
48	0.067	0.062	0.068	0.066	0.004
56	0.068	0.063	0.068	0.066	0.003

Table 18: Growth of *Arthrobacter* sp JM018 on inorganic phosphate, pH 8, with 50 μM zinc

Time (hrs)	O.D. (600nm)	O.D. (600nm)	O.D. (600nm)	Average	95% confidence intervals
0	0.009	0.017	0.009	0.012	0.005
8	0.009	0.018	0.014	0.014	0.005
16	0.008	0.02	0.011	0.013	0.007
24	0.007	0.016	0.009	0.011	0.005
32	-	0.018	0.011	0.015	0.007
40	0.008	0.018	0.008	0.011	0.007
48	0.009	0.019	0.009	0.012	0.007
56	0.009	0.022	0.01	0.014	0.008

Table 19: Growth of *Arthrobacter* sp JM018 on organic phosphate, pH 6, with 50 μM zinc

Time (hrs)	O.D. (600nm)	O.D. (600nm)	O.D. (600nm)	Average	95% confidence intervals
0	0.011	0.017	0.012	0.013	0.004
8	0.017	0.016	0.017	0.017	0.001
16	0.018	0.02	0.018	0.019	0.001
24	0.024	0.028	0.021	0.024	0.004
32	0.036	0.044	0.031	0.037	0.007
40	0.065	0.087	0.052	0.068	0.020
48	0.104	0.091	-	0.098	0.013
56	0.106	0.124	0.106	0.112	0.012
66	0.119	0.122	0.12	0.120	0.002
74	0.124	0.122	0.119	0.122	0.003

Table 20: Growth of *Arthrobacter* sp JM018 on organic phosphate, pH 7, with 50 μM zinc

Time (hrs)	O.D. (600nm)	O.D. (600nm)	O.D. (600nm)	Average	95% confidence intervals
0	0.011	0.01	0.009	0.010	0.001
8	0.026	0.021	0.021	0.023	0.003
16	0.048	0.054	0.05	0.051	0.003
24	0.07	0.076	0.07	0.072	0.004
32	0.081	0.086	0.082	0.083	0.003
40	0.09	0.091	0.089	0.090	0.001
48	0.086	0.097	0.094	0.092	0.006
56	0.086	0.095	0.099	0.093	0.008

Table 21: Growth of *Arthrobacter* sp JM018 on organic phosphate, pH 8, with 50 μM zinc

Time (hrs)	O.D. (600nm)	O.D. (600nm)	O.D. (600nm)	Average	95% confidence intervals
0	0.01	0.009	0.01	0.010	0.001
8	0.013	0.013	0.012	0.013	0.001
16	0.019	0.019	0.019	0.019	0.000
24	0.024	0.025	0.024	0.024	0.001
32	0.035	0.037	0.035	0.036	0.001
40	0.053	0.063	0.054	0.057	0.006
48	0.077	0.074	0.074	0.075	0.002
56	0.08	0.085	0.085	0.083	0.003
66	0.089	0.094	0.094	0.092	0.003
74	0.099	0.092	0.097	0.096	0.004

APPENDIX F

THERMODYNAMICALLY MODELED SATURATION INDICES, CONCENTRATION, ACTIVITY, AND PERCENT AQUEOUS SPECIES OF MODIFIED METAL TOXICITY MEDIUM GENERATED USING VISUAL MINTEQ (V 2.52) UNDER DIFFERENT PH CONDITIONS (6-8)

Table 22: Geochemical modeling of modified metal toxicity medium used in *Arthrobacter* experiments with saturation indices, pH 6 50 μM zinc		
Mineral	log (Ion Activity Product)	Saturation Index
Anhydrite	-8.113	-3.753
Aragonite	-13.091	-4.755
Artinite	-6.8	-16.4
Bianchite	-8.006	-6.241
Brucite	6.848	-10.252
Ca3(PO4)2 (am1)	-38.12	-12.62
Ca3(PO4)2 (am2)	-38.12	-9.87
Ca3(PO4)2 (beta)	-38.12	-9.2
Ca4H(PO4)3:3H2O	-60.883	-12.933
CaCO3xH2O	-13.091	-5.947
CaHPO4	-22.763	-3.488
CaHPO4:2H2O	-22.763	-3.768
Calcite	-13.091	-4.611
Dolomite (disordered)	-26.74	-10.2
Dolomite (ordered)	-26.74	-9.65
Epsomite	-8.671	-6.544
Goslarite	-8.006	-5.995
Gypsum	-8.113	-3.503
Halite	-5.751	-7.301
Huntite	-54.037	-24.069
Hydromagnesite	-47.746	-38.98
Hydroxyapatite	-53.477	-9.144
Hydrozincite	-3.43	-12.13
KCl	-7.34	-8.24
Lime	7.406	-25.294
Magnesite	-13.649	-6.189
Mg(OH)2 (active)	6.848	-11.946
Mg2(OH)3Cl:4H2O	4.364	-21.636
Mg3(PO4)2	-39.792	-16.512
MgCO3:5H2O	-13.649	-9.109
MgHPO4:3H2O	-23.32	-5.145
Mirabilite	-8.356	-7.242
Natron	-13.334	-12.023
Nesquehonite	-13.649	-8.979
Periclase	6.848	-14.736

Table 22: (continued) Thermodynamic modeling of modified metal toxicity medium used in *Arthrobacter* experiments with saturation indices, pH 6 50 μM zinc		
Portlandite	7.406	-15.298
Smithsonite	-12.984	-2.084
Thenardite	-8.356	-8.678
Thermonatrite	-13.334	-13.971
Vaterite	-13.091	-5.178
Zincite	7.513	-3.717
Zincosite	-8.006	-11.936
Zn(OH)2 (am)	7.513	-4.961
Zn(OH)2 (beta)	7.513	-4.241
Zn(OH)2 (delta)	7.513	-4.331
Zn(OH)2 (epsilon)	7.513	-4.021
Zn(OH)2 (gamma)	7.513	-4.221
Zn2(OH)2SO4	-0.493	-7.993
Zn2(OH)3Cl	5.693	-9.498
Zn3(PO4)2:4H2O	-37.798	-2.378
Zn3O(SO4)2	-8.5	-27.413
Zn4(OH)6SO4	14.532	-13.868
Zn5(OH)8Cl2	18.898	-19.602
ZnCl2	-11.153	-18.203
ZnCO3	-12.984	-2.184
ZnCO3:1H2O	-12.984	-2.724
ZnSO4:1H2O	-8.006	-7.368

Table 23: Thermodynamic modeling of modified metal toxicity medium used in *Arthrobacter* experiments final concentrations, activities, and log (activity), pH 6 50 μM zinc

Species	Concentration	Activity	Log activity
Acetate-1	0.002837	0.00263	-2.58
Ca(NH3)2+2	6.8E-19	5.02E-19	-18.299
Ca+2	3.45E-05	2.54E-05	-4.594
Ca-Acetate+	1.09E-06	1.01E-06	-5.994
CaCl+	3.2E-08	2.97E-08	-7.527
CaCO3 (aq)	1.34E-10	1.35E-10	-9.871
CaH2PO4+	1.56E-08	1.45E-08	-7.84
CaHCO3+	2.38E-08	2.2E-08	-7.657
CaHPO4 (aq)	1.87E-08	1.87E-08	-7.728
CaNH3+2	8.71E-12	6.43E-12	-11.192
CaOH+	5.52E-12	5.11E-12	-11.291
CaPO4-	5.37E-11	4.98E-11	-10.303
CaSO4 (aq)	1.76E-06	1.76E-06	-5.753
Cl-1	0.000501	0.000465	-3.333
CO3-2	4.31E-09	3.19E-09	-8.497
H+1	1.08E-06	0.000001	-6
H2CO3* (aq)	0.000153	0.000153	-3.816
H2PO4-	2.74E-05	2.54E-05	-4.595
H3PO4	3.57E-09	3.57E-09	-8.447
H-Acetate (aq)	0.00015	0.00015	-3.823
HCO3-	7.33E-05	6.79E-05	-4.168
HPO4-2	2.18E-06	1.61E-06	-5.793
HSO4-	3.19E-08	2.96E-08	-7.529
K+1	0.000106	9.85E-05	-4.007
K2HPO4 (aq)	2.08E-13	2.08E-13	-12.682
K2PO4-	1.29E-18	1.2E-18	-17.922
K-Acetate (aq)	1.39E-07	1.39E-07	-6.857
KCl (aq)	2.29E-08	2.29E-08	-7.64
KH2PO4 (aq)	4.98E-09	4.99E-09	-8.302
KHPO4-	1.3E-09	1.2E-09	-8.92
KOH (aq)	1.72E-12	1.72E-12	-11.764
KPO4-2	2.44E-15	1.8E-15	-14.745
KSO4-	2.28E-07	2.11E-07	-6.676
Mg(NH3)2+2	3.76E-19	2.78E-19	-18.557
Mg+2	9.55E-06	7.05E-06	-5.152

Table 23: (continued) Thermodynamic modeling of modified metal toxicity medium used in *Arthrobacter* experiments final concentrations, activities, and log (activity), pH 6 50 μM zinc			
Mg2CO3+2	8.34E-16	6.16E-16	-15.21
Mg-Acetate+	3.64E-07	3.37E-07	-6.472
MgCl+	1.41E-08	1.3E-08	-7.885
MgCO3 (aq)	1.87E-11	1.87E-11	-10.729
MgHCO3+	5.3E-09	4.91E-09	-8.309
MgHPO4 (aq)	7.15E-09	7.16E-09	-8.145
MgOH+	2.91E-11	2.7E-11	-10.569
MgPO4-	2.33E-13	2.16E-13	-12.666
MgSO4 (aq)	3.88E-07	3.88E-07	-6.411
Na+1	0.004115	0.003815	-2.419
Na2HPO4 (aq)	2.06E-10	2.06E-10	-9.685
Na2PO4-	4.14E-15	3.84E-15	-14.415
Na-Acetate (aq)	7.6E-06	7.61E-06	-5.119
NaCl (aq)	8.87E-07	8.88E-07	-6.051
NaCO3-	2.44E-10	2.26E-10	-9.645
NaH2PO4 (aq)	1.93E-07	1.93E-07	-6.714
NaHCO3 (aq)	1.3E-07	1.3E-07	-6.886
NaHPO4-	7.78E-08	7.21E-08	-7.142
NaOH (aq)	4.83E-11	4.84E-11	-10.316
NaPO4-2	9.44E-14	6.97E-14	-13.157
NaSO4-	6.85E-06	6.35E-06	-5.198
NH3 (aq)	1.58E-07	1.58E-07	-6.801
NH4+1	0.000299	0.000277	-3.557
NH4SO4-	9.69E-07	8.99E-07	-6.046
OH-	1.09E-08	1.01E-08	-7.997
PO4-3	1.34E-12	6.79E-13	-12.168
SO4-2	0.00041	0.000303	-3.519
Zn-(Acetate)2 (aq)	1.83E-08	1.83E-08	-7.737
Zn(CO3)2-2	8.93E-15	6.59E-15	-14.181
Zn(NH3)2+2	3.46E-14	2.56E-14	-13.592
Zn(NH3)3+2	1.27E-18	9.34E-19	-18.03
Zn(NH3)4+2	2.11E-23	1.56E-23	-22.807
Zn(OH)2 (aq)	4.15E-10	4.16E-10	-9.381
Zn(OH)3-	1.43E-15	1.32E-15	-14.878
Zn(OH)4-2	2.86E-22	2.11E-22	-21.675
Zn(SO4)2-2	7.7E-09	5.69E-09	-8.245
Zn+2	4.41E-05	3.26E-05	-4.487

Table 23: (continued) Thermodynamic modeling of modified metal toxicity medium used in *Arthrobacter* experiments final concentrations, activities, and log (activity), pH 6 50 μM zinc			
Zn2OH+3	2.11E-12	1.07E-12	-11.971
Zn-Acetate+	3.43E-06	3.18E-06	-5.497
ZnCl+	4.71E-08	4.36E-08	-7.36
ZnCl2 (aq)	1.98E-11	1.98E-11	-10.703
ZnCl3-	1.11E-14	1.03E-14	-13.986
ZnCl4-2	3.26E-18	2.4E-18	-17.619
ZnCO3 (aq)	5.96E-09	5.97E-09	-8.224
ZnHCO3+	7.55E-08	7E-08	-7.155
ZnHPO4 (aq)	1.08E-07	1.08E-07	-6.966
ZnNH3+2	1.14E-09	8.42E-10	-9.075
ZnOH+	3.54E-08	3.28E-08	-7.484
ZnSO4 (aq)	2.15E-06	2.16E-06	-5.666

Table 24: Thermodynamic modeling of modified metal toxicity medium used in *Arthrobacter* experiments percent aqueous species, pH 6 50 μM zinc		
Component	% of total Component concentration	Species name
NH4+1	99.624	NH4+1
	0.323	NH4SO4-
	0.053	NH3 (aq)
Ca+2	92.126	Ca+2
	0.086	CaCl+
	4.712	CaSO4 (aq)
	0.05	CaHPO4 (aq)
	0.042	CaH2PO4+
	0.063	CaHCO3+
	2.921	Ca-Acetate+
CO3-2	32.407	HCO3-
	67.485	H2CO3* (aq)
	0.033	ZnHCO3+
	0.011	CaHCO3+
	0.057	NaHCO3 (aq)
K+1	99.629	K+1
	0.13	K-Acetate (aq)
	0.021	KCl (aq)
	0.214	KSO4-
Mg+2	92.462	Mg+2
	0.136	MgCl+
	3.756	MgSO4 (aq)
	0.069	MgHPO4 (aq)
	0.051	MgHCO3+
	3.525	Mg-Acetate+
Na+1	99.619	Na+1
	0.184	Na-Acetate (aq)
	0.021	NaCl (aq)
	0.166	NaSO4-
PO4-3	7.266	HPO4-2
	91.299	H2PO4-
	0.012	H3PO4
	0.024	MgHPO4 (aq)
	0.062	CaHPO4 (aq)
	0.052	CaH2PO4+
	0.259	NaHPO4-

Table 24: (continued) Thermodynamic modeling of modified metal toxicity medium used in *Arthrobacter* experiments percent aqueous species, pH 6 50 μM zinc		
PO4-3 (cont)	0.36	ZnHPO4 (aq)
	0.017	KH2PO4 (aq)
	0.643	NaH2PO4 (aq)
SO4-2	97.065	SO4-2
	0.51	ZnSO4 (aq)
	0.092	MgSO4 (aq)
	0.417	CaSO4 (aq)
	1.621	NaSO4-
	0.054	KSO4-
	0.23	NH4SO4-
Cl-1	99.8	Cl-1
	0.177	NaCl (aq)
Zn+2	88.225	Zn+2
	0.071	ZnOH+
	0.094	ZnCl+
	4.309	ZnSO4 (aq)
	0.015	Zn(SO4)2-2
	0.216	ZnHPO4 (aq)
	0.012	ZnCO3 (aq)
	0.151	ZnHCO3+
	6.867	Zn-Acetate+
	0.037	Zn-(Acetate)2 (aq)
Acetate-1	94.574	Acetate-1
	0.253	Na-Acetate (aq)
	5.004	H-Acetate (aq)
	0.114	Zn-Acetate+
	0.012	Mg-Acetate+
	0.036	Ca-Acetate+

Table 25: Thermodynamic modeling of modified metal toxicity medium used in *Arthrobacter* experiments with saturation indices, pH 7 50 μM zinc		
Mineral	log (Ion Activity Product)	Saturation Index
Anhydrite	-8.118	-3.758
Aragonite	-11.689	-3.353
Artinite	-3.403	-13.003
Bianchite	-8.02	-6.255
Brucite	8.844	-8.256
Ca3(PO4)2 (am1)	-34.602	-9.102
Ca3(PO4)2 (am2)	-34.602	-6.352
Ca3(PO4)2 (beta)	-34.602	-5.682
Ca4H(PO4)3:3H2O	-56.603	-8.653
CaCO3xH2O	-11.689	-4.545
CaHPO4	-22.002	-2.727
CaHPO4:2H2O	-22.002	-3.007
Calcite	-11.689	-3.21
Dolomite (disordered)	-23.937	-7.397
Dolomite (ordered)	-23.937	-6.847
Epsomite	-8.676	-6.55
Goslarite	-8.02	-6.009
Gypsum	-8.118	-3.508
Halite	-5.752	-7.302
Huntite	-48.432	-18.464
Hydromagnesite	-40.145	-31.379
Hydroxyapatite	-47.201	-2.868
Hydrozincite	5.318	-3.382
KCl	-7.341	-8.241
Lime	9.402	-23.297
Magnesite	-12.247	-4.787
Mg(OH)2 (active)	8.844	-9.95
Mg2(OH)3Cl:4H2O	7.355	-18.645
Mg3(PO4)2	-36.275	-12.995
MgCO3:5H2O	-12.247	-7.707
MgHPO4:3H2O	-22.56	-4.385
Mirabilite	-8.358	-7.244
Natron	-11.93	-10.619
Nesquehonite	-12.247	-7.577
Periclase	8.844	-12.74
Portlandite	9.402	-13.302

Table 25: (continued) Thermodynamic modeling of modified metal toxicity medium used in *Arthrobacter* experiments with saturation indices, pH 7 50 μM zinc		
Smithsonite	-11.591	-0.691
Thenardite	-8.358	-8.68
Thermonatrite	-11.93	-12.567
Vaterite	-11.689	-3.776
Zincite	9.5	-1.73
Zincosite	-8.02	-11.95
Zn(OH)2 (am)	9.5	-2.974
Zn(OH)2 (beta)	9.5	-2.254
Zn(OH)2 (delta)	9.5	-2.344
Zn(OH)2 (epsilon)	9.5	-2.034
Zn(OH)2 (gamma)	9.5	-2.234
Zn2(OH)2SO4	1.48	-6.02
Zn2(OH)3Cl	8.667	-6.524
Zn3(PO4)2:4H2O	-34.307	1.113
Zn3O(SO4)2	-6.54	-25.454
Zn4(OH)6SO4	20.48	-7.92
Zn5(OH)8Cl2	26.834	-11.666
ZnCl2	-11.166	-18.216
ZnCO3	-11.591	-0.791
ZnCO3:1H2O	-11.591	-1.331
ZnSO4:1H2O	-8.02	-7.382

Table 26: Thermodynamic modeling of modified metal toxicity medium used in *Arthrobacter* experiments final concentrations, activities, and log (activity), pH 7 50 μM zinc

Species	Concentration	Activity	Log activity
Acetate-1	0.002971	0.002752	-2.56
Ca(NH3)2+2	6.69E-17	4.92E-17	-16.308
Ca+2	3.43E-05	2.52E-05	-4.598
Ca-Acetate+	1.14E-06	1.05E-06	-5.978
CaCl+	3.18E-08	2.94E-08	-7.531
CaCO3 (aq)	3.39E-09	3.39E-09	-8.469
CaH2PO4+	9.01E-09	8.34E-09	-8.079
CaHCO3+	6E-08	5.55E-08	-7.255
CaHPO4 (aq)	1.08E-07	1.08E-07	-6.967
CaNH3+2	8.62E-11	6.34E-11	-10.198
CaOH+	5.48E-11	5.07E-11	-10.295
CaPO4-	3.1E-09	2.87E-09	-8.542
CaSO4 (aq)	1.74E-06	1.74E-06	-5.758
Cl-1	0.000501	0.000464	-3.333
CO3-2	1.1E-07	8.1E-08	-7.092
H+1	1.08E-07	1E-07	-7
H2CO3* (aq)	3.88E-05	3.88E-05	-4.411
H2PO4-	1.59E-05	1.48E-05	-4.831
H3PO4	2.07E-10	2.08E-10	-9.683
H-Acetate (aq)	1.57E-05	1.57E-05	-4.803
HCO3-	0.000187	0.000173	-3.763
HPO4-2	1.27E-05	9.35E-06	-5.029
HSO4-	3.18E-09	2.95E-09	-8.53
K+1	0.000106	9.84E-05	-4.007
K2HPO4 (aq)	1.21E-12	1.21E-12	-11.918
K2PO4-	7.5E-17	6.94E-17	-16.158
K-Acetate (aq)	1.45E-07	1.45E-07	-6.838
KCl (aq)	2.29E-08	2.29E-08	-7.641
KH2PO4 (aq)	2.89E-09	2.9E-09	-8.538
KHPO4-	7.54E-09	6.98E-09	-8.156
KOH (aq)	1.72E-11	1.72E-11	-10.764
KPO4-2	1.42E-13	1.04E-13	-12.981
KSO4-	2.27E-07	2.1E-07	-6.678
Mg(NH3)2+2	3.7E-17	2.72E-17	-16.566
Mg+2	9.5E-06	6.99E-06	-5.156

Table 26: (continued) Thermodynamic modeling of modified metal toxicity medium used in *Arthrobacter* experiments final concentrations, activities, and log (activity), pH 7 50 μM zinc			
Mg2CO3+2	2.09E-14	1.54E-14	-13.813
Mg-Acetate+	3.78E-07	3.5E-07	-6.456
MgCl+	1.39E-08	1.29E-08	-7.889
MgCO3 (aq)	4.7E-10	4.71E-10	-9.327
MgHCO3+	1.34E-08	1.24E-08	-7.907
MgHPO4 (aq)	4.12E-08	4.12E-08	-7.385
MgOH+	2.89E-10	2.67E-10	-9.573
MgPO4-	1.34E-11	1.24E-11	-10.906
MgSO4 (aq)	3.83E-07	3.84E-07	-6.416
Na+1	0.004114	0.00381	-2.419
Na2HPO4 (aq)	1.2E-09	1.2E-09	-8.922
Na2PO4-	2.41E-13	2.23E-13	-12.652
Na-Acetate (aq)	7.94E-06	7.95E-06	-5.099
NaCl (aq)	8.85E-07	8.86E-07	-6.052
NaCO3-	6.2E-09	5.75E-09	-8.241
NaH2PO4 (aq)	1.12E-07	1.12E-07	-6.95
NaHCO3 (aq)	3.29E-07	3.3E-07	-6.482
NaHPO4-	4.52E-07	4.19E-07	-6.378
NaOH (aq)	4.82E-10	4.83E-10	-9.316
NaPO4-2	5.5E-12	4.05E-12	-11.393
NaSO4-	6.82E-06	6.32E-06	-5.199
NH3 (aq)	1.57E-06	1.57E-06	-5.804
NH4+1	0.000297	0.000275	-3.56
NH4SO4-	9.62E-07	8.91E-07	-6.05
OH-	1.09E-07	1.01E-07	-6.997
PO4-3	7.87E-11	3.94E-11	-10.404
SO4-2	0.00041	0.000302	-3.52
Zn-(Acetate)2 (aq)	1.94E-08	1.95E-08	-7.711
Zn(CO3)2-2	5.63E-12	4.14E-12	-11.383
Zn(NH3)2+2	3.34E-12	2.46E-12	-11.61
Zn(NH3)3+2	1.21E-15	8.92E-16	-15.05
Zn(NH3)4+2	2.01E-19	1.48E-19	-18.829
Zn(OH)2 (aq)	4.03E-08	4.04E-08	-7.394
Zn(OH)3-	1.39E-12	1.29E-12	-11.891
Zn(OH)4-2	2.79E-18	2.05E-18	-17.688
Zn(SO4)2-2	7.46E-09	5.49E-09	-8.261
Zn+2	4.3E-05	3.16E-05	-4.5

Table 26: (continued) Thermodynamic modeling of modified metal toxicity medium used in *Arthrobacter* experiments final concentrations, activities, and log (activity), pH 7 50 μM zinc			
Zn2OH+3	2.01E-11	1.01E-11	-10.997
Zn-Acetate+	3.49E-06	3.23E-06	-5.49
ZnCl+	4.57E-08	4.23E-08	-7.373
ZnCl2 (aq)	1.92E-11	1.92E-11	-10.716
ZnCl3-	1.08E-14	1E-14	-14
ZnCl4-2	3.16E-18	2.33E-18	-17.633
ZnCO3 (aq)	1.47E-07	1.47E-07	-6.831
ZnHCO3+	1.87E-07	1.73E-07	-6.762
ZnHPO4 (aq)	6.11E-07	6.11E-07	-6.214
ZnNH3+2	1.11E-08	8.13E-09	-8.09
ZnOH+	3.44E-07	3.19E-07	-6.497
ZnSO4 (aq)	2.09E-06	2.09E-06	-5.68

Table 27: Thermodynamic modeling of modified metal toxicity medium used in *Arthrobacter* experiments percent aqueous species, pH 7 50 μM zinc		
Component	% of total Component concentration	Species name
NH4+1	99.153	NH4+1
	0.321	NH4SO4-
	0.523	NH3 (aq)
Ca+2	91.732	Ca+2
	0.085	CaCl+
	4.658	CaSO4 (aq)
	0.288	CaHPO4 (aq)
	0.024	CaH2PO4+
	0.16	CaHCO3+
	3.035	Ca-Acetate+
CO3-2	0.049	CO3-2
	82.465	HCO3-
	17.156	H2CO3* (aq)
	0.065	ZnCO3 (aq)
	0.083	ZnHCO3+
	0.027	CaHCO3+
	0.146	NaHCO3 (aq)
K+1	99.62	K+1
	0.136	K-Acetate (aq)
	0.021	KCl (aq)
	0.213	KSO4-
Mg+2	91.962	Mg+2
	0.135	MgCl+
	3.71	MgSO4 (aq)
	0.399	MgHPO4 (aq)
	0.129	MgHCO3+
	3.657	Mg-Acetate+
Na+1	99.599	Na+1
	0.192	Na-Acetate (aq)
	0.021	NaCl (aq)
	0.165	NaSO4-
	0.011	NaHPO4-
PO4-3	42.389	HPO4-2
	53.118	H2PO4-
	0.137	MgHPO4 (aq)
	0.359	CaHPO4 (aq)

Table 27: (continued) Thermodynamic modeling of modified metal toxicity medium used in *Arthrobacter* experiments percent aqueous species, pH 7 50 μM zinc		
PO4-3 (cont)	0.01	CaPO4-
	0.03	CaH2PO4+
	1.507	NaHPO4-
	0.025	KHPO4-
	2.035	ZnHPO4 (aq)
	0.374	NaH2PO4 (aq)
SO4-2	97.102	SO4-2
	0.494	ZnSO4 (aq)
	0.091	MgSO4 (aq)
	0.413	CaSO4 (aq)
	1.615	NaSO4-
	0.054	KSO4-
	0.228	NH4SO4-
Cl-1	99.801	Cl-1
	0.176	NaCl (aq)
Zn+2	86.018	Zn+2
	0.688	ZnOH+
	0.081	Zn(OH)2 (aq)
	0.091	ZnCl+
	4.172	ZnSO4 (aq)
	0.015	Zn(SO4)2-2
	0.022	ZnNH3+2
	1.221	ZnHPO4 (aq)
	0.295	ZnCO3 (aq)
	0.373	ZnHCO3+
	6.985	Zn-Acetate+
	0.039	Zn-(Acetate)2 (aq)
Acetate-1	99.039	Acetate-1
	0.265	Na-Acetate (aq)
	0.524	H-Acetate (aq)
	0.116	Zn-Acetate+
	0.013	Mg-Acetate+
	0.038	Ca-Acetate+

Table 28: Thermodynamic modeling of modified metal toxicity medium used in *Arthrobacter* experiments with saturation indices, pH 8 50 μM zinc		
Mineral	log (Ion Activity Product)	Saturation Index
Anhydrite	-8.121	-3.761
Aragonite	-10.624	-2.288
Artinite	-0.34	-9.94
Bianchite	-8.095	-6.33
Brucite	10.842	-6.258
Ca3(PO4)2 (am1)	-32.035	-6.535
Ca3(PO4)2 (am2)	-32.035	-3.785
Ca3(PO4)2 (beta)	-32.035	-3.115
Ca4H(PO4)3:3H2O	-53.752	-5.802
CaCO3xH2O	-10.624	-3.48
CaHPO4	-21.717	-2.442
CaHPO4:2H2O	-21.717	-2.722
Calcite	-10.624	-2.144
Dolomite (disordered)	-21.806	-5.266
Dolomite (ordered)	-21.806	-4.716
Epsomite	-8.678	-6.552
Goslarite	-8.095	-6.084
Gypsum	-8.121	-3.511
Halite	-5.753	-7.303
Huntite	-44.17	-14.202
Hydromagnesite	-33.885	-25.119
Hydroxyapatite	-42.353	1.98
Hydrozincite	13.079	4.379
KCl	-7.341	-8.241
Lime	11.4	-21.3
Magnesite	-11.182	-3.722
Mg(OH)2 (active)	10.842	-7.952
Mg2(OH)3Cl:4H2O	10.35	-15.65
Mg3(PO4)2	-33.708	-10.428
MgCO3:5H2O	-11.182	-6.642
MgHPO4:3H2O	-22.275	-4.1
Mirabilite	-8.359	-7.245
Natron	-10.862	-9.551
Nesquehonite	-11.182	-6.512
Periclase	10.842	-10.742
Portlandite	11.4	-11.304

Table 28: (continued) Thermodynamic modeling of modified metal toxicity medium used in *Arthrobacter* experiments with saturation indices, pH 8 50 μM zinc		
Smithsonite	-10.598	0.302
Thenardite	-8.359	-8.68
Thermonatrite	-10.862	-11.499
Vaterite	-10.624	-2.711
Zincite	11.425	0.195
Zincosite	-8.095	-12.025
Zn(OH)2 (am)	11.425	-1.049
Zn(OH)2 (beta)	11.425	-0.329
Zn(OH)2 (delta)	11.425	-0.419
Zn(OH)2 (epsilon)	11.425	-0.109
Zn(OH)2 (gamma)	11.425	-0.309
Zn2(OH)2SO4	3.33	-4.17
Zn2(OH)3Cl	11.517	-3.674
Zn3(PO4)2:4H2O	-31.958	3.462
Zn3O(SO4)2	-4.765	-23.678
Zn4(OH)6SO4	26.181	-2.219
Zn5(OH)8Cl2	34.46	-4.04
ZnCl2	-11.242	-18.292
ZnCO3	-10.598	0.202
ZnCO3:1H2O	-10.598	-0.338
ZnSO4:1H2O	-8.095	-7.457

Table 29: Thermodynamic modeling of modified metal toxicity medium used in *Arthrobacter* experiments final concentrations, activities, and log (activity), pH 8 50 μM zinc

Species	Concentration	Activity	Log activity
Acetate-1	0.002986	0.002765	-2.558
Ca(NH3)2+2	6.07E-15	4.46E-15	-14.351
Ca+2	3.41E-05	2.51E-05	-4.6
Ca-Acetate+	1.13E-06	1.05E-06	-5.979
CaCl+	3.16E-08	2.92E-08	-7.534
CaCO3 (aq)	3.94E-08	3.94E-08	-7.404
CaH2PO4+	1.73E-09	1.61E-09	-8.794
CaHCO3+	6.97E-08	6.45E-08	-7.19
CaHPO4 (aq)	2.08E-07	2.08E-07	-6.682
CaNH3+2	8.19E-10	6.02E-10	-9.221
CaOH+	5.44E-10	5.04E-10	-9.297
CaPO4-	5.97E-08	5.53E-08	-7.257
CaSO4 (aq)	1.73E-06	1.73E-06	-5.761
Cl-1	0.000501	0.000464	-3.333
CO3-2	1.29E-06	9.47E-07	-6.024
H+1	1.08E-08	1E-08	-8
H2CO3* (aq)	4.54E-06	4.54E-06	-5.343
H2PO4-	3.09E-06	2.86E-06	-5.544
H3PO4	4.01E-12	4.02E-12	-11.396
H-Acetate (aq)	1.58E-06	1.58E-06	-5.801
HCO3-	0.000218	0.000202	-3.695
HPO4-2	2.47E-05	1.81E-05	-4.742
HSO4-	3.19E-10	2.95E-10	-9.53
K+1	0.000106	9.83E-05	-4.007
K2HPO4 (aq)	2.33E-12	2.34E-12	-11.631
K2PO4-	1.45E-15	1.34E-15	-14.871
K-Acetate (aq)	1.46E-07	1.46E-07	-6.836
KCl (aq)	2.28E-08	2.29E-08	-7.641
KH2PO4 (aq)	5.6E-10	5.61E-10	-9.251
KHPO4-	1.46E-08	1.35E-08	-7.869
KOH (aq)	1.72E-10	1.72E-10	-9.764
KPO4-2	2.75E-12	2.02E-12	-11.694
KSO4-	2.27E-07	2.1E-07	-6.678
Mg(NH3)2+2	3.35E-15	2.46E-15	-14.608
Mg+2	9.45E-06	6.95E-06	-5.158

Table 29: (continued) Thermodynamic modeling of modified metal toxicity medium used in *Arthrobacter* experiments final concentrations, activities, and log (activity), pH 8 50 μM zinc			
Mg2CO3+2	2.42E-13	1.78E-13	-12.75
Mg-Acetate+	3.78E-07	3.5E-07	-6.456
MgCl+	1.39E-08	1.28E-08	-7.892
MgCO3 (aq)	5.47E-09	5.47E-09	-8.262
MgHCO3+	1.55E-08	1.44E-08	-7.842
MgHPO4 (aq)	7.94E-08	7.94E-08	-7.1
MgOH+	2.87E-09	2.66E-09	-8.575
MgPO4-	2.59E-10	2.39E-10	-9.621
MgSO4 (aq)	3.81E-07	3.82E-07	-6.418
Na+1	0.004114	0.003809	-2.419
Na2HPO4 (aq)	2.31E-09	2.32E-09	-8.635
Na2PO4-	4.66E-12	4.31E-12	-11.365
Na-Acetate (aq)	7.98E-06	7.99E-06	-5.098
NaCl (aq)	8.85E-07	8.86E-07	-6.053
NaCO3-	7.25E-08	6.72E-08	-7.173
NaH2PO4 (aq)	2.17E-08	2.17E-08	-7.663
NaHCO3 (aq)	3.85E-07	3.86E-07	-6.414
NaHPO4-	8.76E-07	8.11E-07	-6.091
NaOH (aq)	4.82E-09	4.83E-09	-8.316
NaPO4-2	1.07E-10	7.83E-11	-10.106
NaSO4-	6.82E-06	6.32E-06	-5.199
NH3 (aq)	1.5E-05	1.5E-05	-4.824
NH4+1	0.000284	0.000263	-3.58
NH4SO4-	9.18E-07	8.5E-07	-6.07
OH-	1.09E-06	1.01E-06	-5.997
PO4-3	1.53E-09	7.64E-10	-9.117
SO4-2	0.000411	0.000302	-3.52
Zn-(Acetate)2 (aq)	1.65E-08	1.65E-08	-7.781
Zn(CO3)2-2	6.48E-10	4.76E-10	-9.322
Zn(NH3)2+2	2.56E-10	1.88E-10	-9.725
Zn(NH3)3+2	8.89E-13	6.53E-13	-12.185
Zn(NH3)4+2	1.41E-15	1.04E-15	-14.985
Zn(OH)2 (aq)	3.39E-06	3.4E-06	-5.469
Zn(OH)3-	1.17E-09	1.08E-09	-8.966
Zn(OH)4-2	2.35E-14	1.73E-14	-13.763
Zn(SO4)2-2	6.29E-09	4.62E-09	-8.335
Zn+2	3.62E-05	2.66E-05	-4.575

Table 29: (continued) Thermodynamic modeling of modified metal toxicity medium used in *Arthrobacter* experiments final concentrations, activities, and log (activity), pH 8 50 μM zinc			
Zn2OH+3	1.43E-10	7.14E-11	-10.146
Zn-Acetate+	2.95E-06	2.73E-06	-5.563
ZnCl+	3.85E-08	3.56E-08	-7.448
ZnCl2 (aq)	1.61E-11	1.62E-11	-10.792
ZnCl3-	9.09E-15	8.42E-15	-14.075
ZnCl4-2	2.66E-18	1.96E-18	-17.708
ZnCO3 (aq)	1.45E-06	1.45E-06	-5.838
ZnHCO3+	1.84E-07	1.7E-07	-6.769
ZnHPO4 (aq)	9.95E-07	9.96E-07	-6.002
ZnNH3+2	8.89E-08	6.53E-08	-7.185
ZnOH+	2.9E-06	2.68E-06	-5.572
ZnSO4 (aq)	1.76E-06	1.76E-06	-5.755

Table 30: Thermodynamic modeling of modified metal toxicity medium used in *Arthrobacter* experiments percent aqueous species, pH 8 50 μM zinc		
Component	% of total component concentration	Species name
NH4+1	94.672	NH4+1
	0.306	NH4SO4-
	0.03	ZnNH3+2
	4.992	NH3 (aq)
Ca+2	91.238	Ca+2
	0.084	CaCl+
	4.632	CaSO4 (aq)
	0.555	CaHPO4 (aq)
	0.16	CaPO4-
	0.186	CaHCO3+
	0.105	CaCO3 (aq)
	3.031	Ca-Acetate+
CO3-2	0.57	CO3-2
	96.442	HCO3-
	2.006	H2CO3* (aq)
	0.641	ZnCO3 (aq)
	0.081	ZnHCO3+
	0.031	CaHCO3+
	0.017	CaCO3 (aq)
	0.032	NaCO3-
	0.17	NaHCO3 (aq)
K+1	99.615	K+1
	0.137	K-Acetate (aq)
	0.021	KCl (aq)
	0.213	KSO4-
	0.014	KHPO4-
Mg+2	91.518	Mg+2
	0.028	MgOH+
	0.134	MgCl+
	3.69	MgSO4 (aq)
	0.768	MgHPO4 (aq)
	0.053	MgCO3 (aq)
	0.151	MgHCO3+
	3.655	Mg-Acetate+
Na+1	99.587	Na+1
	0.193	Na-Acetate (aq)
Na+1 (cont)	0.021	NaCl (aq)
	0.165	NaSO4-
	0.021	NaHPO4-
PO4-3	82.172	HPO4-2
	10.292	H2PO4-
	0.265	MgHPO4 (aq)
	0.692	CaHPO4 (aq)
	0.199	CaPO4-

Table 30: (continued) Thermodynamic modeling of modified metal toxicity medium used in *Arthrobacter* experiments percent aqueous species, pH 8 50 μM zinc		
	2.92	NaHPO4-
	0.049	KHPO4-
	3.318	ZnHPO4 (aq)
	0.072	NaH2PO4 (aq)
SO4-2	97.194	SO4-2
	0.416	ZnSO4 (aq)
	0.09	MgSO4 (aq)
	0.41	CaSO4 (aq)
	1.615	NaSO4-
	0.054	KSO4-
	0.217	NH4SO4-
Cl-1	99.803	Cl-1
	0.176	NaCl (aq)
Zn+2	72.439	Zn+2
	5.791	ZnOH+
	6.789	Zn(OH)2 (aq)
	0.077	ZnCl+
	3.512	ZnSO4 (aq)
	0.013	Zn(SO4)2-2
	0.178	ZnNH3+2
	1.991	ZnHPO4 (aq)
	2.898	ZnCO3 (aq)
	0.367	ZnHCO3+
	5.907	Zn-Acetate+
	0.033	Zn-(Acetate)2 (aq)
Acetate-1	99.527	Acetate-1
	0.266	Na-Acetate (aq)
	0.053	H-Acetate (aq)
	0.098	Zn-Acetate+
	0.013	Mg-Acetate+
	0.038	Ca-Acetate+

APPENDIX G

TABULATED AND GRAPHICAL REPRESENTATIONS OF CONTINUOUS SEQUENTIAL EXTRACTIONS PERFORMED ON SAMPLES FROM CDAR AND STJOE SITES

Table 31: Continuous Sequential Extraction Data from Sub-Core LCDA-1A (11-7-08)						
	parts per billion					
Volume (mL)	Manganese / 55	Iron / 57	Zinc / 66	Lead / 206	Lead / 207	Lead / 208
50	96.67	150.19	183.42	722.64	836.02	764.47
100	53.77	210.64	42.26	105.46	122.43	122.53
150	42.86	223.07	14.12	22.95	25.88	24.47
200	38.92	206.75	16.14	14.04	16.02	14.69
250	35.47	193.40	14.20	9.51	11.08	9.98
300	36.66	196.23	13.18	8.14	9.45	8.57
350	36.11	197.04	12.19	6.61	7.58	6.72
400	36.11	195.34	11.88	5.23	5.87	5.48
450	36.84	198.26	11.20	4.75	5.41	4.96
500	117.11	1753.88	33.51	22.41	25.13	24.00
550	226.86	2289.16	35.51	15.08	17.69	16.01
600	209.35	2012.80	20.24	8.92	9.94	9.21
650	170.07	1659.54	19.18	6.30	7.15	6.63
700	185.97	1803.14	16.83	7.05	7.76	7.24
750	135.88	1368.53	13.99	6.48	7.27	6.78
800	90.57	953.07	14.02	5.14	5.69	5.32
850	69.41	770.23	8.71	4.25	4.80	4.56
900	48.41	292.96	11.85	3.04	3.44	3.26
950	38.66	245.94	11.35	2.73	3.13	2.84
1000	28.04	176.92	27.56	1.91	2.19	2.01
1050	32.91	739.26	396.95	11.36	12.95	11.88
1100	26.49	328.63	349.22	4.74	5.28	4.83
1150	10.71	167.90	162.02	1.90	2.14	1.99
1200	6.47	85.29	59.83	0.88	1.01	0.93
1250	14.88	110.00	63.06	1.46	1.62	1.56
1300	4.84	70.12	41.20	0.71	0.85	0.74
1350	3.44	52.44	30.76	0.62	0.69	0.64
1400	2.03	36.11	23.57	0.53	0.58	0.55
1450	1.63	32.61	22.33	0.55	0.61	0.57
1500	2.71	41.17	24.97	0.80	0.82	0.77
1550	13.59	612.70	22.20	1.19	1.27	1.25

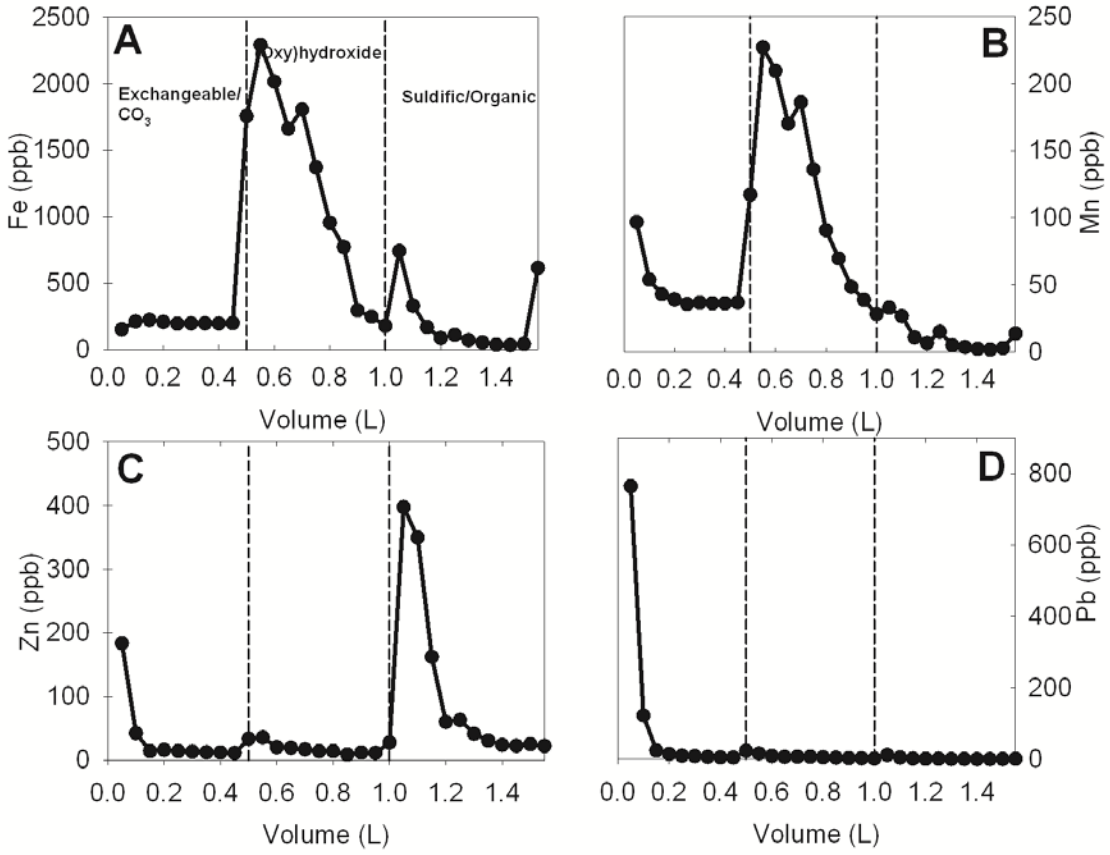

Figure 30: Extractogram of (A) Fe, (B) Mn, (C) Zn, and (D) Pb phases from CDAR 1-A from extraction date 11-7-08. Extractogram shows heavy metal phases as defined by chemical extraction

Table 32: Continuous Sequential Extraction Data from Sub-Core CDAR 1-A (11-10-08)						
	parts per billion					
Volume (mL)	Manganese / 55	Iron / 57	Zinc / 66	Lead / 206	Lead / 207	Lead / 208
50	53.84	107.03	135.97	455.57	523.22	477.52
100	41.67	145.59	52.56	185.61	214.76	195.51
150	34.76	140.78	26.37	37.20	43.45	54.48
200	39.26	168.94	22.00	32.65	37.78	34.59
250	36.38	180.18	15.13	18.15	20.56	18.95
300	36.89	182.57	12.91	12.35	13.96	12.69
350	38.88	202.26	11.65	8.96	10.34	9.45
400	40.57	206.30	11.09	7.42	8.42	7.77
450	42.51	223.64	10.95	6.75	7.69	7.15
500	55.61	460.80	20.77	13.07	14.67	13.47
550	223.27	2382.66	38.78	18.64	21.23	19.39
600	227.58	2099.46	22.76	8.63	9.85	9.00
650	179.95	1696.00	17.86	6.10	7.15	6.54
700	136.97	1343.21	14.84	4.74	5.44	4.97
750	110.61	1117.27	13.61	4.52	5.18	4.70
800	86.44	494.27	13.19	4.26	4.81	4.45
850	67.23	397.29	37.35	3.72	4.31	3.89
900	54.73	327.32	12.81	3.50	4.04	3.76
950	47.94	287.80	21.40	3.35	3.83	3.52
1000	36.01	224.29	17.58	2.78	3.18	2.94
1050	20.48	130.22	9.71	1.06	1.22	1.12
1100	23.62	422.83	482.01	21.37	25.35	23.10
1150	21.43	255.55	282.64	5.57	6.36	5.88
1200	10.94	165.98	117.84	1.79	2.00	1.82
1250	8.58	108.59	67.62	0.95	1.13	1.02
1300	7.21	83.24	39.29	0.79	0.90	0.83
1350	6.02	68.59	23.95	0.80	0.94	0.86
1400	4.15	48.10	14.50	0.63	0.69	0.64
1450	3.07	36.93	11.00	0.54	0.60	0.56
1500	2.63	31.54	8.85	0.52	0.55	0.51
1550	2.15	28.80	8.55	0.48	0.53	0.50
1600	2.39	29.07	7.99	0.52	0.59	0.55

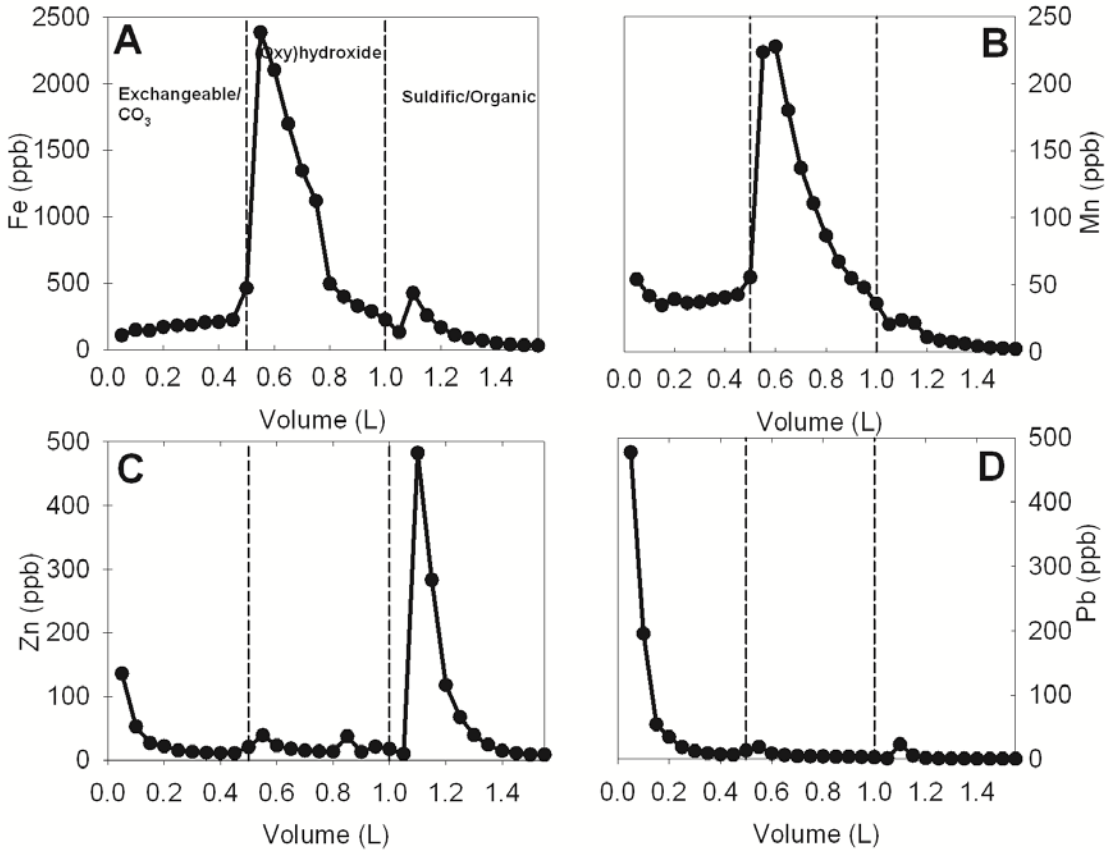

Figure 31: Extractogram of (A) Fe, (B) Mn, (C) Zn, and (D) Pb phases from CDAR 1-A from extraction date 11-10-08. Extractogram shows heavy metal phases as defined by chemical extraction

Table 33: Continuous Sequential Extraction Data from Sub-Core CDAR 1-A (11-11-08)						
	parts per billion					
Volume (mL)	Manganese / 55	Iron / 57	Zinc / 66	Lead / 206	Lead / 207	Lead / 208
50	74.13	122.31	173.34	657.85	749.46	685.72
100	45.34	166.23	50.76	174.48	198.84	181.14
150	50.52	198.50	37.44	65.33	76.87	94.16
200	45.18	200.63	24.58	34.13	38.98	47.55
250	45.25	222.21	19.44	24.10	26.99	24.27
300	45.38	240.17	16.24	14.74	17.23	15.78
350	40.76	221.34	14.49	9.09	10.43	9.51
400	38.90	207.61	11.30	6.30	7.25	6.65
450	37.19	202.14	10.35	4.96	5.74	5.29
500	40.17	224.10	10.61	4.45	5.11	4.66
550	142.39	1910.82	45.67	27.61	32.58	29.59
600	215.87	2165.48	32.80	13.72	15.55	14.41
650	257.28	2410.76	17.87	7.17	8.29	7.55
700	206.71	1959.44	11.49	4.66	5.28	4.90
750	158.79	1534.67	9.00	4.15	4.78	4.32
800	128.67	1291.87	8.87	4.23	4.93	4.53
850	92.34	961.25	7.92	4.15	4.77	4.38
900	66.97	391.16	10.91	3.27	3.79	3.46
950	58.39	339.82	9.09	2.90	3.34	3.03
1000	58.30	340.69	8.94	3.20	3.59	3.33
1050	36.72	207.88	32.47	1.81	2.02	1.89
1100	59.30	1273.76	585.93	46.93	53.76	66.26
1150	50.91	450.77	388.53	8.50	9.74	8.96
1200	41.27	291.49	142.92	2.53	2.85	2.62
1250	34.03	215.88	86.93	1.14	1.30	1.21
1300	27.70	170.71	53.99	0.79	0.90	0.83
1350	21.44	124.70	35.31	0.75	0.83	0.78
1400	9.93	102.99	22.77	0.59	0.70	0.64
1450	7.64	81.18	16.18	0.46	0.53	0.47
1500	6.06	66.67	16.51	0.40	0.44	0.41
1550	6.62	72.51	14.88	0.48	0.54	0.50
1600	33.38	191.72	28.97	1.46	1.65	1.56

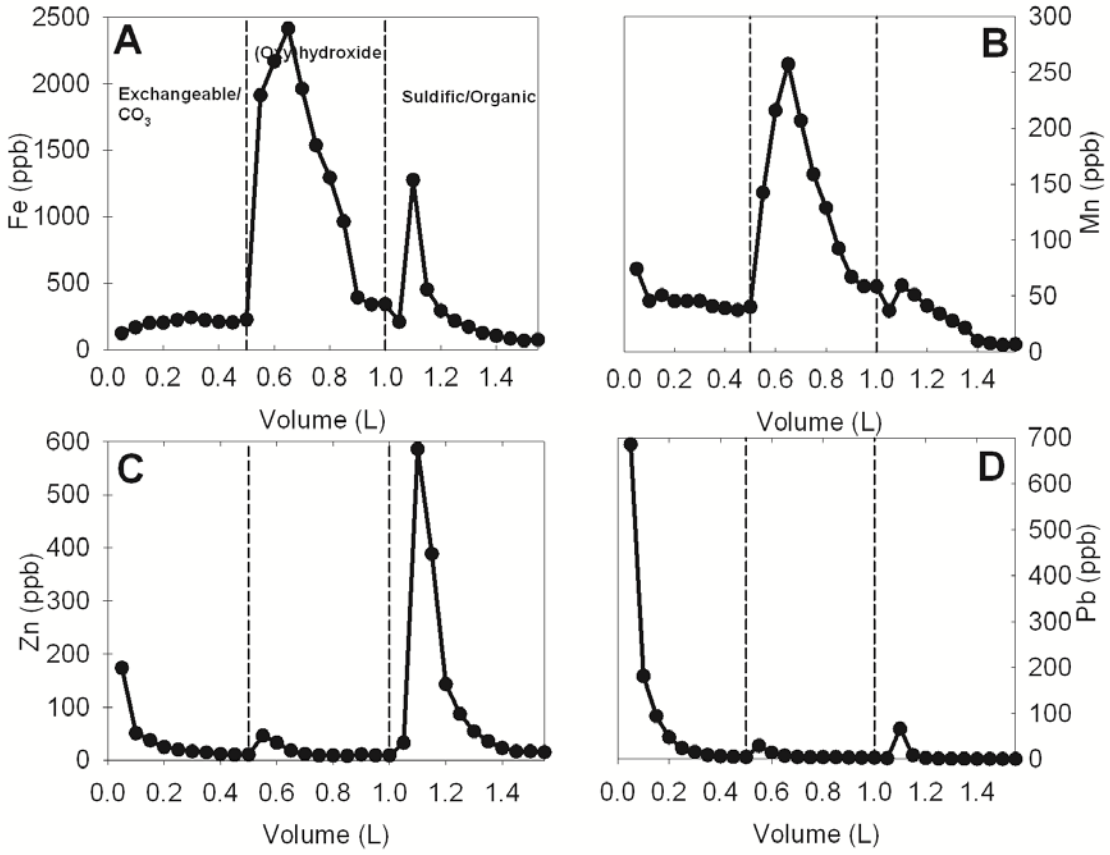

Figure 32: Extractogram of (A) Fe, (B) Mn, (C) Zn, and (D) Pb phases from CDAR 1-A from extraction date 11-11-08. Extractogram shows heavy metal phases as defined by chemical extraction

Table 34: Continuous Sequential Extraction Data from Sub-Core CDAR 1-B						
	parts per billion					
Volume (mL)	Manganese / 55	Iron / 57	Zinc / 66	Lead / 206	Lead / 207	Lead / 208
50	68.99	371.60	319.69	276.55	305.55	285.72
100	62.82	304.99	23.74	50.88	57.71	75.16
150	61.63	304.29	11.52	20.33	23.00	21.42
200	57.75	286.10	8.53	10.48	11.79	11.14
250	55.34	273.35	5.94	7.01	7.96	7.48
300	54.19	268.37	8.40	5.23	5.97	5.59
350	50.80	250.29	4.41	4.01	4.45	4.21
400	47.91	236.49	4.09	3.25	3.64	3.43
450	44.86	222.61	3.94	2.70	3.07	2.89
500	90.05	782.24	12.93	8.28	9.40	8.86
550	155.68	1502.58	12.01	8.33	9.48	8.87
600	116.99	1147.07	9.90	6.53	7.33	6.89
650	82.12	454.88	8.69	4.90	5.51	5.20
700	60.90	338.10	7.89	4.11	4.61	4.36
750	48.17	272.22	9.80	3.71	4.15	3.92
800	38.36	218.81	7.71	3.52	3.91	3.73
850	30.87	177.66	7.56	2.98	3.34	3.15
900	25.09	148.96	8.22	2.62	3.01	2.80
950	20.75	123.90	7.45	2.29	2.63	2.46
1000	9.03	93.39	13.88	1.52	1.69	1.59
1050	9.38	282.71	225.55	32.49	36.63	47.52
1100	9.16	175.78	225.59	2.66	2.96	2.80
1150	7.73	97.57	60.20	0.85	0.97	0.90
1200	5.71	0.00	34.16	0.86	0.97	0.91
1250	4.40	0.00	21.87	0.49	0.56	0.52
1300	3.33	0.00	17.41	0.51	0.57	0.54
1350	2.54	0.00	13.98	0.52	0.58	0.55
1400	2.14	0.00	12.24	0.38	0.41	0.40
1450	1.93	0.00	11.82	0.38	0.40	0.39
1500	0.00	0.00	11.07	0.35	0.40	0.38
1550	2.94	0.00	13.86	0.46	0.50	0.48

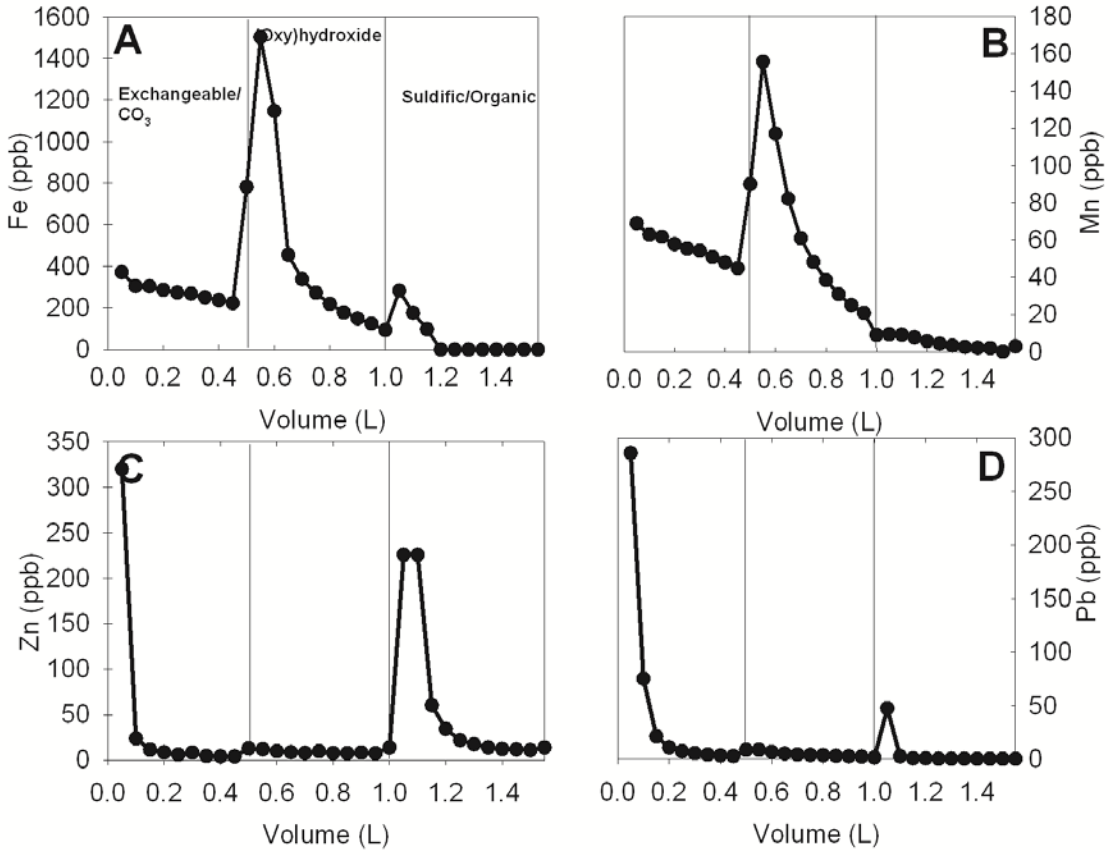

Figure 33: Extractogram of (A) Fe, (B) Mn, (C) Zn, and (D) Pb phases from CDAR 1-B. Extractogram shows heavy metal phases as defined by chemical extraction

Table 35: Continuous Sequential Extraction Data from Sub-Core CDAR 1-C						
	parts per billion					
Volume (mL)	Manganese / 55	Iron / 57	Zinc / 66	Lead / 206	Lead / 207	Lead / 208
50	71.48	296.33	93.14	802.39	901.35	847.54
100	67.86	278.00	28.94	205.74	232.18	216.44
150	50.89	232.05	16.07	47.22	53.44	69.41
200	48.15	230.95	13.34	28.42	31.83	34.01
250	48.60	234.67	8.40	16.91	19.22	17.99
300	49.91	239.37	7.04	16.01	18.10	17.07
350	45.91	223.36	5.20	11.50	12.89	12.18
400	43.23	209.36	4.66	8.69	9.83	9.22
450	42.70	208.61	4.46	7.65	8.66	8.18
500	62.07	397.22	8.23	12.62	14.32	13.45
550	202.53	1825.56	8.83	10.25	11.45	10.83
600	232.23	2033.78	6.47	6.80	7.64	7.19
650	234.09	2052.16	5.25	6.00	6.81	6.36
700	173.47	1538.61	4.28	4.93	5.54	5.23
750	131.06	1208.95	3.95	4.47	5.12	4.81
800	128.21	1206.91	0.00	5.18	5.77	5.48
850	117.25	1116.25	0.00	4.92	5.59	5.28
900	120.01	1132.66	0.00	5.49	6.19	5.83
950	100.58	945.49	0.00	5.27	5.94	5.54
1000	92.86	633.50	0.00	5.14	5.90	5.48
1050	42.91	311.58	67.96	106.91	87.25	106.56
1100	77.95	1469.37	330.59	56.29	64.45	82.65
1150	81.47	1106.11	226.88	9.08	10.31	9.78
1200	69.27	421.68	85.22	2.27	2.61	2.43
1250	55.44	300.18	50.02	0.80	0.89	0.84
1300	43.53	226.63	31.22	0.51	0.57	0.54
1350	33.94	172.87	20.59	0.44	0.50	0.48
1400	21.92	109.38	12.94	0.37	0.40	0.39
1450	10.00	84.98	10.08	0.36	0.39	0.38
1500	8.34	70.18	9.03	0.35	0.36	0.36
1550	9.93	82.74	9.57	0.39	0.44	0.42

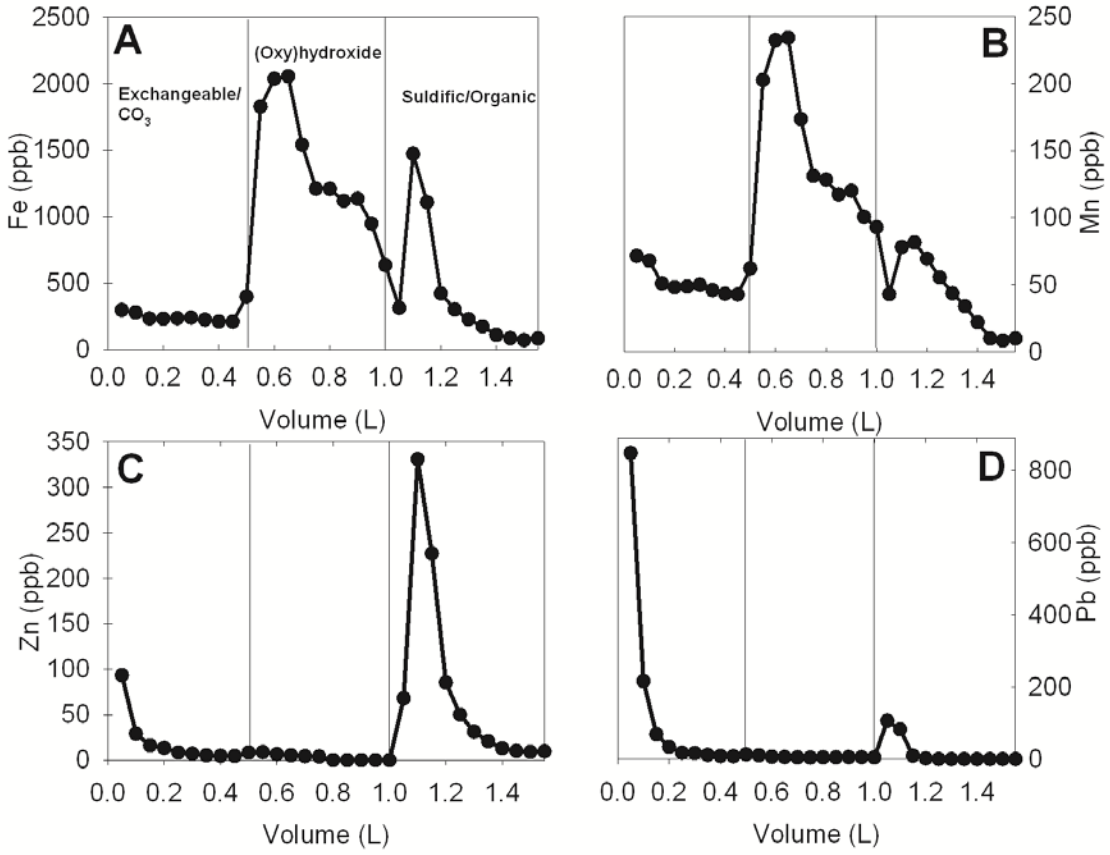

Figure 34: Extractogram of (A) Fe, (B) Mn, (C) Zn, and (D) Pb phases from CDAR 1-C. Extractogram shows heavy metal phases as defined by chemical extraction

Table 36: Continuous Sequential Extraction Data from Sub-Core CDAR 2-A						
	parts per billion					
Volume (mL)	Manganese / 55	Iron / 57	Zinc / 66	Lead / 206	Lead / 207	Lead / 208
50	120.23	1110.71	534.59	717.55	820.34	750.16
100	53.33	242.89	76.54	193.89	220.51	202.19
150	44.63	225.25	40.25	52.89	59.75	74.72
200	45.73	245.85	29.22	30.97	35.51	32.53
250	51.12	283.58	22.94	19.42	22.30	20.48
300	56.97	312.64	19.10	12.91	14.94	13.79
350	58.89	335.69	15.91	9.60	10.95	10.08
400	61.40	339.90	14.76	8.98	10.26	9.39
450	77.51	427.47	16.48	11.11	12.50	11.52
500	194.47	2082.18	41.03	26.18	29.83	27.39
550	430.84	3856.09	39.33	18.58	21.48	19.57
600	459.99	4101.46	31.18	10.27	12.00	11.05
650	362.27	3338.50	24.27	7.30	8.36	7.78
700	286.60	2689.45	22.04	6.59	7.56	6.81
750	222.68	2213.67	20.46	5.67	6.52	5.99
800	178.15	1815.62	20.48	5.12	5.77	5.31
850	138.28	1442.89	19.22	4.45	5.00	4.61
900	109.38	1180.57	19.02	3.85	4.32	4.03
950	96.24	1056.57	19.37	4.21	4.81	4.41
1000	91.83	1047.04	21.88	4.01	4.76	4.31
1050	106.10	2109.86	618.51	66.02	77.07	94.67
1100	107.73	1768.23	689.77	15.26	17.08	15.68
1150	84.39	1108.89	412.00	2.82	3.22	2.97
1200	52.34	344.64	113.87	0.79	0.91	0.84
1250	35.93	230.69	65.37	0.53	0.58	0.55
1300	27.54	174.94	44.23	0.47	0.55	0.49
1350	22.26	135.94	31.73	0.43	0.50	0.45
1400	10.43	112.52	25.74	0.40	0.46	0.42
1450	8.77	94.58	20.96	0.40	0.45	0.42
1500	7.37	79.36	19.99	0.37	0.44	0.38
1550	21.01	118.51	23.24	0.51	0.54	0.51

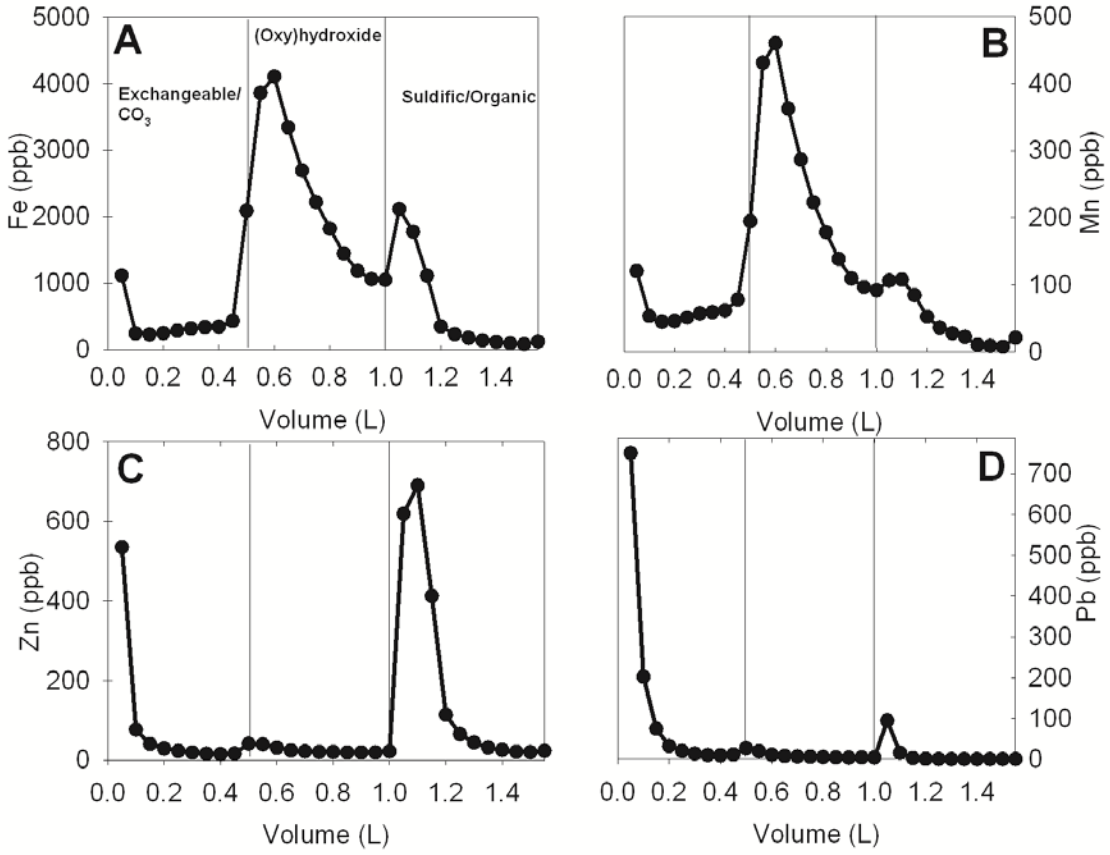

Figure 35: Extractogram of (A) Fe, (B) Mn, (C) Zn, and (D) Pb phases from CDAR 2-A. Extractogram shows heavy metal phases as defined by chemical extraction

Table 37: Continuous Sequential Extraction Data from Sub-Core CDAR 2-B						
	parts per billion					
Volume (mL)	Manganese / 55	Iron / 57	Zinc / 66	Lead / 206	Lead / 207	Lead / 208
50	80.38	436.95	231.94	668.46	748.29	704.74
100	54.56	267.01	46.01	161.75	182.07	169.59
150	42.83	225.27	24.61	33.82	38.09	49.70
200	39.41	216.94	16.65	17.64	19.85	18.58
250	45.10	247.66	13.79	12.08	13.87	12.95
300	47.28	257.85	10.67	8.63	9.78	9.20
350	49.08	267.07	8.90	6.61	7.52	7.06
400	48.39	261.17	7.38	5.39	6.21	5.78
450	46.52	249.24	6.81	4.57	5.24	4.91
500	76.45	989.55	15.66	12.07	13.67	12.85
550	139.89	1387.34	13.43	9.99	11.37	10.63
600	211.89	1979.96	10.68	6.57	7.43	6.96
650	225.98	2123.49	8.94	4.52	5.19	4.82
700	174.33	1705.24	5.74	3.19	3.62	3.42
750	156.33	1558.22	0.00	2.80	3.16	2.98
800	141.73	1437.16	0.00	2.92	3.35	3.13
850	120.86	1265.63	0.00	2.85	3.24	3.07
900	103.16	1100.44	0.00	2.71	3.07	2.90
950	88.03	943.81	0.00	2.46	2.79	2.63
1000	68.79	403.32	6.06	1.66	1.88	1.76
1050	91.72	1702.53	73.59	39.03	44.17	57.12
1100	101.81	1766.81	98.95	16.82	19.27	17.97
1150	81.57	1146.55	71.24	4.88	5.54	5.20
1200	62.24	420.17	43.19	1.17	1.37	1.26
1250	47.67	298.22	25.38	0.50	0.55	0.52
1300	38.07	238.57	15.78	0.33	0.36	0.34
1350	32.14	200.08	10.87	0.27	0.30	0.28
1400	26.67	169.65	7.69	0.24	0.27	0.25
1450	23.30	145.18	6.21	0.23	0.26	0.25
1500	14.34	122.79	0.00	0.23	0.24	0.24
1550	21.86	134.95	0.00	0.25	0.27	0.26

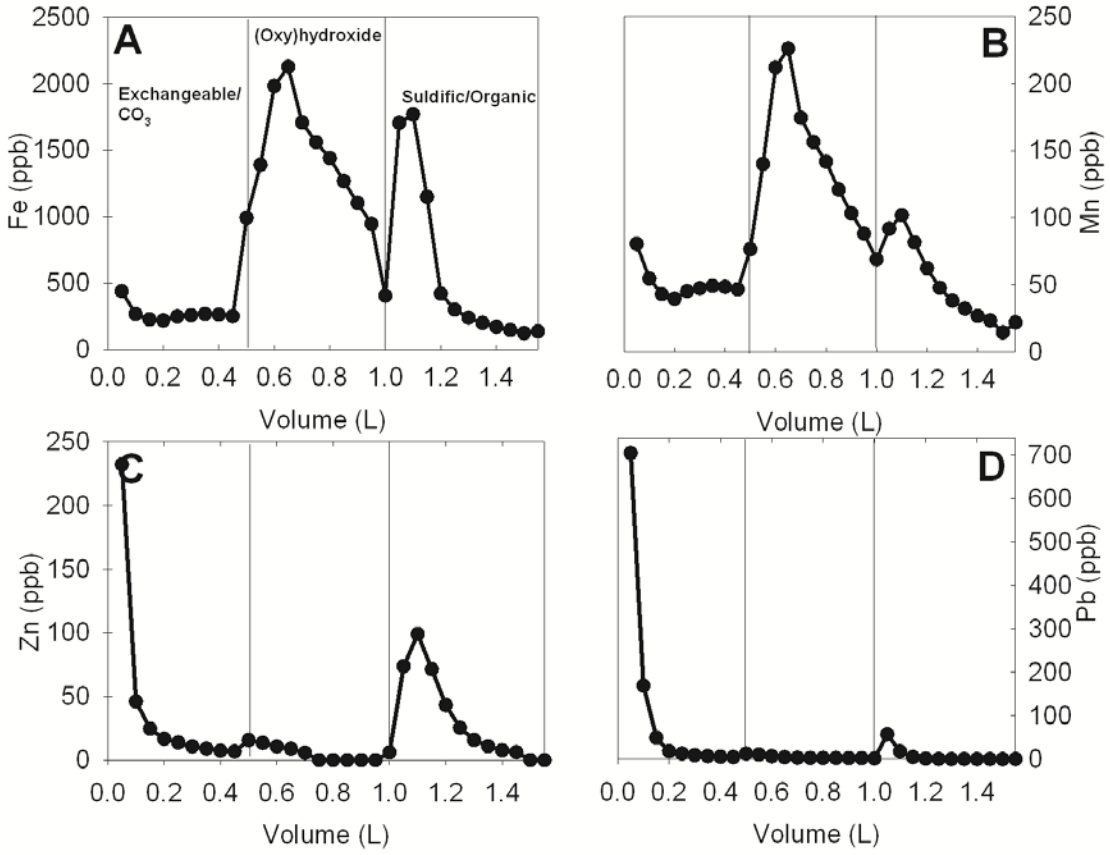

Figure 36: Extractogram of (A) Fe, (B) Mn, (C) Zn, and (D) Pb phases from CDAR 2-B. Extractogram shows heavy metal phases as defined by chemical extraction

Table 38: Continuous Sequential Extraction Data from Sub-Core CDAR 3-A						
	parts per billion					
Volume (mL)	Manganese / 55	Iron / 57	Zinc / 66	Lead / 206	Lead / 207	Lead / 208
50	39.67	227.28	101.27	244.27	277.33	257.26
100	24.40	110.47	24.21	31.70	35.81	46.53
150	21.17	94.35	10.63	9.72	10.87	10.23
200	17.29	97.82	7.76	5.62	6.41	5.96
250	24.26	130.38	7.28	4.36	4.99	4.68
300	25.04	131.87	6.33	3.22	3.64	3.44
350	27.04	142.87	5.35	2.91	3.31	3.12
400	29.39	163.88	5.69	2.57	2.93	2.74
450	33.35	176.51	6.43	2.63	3.01	2.81
500	101.97	1209.00	15.46	8.21	9.38	8.78
550	197.54	1897.06	10.99	4.80	5.43	5.12
600	183.04	1743.89	10.05	3.16	3.62	3.38
650	158.22	1527.51	0.00	1.93	2.19	2.05
700	125.60	1274.75	0.00	1.48	1.68	1.57
750	107.35	1114.12	0.00	1.24	1.42	1.33
800	87.78	798.41	0.00	1.09	1.24	1.17
850	76.47	581.69	0.00	0.91	1.03	0.97
900	69.60	413.50	0.00	0.78	0.90	0.85
950	61.88	378.10	0.00	0.80	0.89	0.84
1000	53.56	323.46	6.15	0.73	0.85	0.79
1050	37.48	277.39	26.49	6.52	7.37	6.94
1100	55.90	607.72	85.95	4.34	4.91	4.61
1150	37.95	276.51	46.62	1.46	1.65	1.55
1200	33.05	220.25	31.20	0.66	0.75	0.71
1250	30.61	192.52	20.84	0.50	0.55	0.52
1300	26.12	160.74	13.98	0.50	0.54	0.51
1350	23.39	143.33	9.71	0.45	0.47	0.46
1400	21.46	131.90	8.29	0.44	0.48	0.46
1450	10.32	106.67	6.85	0.41	0.42	0.41
1500	8.58	89.24	5.36	0.37	0.41	0.39
1550	7.71	79.54	0.00	0.38	0.41	0.40
1600	26.09	153.17	5.19	0.52	0.58	0.55

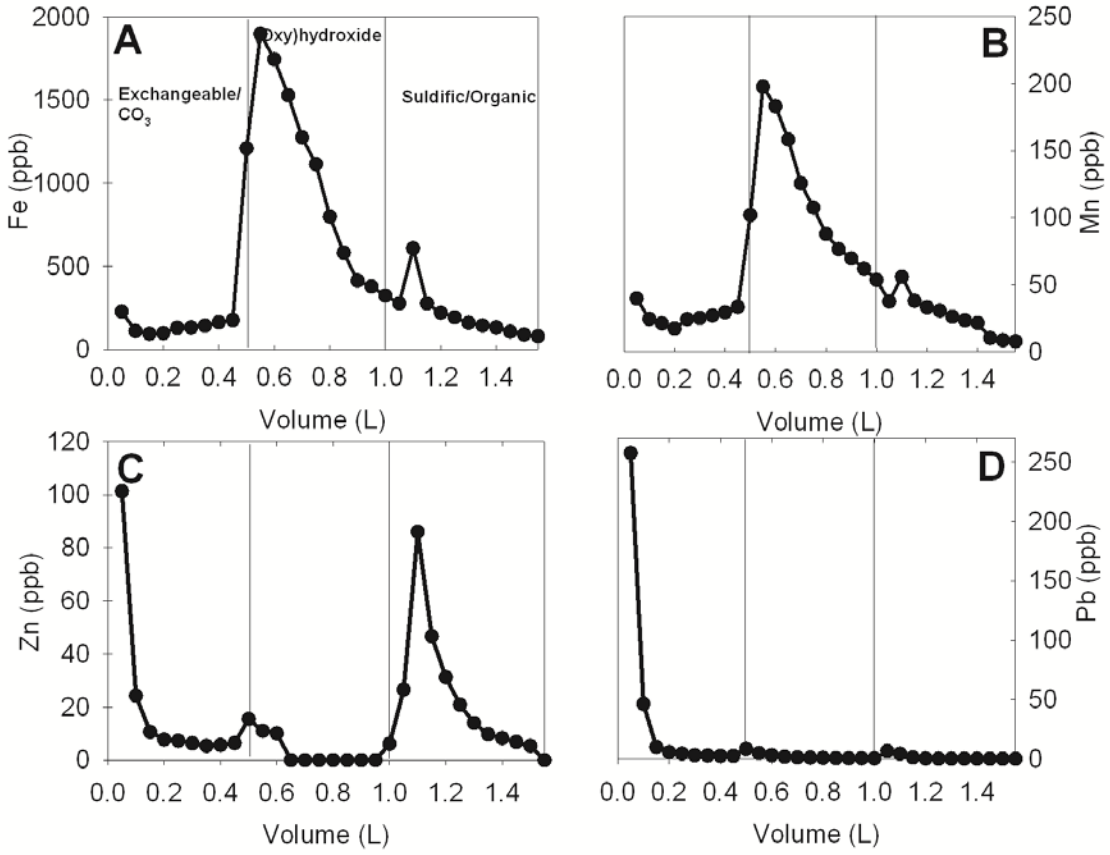

Figure 37: Extractogram of (A) Fe, (B) Mn, (C) Zn, and (D) Pb phases from CDAR 3-A. Extractogram shows heavy metal phases as defined by chemical extraction

Table 39: Continuous Sequential Extraction Data from Sub-Core CDAR 3-B						
	parts per billion					
Volume (mL)	Manganese / 55	Iron / 57	Zinc / 66	Lead / 206	Lead / 207	Lead / 208
50	63.85	246.95	109.04	462.06	519.52	486.87
100	40.52	144.67	26.55	44.55	50.41	65.36
150	38.07	145.26	17.34	21.81	24.33	22.92
200	33.52	139.89	11.97	13.16	14.83	14.07
250	34.56	160.17	10.01	9.81	11.17	10.47
300	33.86	162.10	10.30	9.16	10.35	9.86
350	33.34	162.28	7.45	9.37	10.69	10.06
400	32.28	164.80	5.69	8.03	9.03	8.51
450	33.47	178.45	0.00	5.44	6.28	5.86
500	97.40	1202.45	17.14	13.36	15.17	14.27
550	195.46	1941.96	12.75	6.16	6.98	6.55
600	215.60	2115.19	6.65	2.85	3.21	3.03
650	197.99	1980.61	0.00	1.62	1.87	1.72
700	170.55	1764.58	0.00	1.15	1.32	1.24
750	144.94	1532.41	0.00	0.99	1.12	1.05
800	114.98	1246.33	0.00	0.87	1.00	0.94
850	107.07	1172.60	0.00	0.80	0.91	0.86
900	93.97	1055.55	0.00	0.67	0.74	0.70
950	80.00	772.53	0.00	0.57	0.65	0.60
1000	58.63	369.02	0.00	0.37	0.40	0.39
1050	112.22	1809.44	59.06	7.16	8.21	7.70
1100	78.84	1139.63	52.26	2.91	3.27	3.08
1150	52.02	363.10	49.79	2.13	2.39	2.25
1200	39.48	266.35	37.91	2.01	2.27	2.13
1250	31.32	199.42	18.71	1.88	2.14	2.01
1300	25.54	162.62	14.20	1.88	2.11	2.00
1350	22.10	141.53	9.34	1.84	2.12	1.96
1400	14.03	124.52	6.59	1.91	2.16	2.03
1450	9.76	107.32	5.73	1.97	2.18	2.05
1500	8.61	94.77	0.00	1.87	2.14	2.00

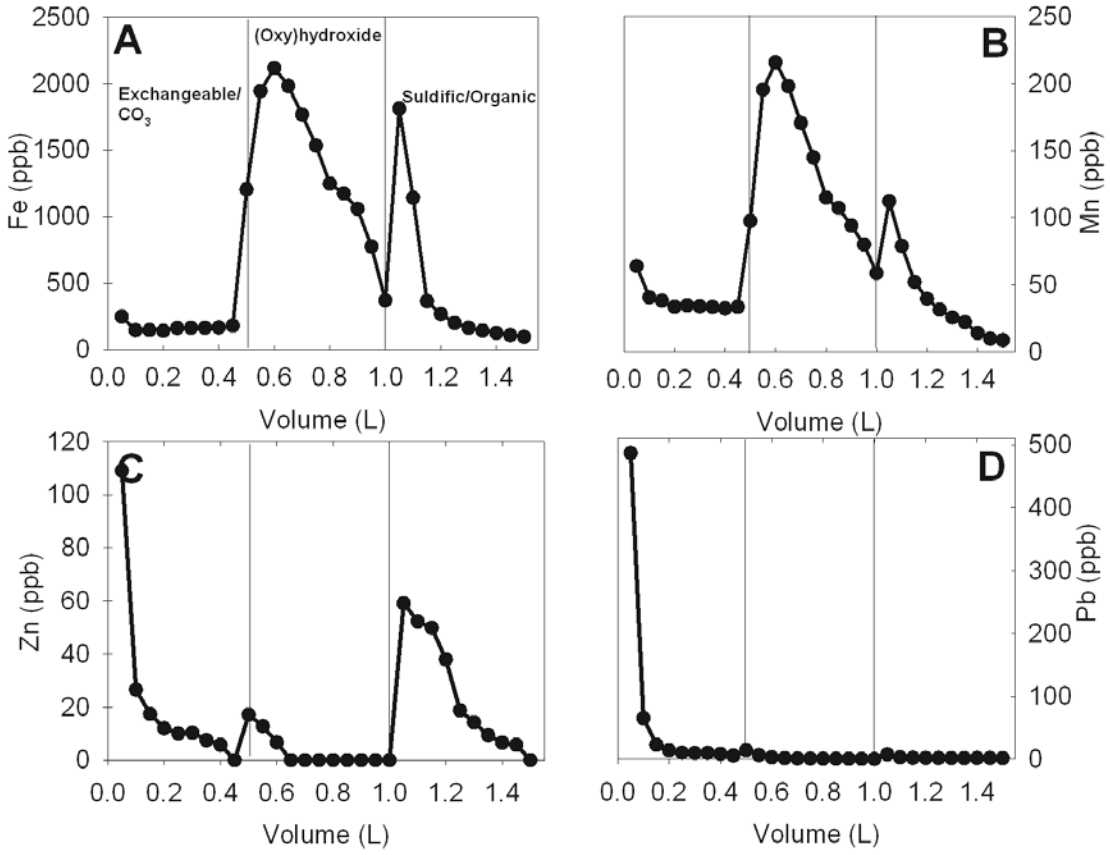

Figure 38: Extractogram of (A) Fe, (B) Mn, (C) Zn, and (D) Pb phases from CDAR 3-B. Extractogram shows heavy metal phases as defined by chemical extraction

Table 40: Continuous Sequential Extraction Data from Sub-Core STJOE 5-A						
	parts per billion					
Volume (mL)	Manganese / 55	Iron / 57	Zinc / 66	Lead / 206	Lead / 207	Lead / 208
50	2.57	0.00	13.88	0.11	0.00	0.00
100	0.00	0.00	2.47	0.00	0.00	0.00
150	0.00	0.00	2.81	0.00	0.00	0.00
200	0.52	0.00	0.00	0.09	0.08	0.09
250	0.00	0.00	0.00	0.08	0.08	0.08
300	0.00	0.00	0.00	0.08	0.08	0.08
350	0.00	0.00	0.00	0.08	0.07	0.08
400	0.00	0.00	0.00	0.07	0.08	0.08
450	0.00	0.00	0.00	0.09	0.08	0.08
500	13.39	315.40	5.27	0.42	0.43	0.43
550	5.59	172.24	0.00	0.20	0.21	0.20
600	3.11	115.32	0.00	0.15	0.16	0.15
650	1.97	80.80	0.00	0.12	0.13	0.13
700	1.53	61.91	0.00	0.12	0.12	0.12
750	1.32	52.33	0.00	0.12	0.11	0.12
800	1.33	51.91	0.00	0.12	0.11	0.12
850	1.28	39.79	0.00	0.14	0.14	0.14
900	1.27	45.71	5.95	0.13	0.13	0.13
950	0.89	43.09	0.00	0.12	0.12	0.11
1000	0.00	35.51	0.00	0.29	0.31	0.30
1050	0.00	0.00	0.00	0.30	0.32	0.31
1100	0.00	0.00	0.00	0.30	0.33	0.32
1150	0.00	0.00	0.00	0.30	0.33	0.31
1200	0.00	0.00	0.00	0.29	0.32	0.30
1250	0.00	0.00	5.93	0.30	0.31	0.31
1300	0.60	0.00	0.00	0.30	0.32	0.31
1350	0.00	0.00	0.00	0.39	0.43	0.41
1400	0.00	0.00	0.00	0.30	0.32	0.31
1450	0.00	0.00	0.00	0.29	0.32	0.31
1500	0.93	0.00	0.00	0.56	0.61	0.59

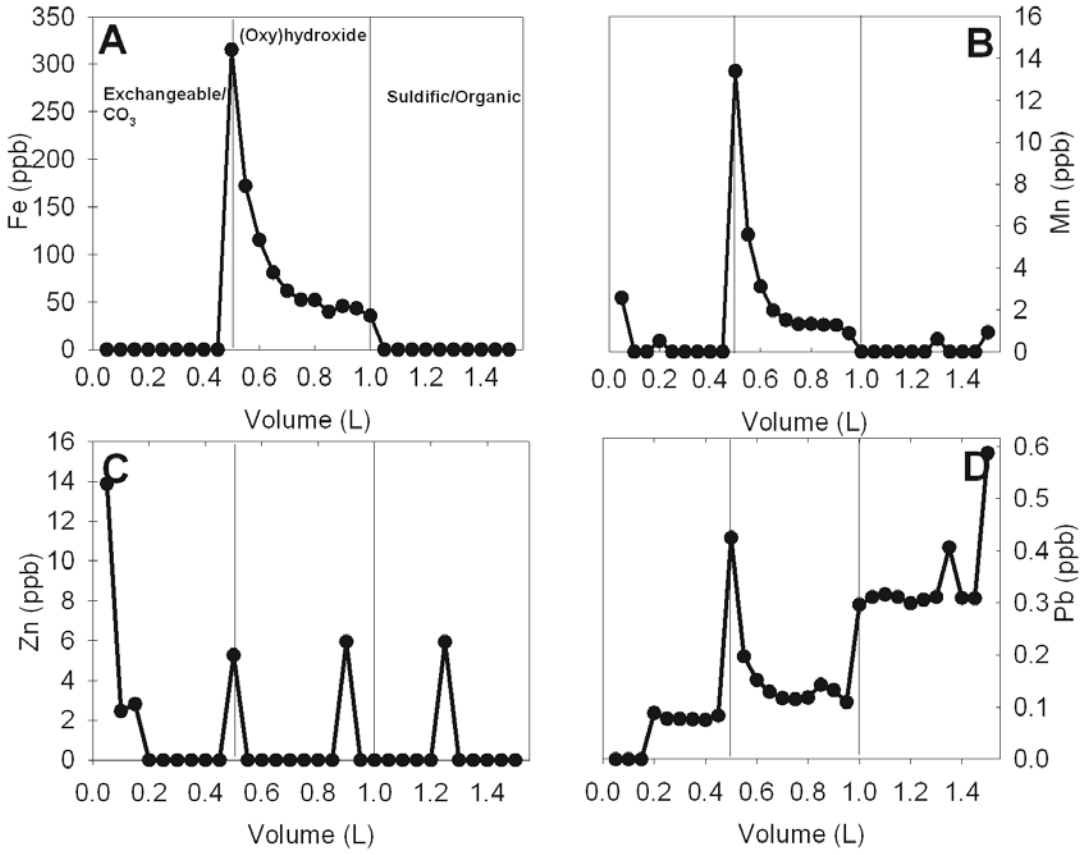

Figure 39: Extractogram of (A) Fe, (B) Mn, (C) Zn, and (D) Pb phases from STJOE 5-A. Extractogram shows heavy metal phases as defined by chemical extraction

Table 41: Continuous Sequential Extraction Data from Sub-Core STJOE 5-B						
	parts per billion					
Volume (mL)	Manganese / 55	Iron / 57	Zinc / 66	Lead / 206	Lead / 207	Lead / 208
50	4.88	0.00	39.59	0.12	0.13	0.12
100	2.13	0.00	12.56	0.19	0.22	0.21
150	0.00	0.00	4.60	0.00	0.00	0.00
200	0.55	0.00	0.00	0.05	0.05	0.05
250	0.00	0.00	0.00	0.05	0.05	0.05
300	0.00	0.00	0.00	0.03	0.00	0.03
350	0.00	0.00	0.00	0.00	0.00	0.03
400	0.00	0.00	0.00	0.03	0.00	0.03
450	0.00	0.00	0.00	0.03	0.00	0.03
500	8.29	240.70	0.00	0.42	0.43	0.42
550	5.07	207.25	0.00	0.85	0.95	0.91
600	4.61	184.76	0.00	0.28	0.31	0.30
650	2.31	128.09	0.00	0.12	0.12	0.12
700	1.23	95.08	0.00	0.08	0.08	0.08
750	0.73	73.55	0.00	0.06	0.06	0.06
800	0.49	62.14	0.00	0.06	0.05	0.06
850	0.00	51.37	0.00	0.05	0.05	0.05
900	0.00	47.50	0.00	0.04	0.04	0.04
950	0.00	45.48	6.16	0.05	0.05	0.05
1000	0.00	36.50	6.86	0.06	0.06	0.06
1050	2.58	49.19	0.00	0.46	0.51	0.49
1100	0.00	0.00	0.00	0.30	0.31	0.31
1150	0.00	0.00	0.00	0.30	0.32	0.30
1200	0.00	0.00	0.00	0.28	0.30	0.29
1250	0.00	0.00	0.00	0.27	0.31	0.29
1300	0.00	0.00	0.00	0.27	0.29	0.28
1350	0.00	0.00	0.00	0.29	0.30	0.29
1400	0.00	0.00	0.00	0.27	0.29	0.29
1450	0.00	0.00	0.00	0.30	0.32	0.30
1500	0.00	0.00	0.00	0.26	0.30	0.28

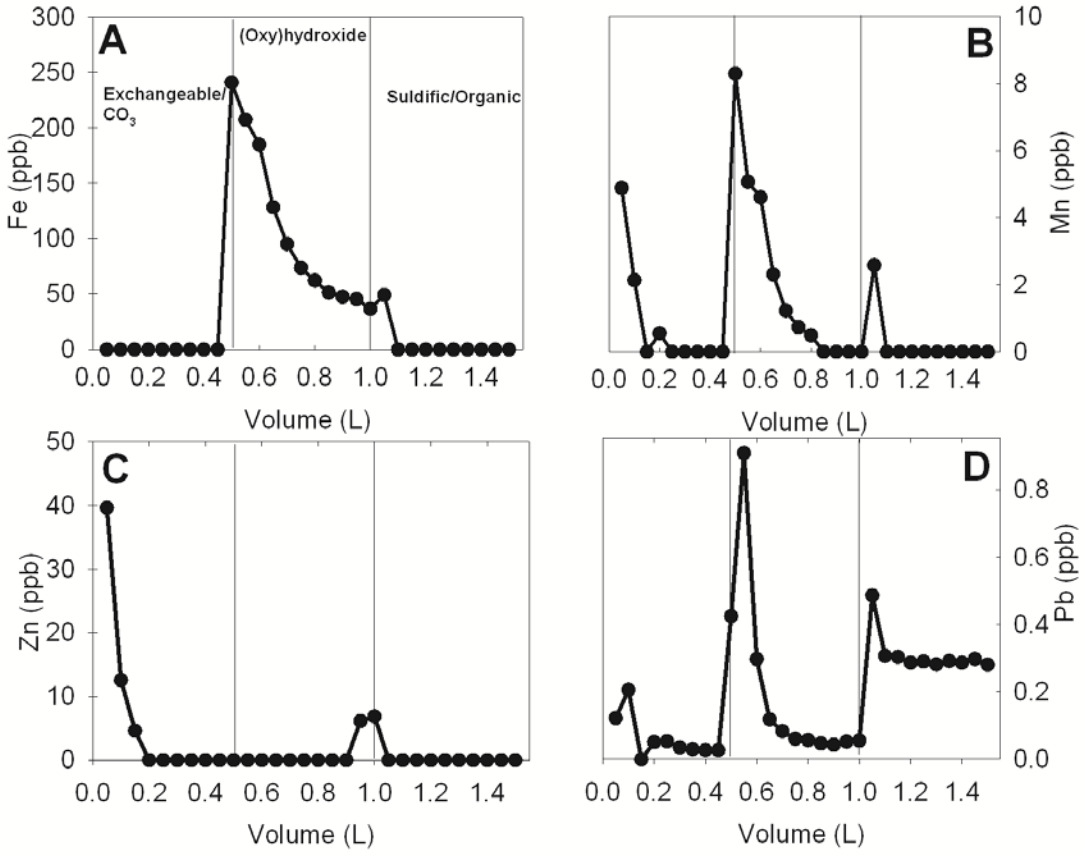

Figure 40: Extractogram of (A) Fe, (B) Mn, (C) Zn, and (D) Pb phases from STJOE 5-B. Extractogram shows heavy metal phases as defined by chemical extraction

Table 42: Continuous Sequential Extraction Data from Sub-Core STJOE 5-C						
	parts per billion					
Volume (mL)	Manganese / 55	Iron / 57	Zinc / 66	Lead / 206	Lead / 207	Lead / 208
50	3.62	0.00	3.02	0.00	0.00	0.00
100	0.00	0.00	0.00	0.00	0.00	0.00
150	0.00	0.00	0.00	0.00	0.00	0.00
200	0.00	0.00	0.00	0.04	0.00	0.04
250	0.00	29.55	0.00	0.19	0.18	0.18
300	0.00	0.00	0.00	0.07	0.08	0.08
350	0.00	0.00	0.00	0.05	0.05	0.06
400	0.00	0.00	0.00	0.05	0.00	0.04
450	0.00	0.00	0.00	0.14	0.16	0.16
500	3.42	195.13	0.00	0.37	0.39	0.38
550	13.76	246.03	0.00	0.23	0.22	0.23
600	4.84	116.19	0.00	0.18	0.18	0.18
650	3.20	97.89	0.00	0.10	0.12	0.10
700	1.64	70.42	0.00	0.08	0.07	0.07
750	1.03	61.99	0.00	0.07	0.08	0.08
800	0.60	47.32	0.00	0.06	0.05	0.05
850	0.00	41.58	0.00	0.06	0.05	0.05
900	0.00	30.63	0.00	0.04	0.05	0.04
950	0.00	108.31	0.00	0.09	0.09	0.10
1000	0.00	182.72	0.00	0.17	0.18	0.17
1050	0.00	101.81	0.00	0.28	0.31	0.29
1100	0.00	66.35	0.00	0.34	0.34	0.33
1150	0.00	32.19	0.00	0.30	0.31	0.31
1200	0.00	30.07	0.00	0.30	0.30	0.30
1250	0.00	34.83	0.00	0.29	0.32	0.31
1300	0.00	34.09	0.00	0.29	0.29	0.29
1350	0.00	33.79	0.00	0.30	0.32	0.31
1400	0.00	33.20	0.00	0.28	0.31	0.30
1450	0.00	30.11	0.00	0.30	0.33	0.31
1500	0.00	0.00	0.00	0.28	0.33	0.30
1550	0.00	36.05	6.03	0.49	0.52	0.51

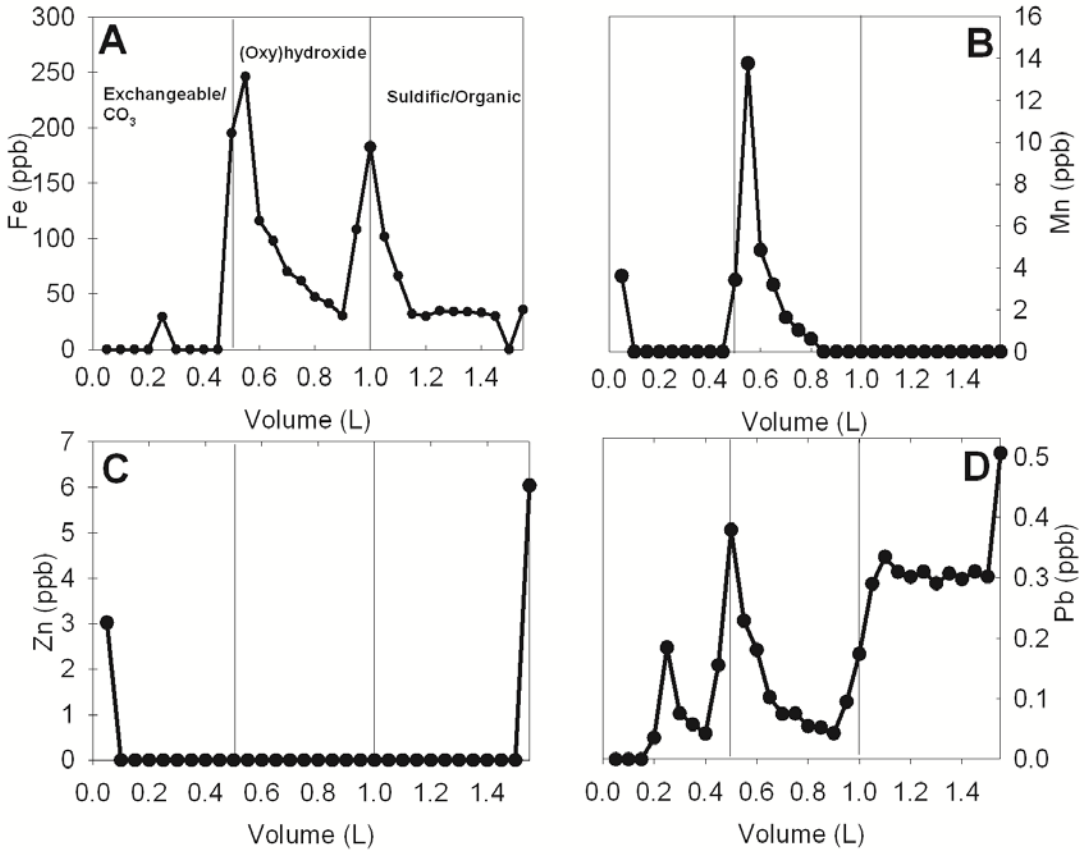

Figure 41: Extractogram of (A) Fe, (B) Mn, (C) Zn, and (D) Pb phases from STJOE 5-C. Extractogram shows heavy metal phases as defined by chemical extraction

LITERATURE CITED

1. Horowitz, A.J., K.A. Elrick, and R.B. Cook, *Effect of mining-related activities on the sediment-trace element geochemistry of Lake Coeur d'Alene, Idaho, USA. Part 1, Surface sediments*, in G.S. (U.S.), Editor. 1992, U.S. Dept. of the Interior, U.S. Geological Survey; U.S. Geological Survey, Open-File Reports Section [distributor],: Doraville, Ga. Denver, Colo.

2. Horowitz, A.J., *The effect of mining and related activities on the sediment-trace element geochemistry of Lake Coeur d'Alene, Idaho. Part II, Surface sediments*, in G.S. (U.S.), Editor. 1993, U.S. Dept. of the Interior, U.S. Geological Survey ; Earth Science Information Center, Open-File Reports Section [distributor],: Atlanta, Ga. Denver, CO.

3. Horowitz, A.J., K.A. Elrick, J.A. Robbins, and R.B. Cook, *A summary of the effects of mining and related activities on the sediment-trace element geochemistry of Lake Coeur d'Alene, Idaho, USA.* Journal of Geochemical Exploration 1995. **52**(1-2): p. 135-144.

4. Balistrieri, L.S., S.E. Box, and J.W. Tonkin, *Modeling precipitation and sorbtion of elements during mixing of river water and porewater in Coeur d'Alene River Basin.* Environmental Science & Technology, 2003(37): p. 4694-4701.

5. Kuwabara, J.S., J.L. Carter, B.R. Topping, S.V. Fend, P.F. Woods, W.M. Berelson, and L.S. Balistrieri, *Importance of Sediment-Water Interactions in Coeur d'Alene Lake, Idaho, USA: Management Implications.* Environmental Management 2003. **32**(3): p. 348-359.

6. Tonkin, J., L. Balistrieri, and J. Murray, *Modeling metal removal onto natural particles formed during mixing of acid rock drainage with ambient surface water.* Environmental Science & Technology, 2002. **36**(3): p. 484-492.

7. Leach, D.L., G.P. Landis, and A.H. Hofstra, *Metamorphic origin of the Coeur d'Alene base- and precious-metal veins in the Belt basin, Idaho and Montana.* Geology 1985. **16**(2): p. 122-125.

8. Mauk, J.L. and B.G. White, *Stratigraphy of the proterozoic Revett Formation and its control on Ag-Pb-Zn vein mineralization in the Coeur d'Alene district, Idaho.* Economic Geology and the Bulletin of the Society of Economic Geologists, 2004. **99**(2): p. 295-312.

9. Fleck, R.J., R.E. Criss, G.F. Eaton, R.W. Cleland, C.S. Wavra, and W.D. Bond, *Age and origin of base and precious metal veins of the Coeur d'Alene mining district, Idaho.* Economic Geology and the Bulletin of the Society of Economic Geologists, 2002. **97**(1): p. 23-42.

10. Rosenberg, P.E. and P.B. Larson, *Isotope Geochemistry of Ankerite-Bearing Veins Associated with the Coeur d'Alene Mining District, Idaho.* Economic Geology, 2000. **95**(8): p. 1689-1699.

11. Panneerselvam, K., A.W. Macfarlane, and V.J.M. Salters, *Provenance of Ore Metals in Base and Precious Metal Deposits of Central Idaho as Infered from Lead Isotopes.* Economic Geology, 2006. **101**(5): p. 1063-1077.

12. Cummings, D.E., A.W. March, B. Bostick, S. Spring, F. Caccavo, S. Fendorf, and R.F. Rosenzweig, *Evidence for microbial Fe(III) reduction in anoxic, mining-impacted lake sediments (Lake Coeur d'Alene, Idaho).* Applied and Environmental Microbiology, 2000. **66**(1): p. 154-162.

13. Farrand, W.H. and J.C. Harsanyi, *Mapping the distribution of mine tailings in the Coeur d'Alene River Valley, Idaho, through the use of a constrained energy minimization technique.* Remote Sensing of Environment 1997. **59**(1): p. 64-76.

14. Toevs, G.R., M.J. Morra, M.L. Polizzotto, D.G. Strawn, B.C. Bostick, and S. Fendorf, *Metal(loid) diagenesis in mine-impacted sediments of Lake Coeur d'Alene, Idaho.* Environmental Science & Technology, 2006. **40**(8): p. 2537-2543.

15. Grieco, R.A., *Petrology and geochemistry of carbonate veins in the Moe-Reindeer Queen mineral belt of the Coeur d'Alene mining district, Idaho-Montana*, 1981, Thesis (M.S.), Washington State University, 1981.,

16. Horowitz, A.J., K.A. Elrick, J.A. Robbins, and R.B. Cook, *Effect of Mining and Related Activities on the Sediment Trace-Element Geochemistry of Lake Coeur-Dalene, Idaho, USA .2. Subsurface Sediments.* Hydrological Processes, 1995. **9**(1): p. 35-54.

17. Harrington, J.M., S.E. Fendorf, and R.F. Rosenzweig, *Biotic generation of arsenic(III) in metal(loid)-contaminated freshwater lake sediments.* Environmental Science & Technology, 1998. **32**(16): p. 2425-2430.

18. Harrington, J.M., M.J. LaForce, W.C. Rember, S.E. Fendorf, and R.F. Rosenzweig, *Phase associations and mobilization of iron and trace elements in Coeur d'Alene Lake, Idaho.* Environmental Science & Technology, 1998. **32**(5): p. 650-656.

19. La Force, M.J., S. Fendorf, G.C. Li, and R.F. Rosenzweig, *Redistribution of trace elements from contaminated sediments of Lake Coeur d'Alene during oxygenation.* Journal of Environmental Quality 1999. **28**(4): p. 1195-1200.

20. La Force, M.J., S.E. Fendorf, G.C. Li, G.M. Schneider, and R.F. Rosenzweig, *A laboratory evaluation of trace element mobility from flooding and nutrient loading of Coeur d'Alene River sediments.* Journal of Environmental Quality 1998. **27**(2): p. 318-328.

21. Maxfield, D., J.M. Rodriguez, M. Buettner, J. Davis, L. Forbes, R. Kovacs, W. Russel, L. Schultz, R. Smith, J. Stanton, and C.M. Wai, *Heavy metal content in the sediments of the southern part of the Coeur d'Alene Lake.* Environmental Pollution (1970) 1974. **6**(4): p. 263-266.

22. Reece, D.E., J.R. Felkey, and C.M. Wai, *Heavy metal pollution in the sediments of the Coeur d'Alene River, Idaho.* Environmental Geology, 1978. **2**(5): p. 289-293.

23. Winowiecki, L., *Geochemical cycling of heavy metals in the sediment of Lake Coeur d'Alene, Idaho*, 2002, Masters Thesis, University of Idaho, Moscow, Idaho,

24. Woods, P.F. and M.A. Beckwith, *Nutrient and trace-element enrichment of Coeur d'Alene Lake, Idaho.* U. S. Geological Survey water-supply paper, 1997(2485): p. 1-93.

25. Sprenke, K.F., W.C. Rember, S.F. Bender, M.L. Hoffmann, F. Rabbi, and V.E. Chamberlain, *Toxic metal contamination in the lateral lakes of the Coeur d'Alene River valley, Idaho.* Environmental Geology 2000. **39**(6): p. 575-586.

26. Bostick, B.C., C.M. Hansel, M.J. La Force, and S. Fendorf, *Seasonal fluctuations in zinc speciation within a contaminated wetland.* Environmental Science & Technology, 2001. **35**(19): p. 3823-3829.

27. Farag, A.M., M.J. Suedkamp, J.S. Meyer, R. Barrows, and D.F. Woodward, *Distribution of metals during digestion by cutthroat trout fed benthic invertebrates contaminated in the Clark Fork River, Montana and the Coeur d'Alene River, Idaho, USA, and fed artificially contaminated Artemia.* Journal of Fish Biology 2000. **56**(1): p. 173-190.

28. Farag, A.M., D.F. Woodward, J.N. Goldstein, W. Brumbaugh, and J.S. Meyer, *Concentrations of metals associated with mining waste in sediments, biofilm, benthic macroinvertebrates, and fish from the Coeur d'Alene River Basin, Idaho.* Archives of Environmental Contamination and Toxicology 1998. **34**(2): p. 119-127.

29. Maxfield, D., J.M. Rodriguez, M. Buettner, J. Davis, L. Forbes, R. Kovacs, W. Russel, L. Schultz, R. Smith, J. Stanton, and C.M. Wai, *Heavy metal pollution in the sediments of the Coeur d'Alene river delta.* Environmental Pollution (1970) 1974. **7**(1): p. 1-6.

30. Paulson, A.J., *The transport and fate of Fe, Mn, Cu, Zn, Cd, Pb and SO4 in a groundwater plume and in downstream surface waters in the Coeur d'Alene Mining District, Idaho, U.S.A.* Applied Geochemistry 1997. **12**(4): p. 447-464.

31. Balistrieri, L.S., S.E. Box, and J.W. Tonkin, *Modeling precipitation and sorption of elements during mixing of river water and porewater in the Coeur d'Alene River basin.* Environmental Science & Technology, 2003. **37**(20): p. 4694-4701.

32. Box, S.E., United States. Forest Service., United States. Bureau of Land Management., and Geological Survey (U.S.), *Stream-sediment geochemistry in mining-impacted streams : Prichard, Eagle, and Beaver Creeks, Northern Coeur d'Alene Mining District, northern Idaho*. Scientific investigations report ; 2004-5284. 2005, Reston, Va. Denver, CO: U.S. Dept. of the Interior. v, 62 p.

33. Moberly, J., T. Borch, R. Sani, N. Spycher, S. Şengör, T. Ginn, and B. Peyton, *Heavy Metal–Mineral Associations in Coeur d'Alene River Sediments: A Synchrotron-Based Analysis.* Water, Air, & Soil Pollution, 2009. **201**(1-4): p. 195-208.

34. Grosbois, C.A., A.J. Horowitz, J.J. Smith, and K.A. Elrick, *The effect of mining and related activities on the sediment-trace element geochemistry of Lake Coeur d'Alene, Idaho, USA. Part III. Downstream effects: the Spokane River Basin.* Hydrological Processes, 2001. **15**(5): p. 855-875.

35. Horowitz, A.J., K.A. Elrick, and R.B. Cook, *Comment on "Phase Associations and Mobilization of Iron and trace elements in Coeur d'Alene Lake, Idaho"*. Environmental Science & Technology, 1999(32): p. 201-202.

36. Kalnejais, L.H., W.R. Martin, R.P. Signell, and M.H. Bothner, *Role of Sediment Resuspension in the Remobilization of Particulate-Phase Metals from Coastal Sediments.* Environmental Science & Technology, 2007. **41**(7): p. 2282-2288.

37. Lothenbach, B., G. Furrer, and R. Schulin, *Immobilization of heavy metals by polynuclear aluminium and montmorillonite compounds.* Environmental Science & Technology 1997. **31**(5): p. 1452-1462.

38. Fredrickson, J.K., J.M. Zachara, R.K. Kukkadapu, Y.A. Gorby, S.C. Smith, and C.F. Brown, *Biotransformation of Ni-substituted hydrous ferric oxide by an Fe(III)-reducing bacterium.* Environmental Science & Technology, 2001. **35**(4): p. 703-712.

39. Sengör, S., N.F. Spycher, T.R. Ginn, R.K. Sani, and B. Peyton, *Biogeochemical reactive-diffusive transport of heavy metals in Lake Coeur d'Alene sediments.* Applied Geochemistry, 2007. **22**(12): p. 2569-2594.

40. Oberdorster, G., E. Oberdorster, and J. Oberdorster, *Nanotoxicology: An emerging discipline evolving from studies of ultrafine particles.* Environmental Health Perspectives, 2005. **113**(7): p. 823-839.

41. Atkinson, C.A., D.F. Jolley, and S.L. Simpson, *Effect of overlying water pH, dissolved oxygen, salinity and sediment disturbances on metal release and sequestration from metal contaminated marine sediments.* Chemosphere, 2007. **69**(9): p. 1428-1437.

42. Haus, K.L., R.L. Hooper, L.A. Strumness, and J.B. Mahoney, *Analysis of arsenic speciation in mine contaminated lacustrine sediment using selective sequential extraction, HR-ICPMS and TEM.* Applied Geochemistry, 2007. **23**(4): p. 692-704.

43. Nies, D.H., *Microbial heavy-metal resistance.* Applied and Environmental Microbiology 1999. **51**(6): p. 730-750.

44. Lefcort, H., E. Ammann, and S.M. Eiger, *Antipredatory behavior as an index of heavy-metal pollution? A test using snails and caddisflies.* Archives of Environmental Contamination and Toxicology 2000. **38**(3): p. 311-316.

45. Weis, J.S., G. Smith, and C. Santiago-Bass, *Predator/prey interactions: A link between the individual level and both higher and lower level effects of toxicants in aquatic ecosystems.* Journal of Aquatic Ecosystem Stress and Recovery (Formerly Journal of Aquatic Ecosystem Health), 2000. **7**(2): p. 145-153.

46. Meyer, J.S., M.J. Suedkamp, J.M. Morris, and A.M. Farag, *Leachability of protein and metals incorporated into aquatic invertebrates: Are species and metals-exposure history important?* Archives of Environmental Contamination and Toxicology, 2006. **50**(1): p. 79-87.

47. Schaumloffel, J.C., R.H. Filby, and B.C. Moore, *Ponderosa pine tree rings as historical monitors of zinc and cadmium pollution.* Journal of Environmental Quality 1998. **27**(4): p. 851-859.

48. Spears, B.L., J.A. Hansen, and D.J. Audet, *Blood lead concentrations in waterfowl utilizing lake Coeur d'Alene, Idaho.* Archives of Environmental Contamination and Toxicology, 2007. **52**(1): p. 121-128.

49. Sani, R.K., B.A. Peyton, and M. Jandhyala, *Toxicity of lead in aqueous medium to Desulfovibrio desulfuricanis G20.* Environmental Toxicology and Chemistry, 2003. **22**(2): p. 252-260.

50. Sani, R.K., B.M. Peyton, and L.T. Brown, *Copper induced inhibition of growth of Desulfovibrio desulfuricans G20: Assessment of its toxicity and correlation with those of zinc and lead.* Applied and Environmental Microbiology 2001(67): p. 4765-4772.

51. Gadd, G.M., *Metals and Microorganisms - a Problem of Definition.* Fems Microbiology Letters, 1992. **100**(1-3): p. 197-203.

52. Morton, J.D., K.F. Hayes, and J.D. Semrau, *Effect of copper speciation on whole-cell soluble methane monooxygenase activity in Methylosinus trichosporium OB3b.* Applied and Environmental Microbiology, 2000. **66**(4): p. 1730-1733.

53. Dinning, A.J., I.S.I. Al-Adham, I.M. Eastwood, P. Austin, and P.J. Collier, *Pyrithione biocides as inhibitors of bacterial ATP synthesis.* Journal of Applied Microbiology, 1998. **85**(1): p. 141-146.

54. Sillanpaa, M. and A. Oikari, *Assessing the impact of complexation by EDTA and DTPA on heavy metal toxicity using microtox bioassay.* Chemosphere, 1996. **32**(8): p. 1485-1497.

55. Schets, F.M. and G.J. Medema, *Prevention of Toxicity of Metal-Ions to Aeromonas and Other Bacteria in Drinking-Water Samples Using Nitrilotriacetic Acid (Nta) Instead of Ethylenediaminetetraacetic Acid (Edta).* Letters in Applied Microbiology, 1993. **16**(2): p. 75-76.

56. Lloyd, J.R. and D.R. Lovley, *Microbial detoxification of metals and radionuclides.* Current Opinion in Biotechnology, 2001. **12**(3): p. 248-253.

57. Morse, J.W., *Interactions of Trace-Metals with Authigenic Sulfide Minerals - Implications for Their Bioavailability.* Marine Chemistry, 1994. **46**(1-2): p. 1-6.

58. Stohs, S.J. and D. Bagchi, *Oxidative Mechanisms in the Toxicity of Metal-Ions.* Free Radical Biology and Medicine, 1995. **18**(2): p. 321-336.

59. Gadd, G.M., *Interactions of Fungi with Toxic Metals.* New Phytologist, 1993. **124**(1): p. 25-60.

60. Cummings, D.E., O.L. Snoeyenbos-West, D.T. Newby, A.M. Niggemyer, D.R. Lovley, L.A. Achenbach, and R.F. Rosenzweig, *Diversity of geobacteraceae species inhabiting metal-polluted freshwater lake sediments ascertained by 16S rDNA analyses.* Microbial Ecology, 2003. **46**(2): p. 257-269.

61. Roane, T.M. and S.T. Kellogg, *Characterization of bacterial communities in heavy metal contaminated soils.* Canadian Journal of Microbiology, 1996(42): p. 593-603.

62. Niggemyer, A., S. Spring, E. Stackebrandt, and R.F. Rosenzweig, *Isolation and characterization of a novel As(V)-reducing bacterium: Implications for arsenic mobilization and the genus Desulfitobacterium.* Applied and Environmental Microbiology, 2001. **67**(12): p. 5568-5580.

63. Sani, R.K., B.M. Peyton, J.E. Amonette, and G.G. Geesey, *Reduction of uranium(VI) under sulfate-reducing conditions in the presence of Fe(III)-(hydr)oxides.* Geochimica Et Cosmochimica Acta 2004. **68**(12): p. 2639-2648.

64. Sani, R.K., B.M. Peyton, A. Dohnalkova, and J.E. Amonette, *Reoxidation of reduced uranium with iron(III) (hydr)oxides under sulfate-reducing conditions.* Environmental Science & Technology 2005. **39**(7): p. 2059-2066.

65. Kukkadapu, R.K., J.M. Zachara, S.C. Smith, J.K. Fredrickson, and C.X. Liu, *Dissimilatory bacterial reduction of Al-substituted goethite in subsurface sediments.* Geochimica et Cosmochimica Acta, 2001. **65**(17): p. 2913-2924.

66. Zachara, J.M., J.K. Fredrickson, S.C. Smith, and P.L. Gassman, *Solubilization of Fe(III) oxide-bound trace metals by a dissimilatory Fe(III) reducing bacterium.* Geochimica Et Cosmochimica Acta, 2001. **65**(1): p. 75-93.

67. Cummings, D.E., F. Caccavo, S. Fendorf, and R.F. Rosenzweig, *Arsenic mobilization by the dissimilatory Fe(III)-reducing bacterium Shewanella alga BrY.* Environmental Science & Technology, 1999. **33**(5): p. 723-729.

68. Balistrieri, L., S.E. Box, A.A. Bookstrom, and M. Ikramuddin, *Assessing the Influence of Reacting Pyrite and Carbonate Minerals on the Geochemistry of Drainage in the Coeur d'Alene Mining District.* Environmental Science & Technology, 1999(33): p. 3347-3353.

69. Schwarz, A.O. and B.E. Rittmann, *Analytical-modeling analysis of how pore-water gradients of toxic metals confer community resistance.* Advances in Water Resources, 2007. **30**(6-7): p. 1562-1570.

70. Schwarz, A.O. and B.E. Rittmann, *Modeling bio-protection and the gradient-resistance mechanism.* Biodegradation, 2007. **18**(6): p. 693-701.

71. Paulson, A.J., *Biogeochemical removal of Zn and Cd in the Coeur d'Alene River (Idaho, USA), downstream of a mining district.* Science of the Total Environment, The, 2001. **278**(1-3): p. 31-44.

72. van Leeuwen, H.P., R.M. Town, J. Buffle, R.F.M.J. Cleven, W. Davison, J. Puy, W.H. van Riemsdijk, and L. Sigg, *Dynamic speciation analysis and bioavailability of metals in aquatic systems.* Environmental Science & Technology, 2005. **39**(22): p. 8545-8556.

73. Meylan, S., R. Behra, and L. Sigg, *Influence of metal speciation in natural freshwater on bioaccumulation of copper and zinc in periphyton: A microcosm study.* Environmental Science & Technology, 2004. **38**(11): p. 3104-3111.

74. Nurenberg, W., *Voltametric trace analysis in ecological chemistry of toxic metals.* Pure and Applied Chemistry, 1982. **54**(4): p. 853-878.

75. D'Imperio, S., C.R. Lehr, H. Oduro, G. Druschel, M. Kuhl, and T.R. McDermott, *Relative Importance of H2 and H2S as Energy Sources for Primary Production in Geothermal Springs.* Applied and Environmental Microbiology, 2008. **74**(18): p. 5802-5808.

76. Parkhurst, D. and C. Appelo, *User's guide to PHREEQC (version 2)—a computer program for speciation, batch-reaction, one-dimensional transport, and inverse geochemical calculations.* US Geological Survey Water-Resources Investigations Report, 1999. **99**(4259): p. 310.

77. Allison, J.D., D.S. Brown, and K.J. Novo-Gradac, *MINTEQA2/PORODEFA2, a geochemical assessment model for environmental systems version 3.0 user's manual.* Washington DC: US Environmental Protection Agency 1991.

78. Spycher, N.F., A. Massoudieh, S.S. Sengor, T.R. Ginn, B.M. Peyton, R.K. Sani, and J. Moberly. *Modeling iron (hydr)oxide reductive dissolution and metal transport in mining-impacted riverine and lacustrine sediments*. in *Computation Methods in Water Resources XVII International Conference*. 2008. San Francisco, California.

79. Brown, P. and S. Markich, *Evaluation of the free ion activity model of metal-organism interaction: extension of the conceptual model.* Aquatic Toxicology, 2000. **51**(2): p. 177-194.

80. Mertens, J., F. Degryse, D. Springael, and E. Smolders, *Zinc toxicity to nitrification in soil and soilless culture can be predicted with the same biotic ligand model.* Environmental Science & Technology, 2007. **41**(8): p. 2992-2997.

81. Van Nostrand, J.D., A.G. Sowder, P.M. Bertsch, and P.J. Morris, *Effect of pH on the toxicity of nickel and other divalent metals to Burkholderia cepacia Pr1(301).* Environmental Toxicology and Chemistry, 2005. **24**(11): p. 2742-2750.

82. Janssen, C.R., D.G. Heijerick, K.A.C. De Schamphelaere, and H.E. Allen, *Environmental risk assessment of metals: tools for incorporating bioavailability.* Environment International, 2003. **28**(8): p. 793-800.

83. De Schamphelaere, K.A.C., J.L. Stauber, K.L. Wilde, S.J. Markich, P.L. Brown, N.M. Franklin, N.M. Creighton, and C.R. Janssen, *Toward a Biotic Ligand Model for Freshwater Green Algae: Surface-Bound and Internal Copper Are Better Predictors of Toxicity than Free Cu2+-Ion Activity When pH Is Varied.* Environmental Science & Technology, 2005. **39**(7): p. 2067-2072.

84. Kirpichtchikova, T.A., A. Manceau, L. Spadini, F. Panfili, M.A. Marcus, and T. Jacquet, *Speciation and solubility of heavy metals in contaminated soil using X-ray microfluorescence, EXAFS spectroscopy, chemical extraction, and thermodynamic modeling.* Geochimica et Cosmochimica Acta 2006. **70**(9): p. 2163-2190.

85. Miro, M., E.H. Hansen, R. Chomchoei, and W. Frenzel, *Dynamic flow-through approaches for metal fractionation in environmentally relevant solid samples.* Trac-Trends in Analytical Chemistry, 2005. **24**(8): p. 759-771.

86. Shiowatana, J., N. Tantidanai, S. Nookabkaew, and D. Nacapricha, *A novel continuous-flow sequential extraction procedure for metal speciation in solids.* Journal of Environmental Quality, 2001. **30**(4): p. 1195-1205.

87. van Hullebusch, E.D., S. Utomo, M.H. Zandvoort, and P.N.L. Lens, *Comparison of three sequential extraction procedures to describe metal fractionation in anaerobic granular sludges.* Talanta, 2005. **65**(2): p. 549-558.

88. Wisotzky, F. and N. Cremer, *Sequential extraction procedure in columns. Part 1: Development and description of a new method.* Environmental Geology, 2003. **44**(7): p. 799-804.

89. Gasser, U., W. Walker, R. Dahlgren, R. Borch, and R. Burau, *Lead release from smelter and mine waste impacted materials under simulated gastric conditions and relation to speciation.* Environmental Science & Technology, 1996. **30**(3): p. 761-769.

90. Brown, G.E., A.L. Foster, and J.D. Ostergren, *Mineral surfaces and bioavailability of heavy metals: A molecular-scale perspective.* Proceedings of the National Academy of Sciences of the United States of America, 1999. **96**(7): p. 3388-3395.

91. Manceau, A., M.A. Marcus, N. Tamura, O. Proux, N. Geoffroy, and B. Lanson, *Natural speciation of Zn at the micrometer scale in a clayey soil using X-ray fluorescence, absorption, and diffraction.* Geochimica Et Cosmochimica Acta, 2004. **68**(11): p. 2467-2483.

92. Cummings, D.E., F. Caccavo, S. Spring, and R.F. Rosenzweig, *Ferribacterium limneticum, gen. nov., sp. nov., an Fe(III)-reducing microorganism isolated from mining-impacted freshwater lake sediments.* Archives of Microbiology, 1999. **171**(3): p. 183-188.

93. Ramamoorthy, S., J.S. Piotrowski, H.W. Langner, W.E. Holben, M.J. Morra, and R.F. Rosenzweig, *Ecology of Sulfate-Reducing Bacteria in an Iron-Dominated, Mining-Impacted Freshwater Sediment.* Journal of Environmental Quality, 2009. **38**(2): p. 675-684.

94. Sass, H., S. Ramamoorthy, C. Yarwood, H. Langner, P. Schumann, R.M. Kroppenstedt, S. Spring, and R.F. Rosenzweig, *Desulfovibrio idahonensis sp. nov., sulfate-reducing bacteria isolated from a metal(loid)-contaminated freshwater sediment.* International Journal of Systems and Evolutionary Microbiology, 2009. **59**(9): p. 2208-2214.

95. Rastogi, G., R. Sani, B. Peyton, J. Moberly, and T. Ginn, *Molecular Studies on the Microbial Diversity Associated with Mining-Impacted Coeur d'Alene River Sediments.* Microbial Ecology, 2008.

96. Rothberg, J. and J. Leamon, *The development and impact of 454 sequencing.* Nature Biotechnology, 2008. **26**(10): p. 1117-1124.

97. He, Z., T.J. Gentry, C.W. Schadt, L. Wu, J. Liebich, S.C. Chong, Z. Huang, W. Wu, B. Gu, P. Jardine, C. Criddle, and J. Zhou, *GeoChip: a comprehensive microarray for investigating biogeochemical, ecological and environmental processes.* International Society for Microbial Ecology Journal. **1**(1): p. 67-77.

98. Nocker, A., C.-Y. Cheung, and A.K. Camper, *Comparison of propidium monoazide with ethidium monoazide for differentiation of live vs. dead bacteria by selective removal of DNA from dead cells.* Journal of Microbiological Methods, 2006. **67**(2): p. 310-320.

99. Chapelle, F.H., *Ground-water Microbiology and Geochemistry*. 2nd ed. . 2001, New York: John Wiley and sons. 55-56, 181-183, 343-347.

100. Mongodin, E.F., N. Shapir, S.C. Daugherty, R.T. Deboy, J.B. Emerson, A. Shvartzbeyn, D. Radune, J. Vamathevan, F. Riggs, V. Grinberg, H. Khouri, L.P. Wackett, K.E. Nelson, and M.J. Sadowsky, *Secrets of soil survival revealed by the genome sequence of Arthrobacter aurescens TC1.* Plos Genetics, 2006. **2**(12): p. 2094-2106.

101. Roane, T.M., K.L. Josephson, and I.L. Pepper, *Dual-Bioaugmentation Strategy To Enhance Remediation of Cocontaminated Soil.* Applied and Environmental Microbiology, 2001. **67**(7): p. 3208-3215.

102. Brim, H., H. Heuer, E. Krogerrecklenfort, M. Mergeay, and K. Smalla, *Characterization of the bacterial community of a zinc-polluted soil.* Canadian Journal of Microbiology 1999. **45**(4): p. 326-338.

103. Trajanovska, S., M.L. Britz, and M. Bhave, *Detection of heavy metal ion resistance genes in Gram-positive and Gram-negative bacteria isolated from a lead-contaminated site.* Biodegradation 1997. **8**(2): p. 113-124.

104. Coombs, J.M. and T. Barkay, *Molecular Evidence for the Evolution of Metal Homeostasis Genes by Lateral Gene Transfer in Bacteria from the Deep Terrestrial Subsurface.* Applied and Environmental Microbiology, 2004. **70**(3): p. 1698-1707.

105. Zhang, H.B., C.Q. Duan, Q.Y. Shao, W.M. Ren, T. Sha, L.Z. Cheng, Z.W. Zhao, and B. Hu, *Genetic and physiological diversity of phylogenetically and geographically distinct groups of Arthrobacter isolated from lead-zinc mine tailings.* Fems Microbiology Ecology 2004. **49**(2): p. 333-341.

106. Horton, R.N., W.A. Apel, V.S. Thompson, and P.P. Sheridan, *Low temperature reduction of hexavalent chromium by a microbial enrichment consortium and a novel strain of Arthrobacter aurescens.* Bmc Microbiology 2006. **6**.

107. Kurek, E., R. Kaczorowska, I. Nadulska, M. Ochal, E. Puacz, and E. Patkowska, *Retention of Cd by soil constituents under different environmental conditions.* Chemosphere, 1996. **33**(2): p. 277-284.

108. Konopka, A. and T. Zakharova, *Quantification of bacterial lead resistance via activity assays.* Journal of Microbiological Methods, 1999. **37**(1): p. 17-22.

109. Jo, J.K., Y.S. Jang, K.Y. Kim, M.H. Kim, I.J. Kim, and W.I. Chung, *Isolation of ALU1-P gene encoding a protein with aluminum tolerance activity from Arthrobacter viscosus.* Biochemical and Biophysical Research Communications 1997. **239**(3): p. 835-839.

110. Nies, D., *Heavy metal-resistant bacteria as extremophiles: molecular physiology and biotechnological use of Ralstonia sp. CH34.* Extremophiles 2000(4): p. 77-82.

111. Amor, L., C. Kennes, and M.C. Veiga, *Kinetics of inhibition in the biodegradation of monoaromatic hydrocarbons in presence of heavy metals.* Bioresource Technology 2001. **78**(2): p. 181-185.

112. Benka-Coker, M.O. and J.A. Ekundayo, *Effects of heavy metals on growth of species of Micrococcus and Pseudomonas in a crude oil/mineral salts medium.* Bioresource Technology 1998. **66**(3): p. 241-245.

113. Berg, J. and Y. Shi, *The galvanization of biology: a growing appreciation for the roles of zinc.* Science, 1996. **271**(5252): p. 1081.

114. Barua, S., *Microbial Diversity and Zinc Toxicity to Pseudomonas sp. from Coeur d'Alene River Sediments,* 2007, Masters Thesis, Montana State University, Bozeman, Montana.

115. Brandis, A. and R. Thauer, *Growth of Desulfovibrio species on hydrogen and sulphate as sole energy source.* Journal of General Microbiology, 1981. **126**(1): p. 249.

116. McGinnis, S. and T. Madden, *BLAST: at the core of a powerful and diverse set of sequence analysis tools.* Nucleic Acids Research, 2004. **32**(Web Server Issue): p. W20.

117. Sani, R.K., G. Geesey, and B.M. Peyton, *Assessment of lead toxicity to Desulfovibrio desulfuricans G20: influence of components of Lactate C medium.* Advances in Environmental Research 2001. **5**(3): p. 269-276.

118. Ihaka, R. and R. Gentleman, *R: a language for data analysis and graphics.* Journal of Computational and Graphical Statistics, 1996. **5**(3): p. 299-314.

119. Beard, S.J., R. Hashim, G.H. Wu, M.R.B. Binet, M.N. Hughes, and R.K. Poole, *Evidence for the transport of zinc(II) ions via the Pit inorganic phosphate transport system in Escherichia coli.* Fems Microbiology Letters, 2000. **184**(2): p. 231-235.

120. Harris, R.M., D.C. Webb, S.M. Howitt, and G.B. Cox, *Characterization of PitA and PitB from Escherichia coli.* Journal of Bacteriology, 2001. **183**(17): p. 5008-5014.

121. Jackson, R.J., M.R.B. Binet, L.J. Lee, R. Ma, A.I. Graham, C.W. McLeod, and R.K. Poole, *Expression of the PitA phosphate/metal transporter of Escherichia coli is responsive to zinc and inorganic phosphate levels.* Fems Microbiology Letters, 2008. **289**(2): p. 219-224.

122. van Veen, H.W., *Phosphate transport in prokaryotes: molecules, mediators and mechanisms.* Antonie van Leeuwenhoek, 1997. **72**(4): p. 299-315.

123. Hayashi, S., J. Koch, and E. Lin, *Active transport of L-α-glycerophosphate in Escherichia coli.* Journal of Biological Chemistry, 1964. **239**(9): p. 3098-3105.

124. Maloney, P., S. Ambudkar, V. Anatharam, L. Sonna, and A. Varadhachary, *Anion-exchange mechanisms in bacteria.* Microbiology and Molecular Biology Reviews, 1990. **54**(1): p. 1-17.

125. Kanehisa, M. and S. Goto, *KEGG: Kyoto encyclopedia of genes and genomes.* Nucleic Acids Research, 2000. **28**(1): p. 27.

126. Noll, M. and S. Lutsenko, *Expression of ZntA, a zinc-transporting P-1-type ATPase, is specifically regulated by zinc and cadmium.* Iubmb Life, 2000. **49**(4): p. 297-302.

127. Bøttger, P. and L. Pedersen, *Evolutionary and experimental analyses of inorganic phosphate transporter PiT family reveals two related signature sequences harboring highly conserved aspartic acids critical for sodium-dependent phosphate transport function of human PiT2.* FEBS Journal, 2005. **272**: p. 3060-3074.

128. Paulson, A.J. and L. Balistrieri, *Modeling removal of Cd, Cu, Pb, and Zn in acidic groundwater during neutralization by ambient surface waters and groundwaters.* Environmental Science & Technology, 1999. **33**(21): p. 3850-3856.

129. Feris, K., P. Ramsey, C. Frazar, J.N. Moore, J.E. Gannon, and W.E. Holben, *Differences in Hyporheic-Zone Microbial Community Structure along a Heavy-Metal Contamination Gradient.* Applied and Environmental Microbiology, 2003. **69**(9): p. 5563-5573.

130. Feris, K.P., P.W. Ramsey, C. Frazar, M. Rillig, J.N. Moore, J.E. Gannon, and W.E. Holben, *Seasonal Dynamics of Shallow-Hyporheic-Zone Microbial Community Structure along a Heavy-Metal Contamination Gradient.* Applied and Environmental Microbiology, 2004. **70**(4): p. 2323-2331.

131. Feris, K.P., P.W. Ramsey, M. Rillig, J.N. Moore, J.E. Gannon, and W.E. Holben, *Determining Rates of Change and Evaluating Group-Level Resiliency Differences in Hyporheic Microbial Communities in Response to Fluvial Heavy-Metal Deposition.* Applied and Environmental Microbiology, 2004. **70**(8): p. 4756-4765.

132. Gillan, D.C., B. Danis, P. Pernet, G. Joly, and P. Dubois, *Structure of Sediment-Associated Microbial Communities along a Heavy-Metal Contamination Gradient in the Marine Environment.* Applied and Environmental Microbiology, 2005. **71**(2): p. 679-690.

133. Brodie, E.L., T.Z. DeSantis, D.C. Joyner, S.M. Baek, J.T. Larsen, G.L. Andersen, T.C. Hazen, P.M. Richardson, D.J. Herman, and T.K. Tokunaga, *Application of a High-Density Oligonucleotide Microarray Approach To Study Bacterial Population Dynamics during Uranium Reduction and Reoxidation†.* Applied and Environmental Microbiology 2006. **72**(9): p. 6288-6298.

134. Lozupone, C. and R. Knight, *UniFrac: a New Phylogenetic Method for Comparing Microbial Communities.* Applied and Environmental Microbiology 2005. **71**(12): p. 8228-8235.

135. Mossop, K.F. and C.M. Davidson, *Comparison of original and modified BCR sequential extraction procedures for the fractionation of copper, iron, lead, manganese and zinc in soils and sediments.* Analytica Chimica Acta, 2003. **478**(1): p. 111-118.

136. Traina, S. and V. Laperche, *Contaminant bioavailability in soils, sediments, and aquatic environments.* Proceedings of the National Academy of Sciences, 1999. **96**(7): p. 3365.

137. Yan, W., *Singular-Value Partitioning in Biplot Analysis of Multienvironment Trial Data.* Agronomy Journal, 2002. **94**(5): p. 990-996.

138. Yan, W., P. Cornelius, J. Crossa, and L. Hunt, *Two types of GGE biplots for analyzing multi-environment trial data.* Crop Science, 2001. **41**(3): p. 656.

139. Yan, W., M.S. Kang, B. Ma, S. Woods, and P.L. Cornelius, *GGE Biplot vs. AMMI Analysis of Genotype-by-Environment Data.* Crop Science, 2007. **47**(2): p. 643-653.

140. Krauskopf, K., *International Series in the Earth and Planetary Sciences*. 1st ed. Introduction to Geochemistry, ed. F. Press. 1967, New York: McGraw-Hill

141. Almendras, M.-L., M. Carballa, L. Diels, K. Vanbroekhoven, and R. Chamy, *Prediction of Heavy Metals Mobility and Bioavailability in Contaminated Soil Using Sequential Extraction and Biosensors.* Journal of Environmental Engineering, 2009. **135**(9): p. 839-844.

142. Schwertmann, U. and R.M. Cornell, *Iron oxides in the laboratory*. 2nd ed. 2000, Weinheim, Germany: Wiley-VCH 14, 103-112.

143. Fredrickson, J., J. Zachara, D. Kennedy, H. Dong, T. Onstott, N. Hinman, and S. Li, *Biogenic iron mineralization accompanying the dissimilatory reduction of hydrous ferric oxide by a groundwater bacterium.* Geochimica et Cosmochimica Acta, 1998. **62**(19-20): p. 3239-3257.

144. Ben-Dov, E., A. Brenner, and A. Kushmaro, *Quantification of sulfate-reducing bacteria in industrial wastewater, by real-time polymerase chain reaction (PCR) using dsrA and apsA genes.* Microbial Ecology, 2007. **54**(3): p. 439-451.

145. Lovley, D.R. and E.J.P. Phillips, *Rapid Assay for Microbially Reducible Ferric Iron in Aquatic Sediments.* Applied and Environmental Microbiology 1987. **53**(7): p. 1536-1540.

146. Park, H., S. Lin, and G. Voordouw, *Ferric iron reduction by Desulfovibrio vulgaris Hildenborough wild type and energy metabolism mutants.* Antonie van Leeuwenhoek, 2008. **93**(1): p. 79-85.

147. Dyer, J.A., P. Trivedi, N.C. Scrivner, and D.L. Sparks, *Surface complexation modeling of zinc sorption onto ferrihydrite.* Journal of Colloid and Interface Science, 2004. **270**(1): p. 56-65.

148. Harrison, J. and V. Berkheiser, *Anion interactions with freshly prepared hydrous iron oxides.* Clays Clay Miner, 1982. **30**(2): p. 97-102.

149. Coleman, M., D. Hedrick, D. Lovley, D. White, and K. Pye, *Reduction of Fe (III) in sediments by sulphate-reducing bacteria.* Letters to Nature, 1993. **361**: p. 436-438.

150. Elias, D., J. Suflita, M. McInerney, and L. Krumholz, *Periplasmic cytochrome c3 of Desulfovibrio vulgaris is directly involved in H2-mediated metal but not sulfate reduction.* Applied and Environmental Microbiology, 2004. **70**(1): p. 413.

151. Herbert, R., S. Benner, A. Pratt, and D. Blowes, *Surface chemistry and morphology of poorly crystalline iron sulfides precipitated in media containing sulfate-reducing bacteria.* Chemical Geology, 1998. **144**(1-2): p. 87-97.

152. Neal, A.L., S. Techkarnjanaruk, A. Dohnalkova, D. McCready, B.M. Peyton, and G.G. Geesey, *Iron sulfides and sulfur species produced at hematite surfaces in the presence of sulfate-reducing bacteria.* Geochimica Et Cosmochimica Acta 2001. **65**(2): p. 223-235.

153. Hansel, C.M., S.G. Benner, and S. Fendorf, *Competing Fe(II)-induced mineralization pathways of ferrihydrite.* Environmental Science & Technology 2005. **39**(18): p. 7147-7153.